

ANALYSIS OF THE METAL CUTTING PROCESS
USING THE SHEAR PLANE MODEL

by

Cameron Kai-Ming Chen

A thesis submitted in partial fulfillment
of the requirements for the degree

of

Master of Science

in

Mechanical Engineering

MONTANA STATE UNIVERSITY
Bozeman, Montana

August 2010

©COPYRIGHT

by

Cameron Kai-Ming Chen

2010

All Rights Reserved

APPROVAL

of a thesis submitted by

Cameron Kai-Ming Chen

This thesis has been read by each member of the thesis committee and has been found to be satisfactory regarding content, English usage, format, citation, bibliographic style, and consistency and is ready for submission to the Division of Graduate Education.

Dr. David Miller

Approved for the Department of Mechanical Engineering

Dr. Christopher Jenkins

Approved for the Division of Graduate Education

Dr. Carl A. Fox

STATEMENT OF PERMISSION TO USE

In presenting this thesis in partial fulfillment of the requirements for a master's degree at Montana State University, I agree that the Library shall make it available to borrowers under rules of the Library.

If I have indicated my intention to copyright this thesis by including a copyright notice page, copying is allowable only for scholarly purposes, consistent with "fair use" as prescribed in the U.S. Copyright Law. Requests for permission for extended quotation from or reproduction of this thesis in whole or in parts may be granted only by the copyright holder.

Cameron Kai-Ming Chen

August 2010

TABLE OF CONTENTS

1. INTRODUCTION	1
Brief History of Metal Cutting.....	1
Mathematical Concepts of Mechanics of Materials.....	11
Yield Criteria.....	11
Equilibrium Equations	12
Constant Volume Condition	12
The Isotropic Condition	13
Metal Cutting Models	15
Slipline Field Theory	15
The Shear Plane Model	17
The Parallel Sided Shear Plane Model.....	19
The Johnson Cook Constitutive Model for Flow Stress	20
2. DESCRIPTION OF THE METAL CUTTING PROCESS CALCULATION.....	21
The Calculation Routine	22
Module #1	23
Module #2	31
Module #3	37
Module #4	41
Module #5	44
Module #6	45
Module #7	46
Modifications to the Calculation Routine	48
3. PARAMETRIC STUDY OF THE SIMULATION.....	54
Cutting Force	54
Thrust Force	56
Shear Plane Temperature	58
Average Chip Temperature	60
Tool-Chip Interface Temperature	61
Shear Plane Angle	63
Chip Thickness.....	65
Shear Strain Rate at the Shear Plane.....	66
Friction Force.....	67
Shear Stress at the Tool-Chip Interface.....	69
Shear Stress at the Shear Plane	70

TABLE OF CONTENTS - CONTINUED

4. COMPARISON OF METAL CUTTING PREDICTIONS WITH EXPERIMENT	71
Case Study of 1006 Steel	72
Case Study of 6Al-4V Titanium	74
Case Study of 2024-T3 Aluminum as the Workpiece.....	76
Case Study with OFE Copper as the Workpiece.....	81
5. CONCLUSION.....	83
REFERENCES CITED.....	85
APPENDICES	89
APPENDIX A: Calculation Method	90
APPENDIX B: Defining the Shear Thickness Ratio	100

LIST OF TABLES

Table	Page
1. Johnson Cook parameters	23

LIST OF FIGURES

Figure	Page
1. Excerpts from 'Handbuch der Maschinen'. a.)images depicting the chip formation process. b.) tabulated information regarding speeds and feeds for a given workpiece material[6].	2
2. Illustrations from "Memoirs sur le Rabotage de Metaux"[7]. a.) a model of the chip formation process, b.) detailed illustrations of metallic chips, presumably formed by a variety of different metal cutting techniques.	3
3. Illustration by Mallock [8] of the chip formation zone during a metal cutting process for a.) wrought iron, b.) hard stee, c.) cast iron and d.) gun metal. Note the contrast between the workpiece and chip, indicating the presence of a distinct 'shear plane'	4
4. Illustrations by Mallock of the chip formation zone with copper as the workpiece. Of interest is the different configuration of the chip formation zone with and without the use of a lubricant.	5
5. The shear plane model, as first proposed by Mallock in 1881[8].....	6
6. Figure 6: An illustration of the force equilibrium, as depicted by 'Merchant's Circle'[9].	7
7. The shear plane model with the tool positioned at an oblique angle relative to the workpiece[2].....	8
8. A depiction of the model derived by N.Fang to describe metal cutting using a tool with a rounded edge.	8
9. A example of simulation results from AdvantEdge software.....	9
10. Mohr's circles for plane strain conditions: (a) stress circle; (b) strain-rate circle[2].	14

LIST OF FIGURES - CONTINUED

Figure	Page
11. Curvilinear element bounded by sliplines showing stresses acting on sliplines[2].....	15
12. (a) The shear plane model. (b). forces associated with the shear plane model.	17
13. The shear plane model (9).....	20
14. Flow chart of calculation routine.	22
15. The shear plane model showing relevant parameters for preliminary calculations.	24
16. Layout of the orthogonal machining experiment used by Stevenson and Oxley (11).	26
17. A typical observation of plastic deformation in the shear zone from experiments conducted by Stevenson and Oxley.	26
18. Shear strain-rate as a function of shear plane velocity and feed.	27
19. Shear strain-rate as a function of shear plane velocity and shear plane length.	28
20. The shear plane model showing the relationship between the shear plane velocity (V_s) and the velocity component normal the the shear plane (V_n).	29
21. The parallel sided shear plane model. The chip formation zone is approximately bounded by planes CD and EF, which are parallel to the shear plane.	29
22. Thermal conductivity as a function of temperature for the workpiece materials under study.	32
23. Specific heat as a function of temperatures for the workpiece materials under study.	33

LIST OF FIGURES - CONTINUED

Figure	Page
24. Theoretical and experimental results for beta: line represents Weiner's theoretical results; open circle represents Nakayama's experimental results; closed triangle, closed square and closed circle represent boothroyd's results, '+' symbol represents results calclated by Tay et al. using finite element method[2].....	35
25. Mohr's stress circle and slipline field element showing stress-free surface condition[2].	38
26. Heat Generation models considered in the numerical method used to evaluate the maximum temperature rise at the chip interface[1].	44
27. Calculated and experimental tool-chip interface results: full line represents numerical results assuming rectangular plastic zone and broken line represents numerical results assuming triangular plastic zone; symbols represent experimental results.	45
28. A sample plot of total work rate as a function of shear thickness ratio, with $\alpha = 5^\circ$, $w=3\text{mm}$, $t_1 = 0.07\text{mm}$, $V_C = 200 \text{ m/min}$	49
29. A sample plot of the determination of δ with 1006 steel as the workpiece.	50
30. Determination of δ with 1006 steel as the workpiece: the relationship of the power law constant (n) as a function of cutting velocity (V_C)	51
31. Determination of δ with 1006 steel as the workpiece: the relationship of the power law constant (A) as a function of cutting velocity (V_C)......	52
32. Predicted cutting force as a function of cutting speed and feed.	55

LIST OF FIGURES - CONTINUED

Figure	Page
33. Predicted thrust force as a function of cutting speed and feed.....	57
34. Predicted shear plane temperature as a function of cutting speed and feed.....	59
35. Average chip temperature as a function of cutting speed and feed.....	60
36. Tool-chip interface temperature as a function of cutting speed and feed.....	62
37. Shear plane angle as a function of cutting speed and feed.....	64
38. Chip thickness as a function of cutting speed and feed.....	65
39. Shear strain rate as a function of cutting speed and feed.....	67
40. Predicted friction force.	68
41. Shear stress at the tool-chip interface.	69
42. Shear stress at the shear plane.....	70
43. Comparison of cutting forces from experiment and from simulation.....	73
44. Comparison of observed and predicted tool forces with 6Al-4V titanium as the workpiece.	75
45. Comparison of predicted cutting force with experimental data for 2024-T3.....	77
46. Comparison of predicted thrust force with experimental data for 2024-T3.....	78

LIST OF FIGURES - CONTINUED

Figure	Page
47. Comparison of predicted chip thickness with experimental data for 2024-T3.....	79
48. Chip thickness as a function of shear plane angle with $a = 0^\circ$ and $t_1 = 0.08\text{mm}$	80
49. Comparison of predicted cutting force with experimental data for OFE copper as the workpiece.....	81
50. Comparison of predicted thrust force with experimental data for OFE copper as the workpiece.....	82
51. Determination of δ with 6Al-4V Ti as the workpiece: shear thickness ratio v. cutting velocity and feed - power law fit.	101
52. Determination of δ with 6Al-4V Ti as the workpiece: the relationship of the power law constant (n) as a function of cutting velocity (V_c) - 2nd order polynomial fit.....	102
53. Determination of δ with 6Al-4V Ti as the workpiece: the relationship of the power law constant (A) as a function of cutting velocity (V_c) - a power law fit.	102
54. Determination of δ with OFE copper as the workpiece: shear thickness ratio v. cutting velocity and feed - power law fit.	103
55. Determination of δ with OFE copper as the workpiece: the relationship of the power law constant (n) as a function of cutting velocity (V_c) - 2nd order polynomial fit.	103
56. Determination of δ with OFE copper as the workpiece: the relationship of the power law constant (A) as a function of cutting velocity (V_c) - power law fit.	104

LIST OF FIGURES - CONTINUED

Figure	Page
57. Determination of δ with 2024-T3 aluminum as the workpiece: shear thickness ratio v. cutting velocity and feed - power law fit.	104
58. Determination of δ with 2024-T3 aluminum as the workpiece: the relationship of the power law constant (n) as a function of cutting velocity (V_c) - 2nd order polynomial fit.	105
59. Determination of δ with 2024-T3 aluminum as the workpiece: the relationship of the power law constant (A) as a function of cutting velocity (V_c) - power law fit.	105
60. Determination of δ with 1006 steel as the workpiece: shear thickness ratio v. cutting velocity and feed - power law fit.	106
61. Determination of δ with 1006 steel as the workpiece: the relationship of the power law constant (n) as a function of cutting velocity (V_c) - 2nd order polynomial fit.....	106
62. Determination of δ with 1006 steel as the workpiece: the relationship of the power law constant (A) as a function of cutting velocity (V_c) - power law fit.....	107

ABSTRACT

The objective of the metal cutting process is to reshape a piece of metal, or workpiece, of initial geometry into a new geometry of desired shape. Although there are a variety of ways to cut metal, this study focuses on the type of cutting where metal is sheared away from the workpiece as is commonly done with machine tools such as the lathe or mill. Typically, the correct machine settings can be found from reference guides that summarize a great amount of empirical data on metal cutting. Trial and error when combined with experience, often suffices to select the proper process parameters. The aim of this study is to predict the outcome of a metal cutting process given the properties of the workpiece, feed and cutting speed in order to understand the cutting process and predict optimum conditions. The shear plane model is well known, having been developed in the early and mid-20th century. However the empirical nature of the model and approximations made in making predictions of the metal cutting process serve to limit the usefulness of this model. A calculation routine devised by P.L.B Oxley to predict how to cut steel was created with modifications allowing predictions of the metal cutting process with any metal. A comparative study was done with 1006 steel, 6Al-4V titanium, 2024-T3 aluminum and OFE copper regarding the differences in tool forces and temperatures that would result if each metal was cut with the same process. A quantitative prediction of the metal cutting process was made for the four metals under study. Although there is no experimental data with which to evaluate these predictions, a number of case studies were performed. These case studies involved the prediction of experimental data presented in literature from other laboratories. The metal cutting model presented here has great promise as a guide to predict the best machine tool parameters.

INTRODUCTION

Brief History of Metal Cutting

According to Finnie's narrative [3] on the history of metal cutting, the earliest reference that could be found relating to scientific studies of the cutting process is from Cocquihhat [4] in 1851. His cutting experiments involved rotating the workpiece while cutting with a drill held fixed. The drill advanced at a constant speed while torque was measured with a weight balance. The data collected were the work required per unit volume and force per unit area of the cut. Experiments were carried out for cast iron, malleable iron, brass, stone and other materials. Cocquihhat then used this data to estimate the cost of creating tunnels and trenches. In 1861, Weibe [5] extended the work of Cocquihhat and published the formula,

$$P = K * E * B \quad (1)$$

where P is the work required to remove a piece of material of width B and thickness E. K is a constant of the material. This formula is the first attempt to analyze and predict the outcome of a metal cutting process.

In 1873, Hartig [6] published “Handbuch der Maschinen”; a comprehensive reference guide containing tabulated values for machining metals. These tabulations were made from observations of the metal cutting process. Hartig’s book, similar in function to today’s “Machinery’s Handbook”, was the first of its kind and apparently was the definitive reference for machining in its day. Shown in fig. 1a is a collection of several illustrations depicting the chip formation process of several types cutting

processes. Shown in Figure 1 is an example of tabulated values of feeds and speeds for a given workpiece material.

§. 94. Theorie der mechanischen Werkzeuge.		533	172 Materialien zum Schneiden. — Eisen.				
Af	Material.	Belastung bis zum Bröcken				Kilogramm.	
		auf einen Querschnitt von 4 Quadratlinien weitt.	auf einen Querschnitt von 1 Quadratlinie weitt.	auf einen Querschnitt von 1 Quadratlinie profilös.	auf einen Querschnitt von 1 Quadratcentimeter.		
5	Reber Schmiedeisen .	Wörrt. Pf.	Wörrt. Pf.	Schlägt.			
		4100	4500				
		4340	105500	84500	6176		
6	Cementeisen	6160	6410				
		6316	157750	12300	8979		
7	Raffiniertes Schmiedeisen R°	4250	5250				
		4770	119250	92900	6788		
8	nn	4510	5910				
		5050	126250	98300	7186		
9	F°	4660	6510				
		5340	133500	10400	7599		
10	Gußeisen F	4660	5660				

Figure 1: Excerpts from 'Handbuch der Maschinen'. a.)images depicting the chip formation process. b.) tabulated information regarding speeds and feeds for a given workpiece material[6].

One of the first attempts to analyze chip formation was performed by Tresca [7] in 1873, see Figure 2.

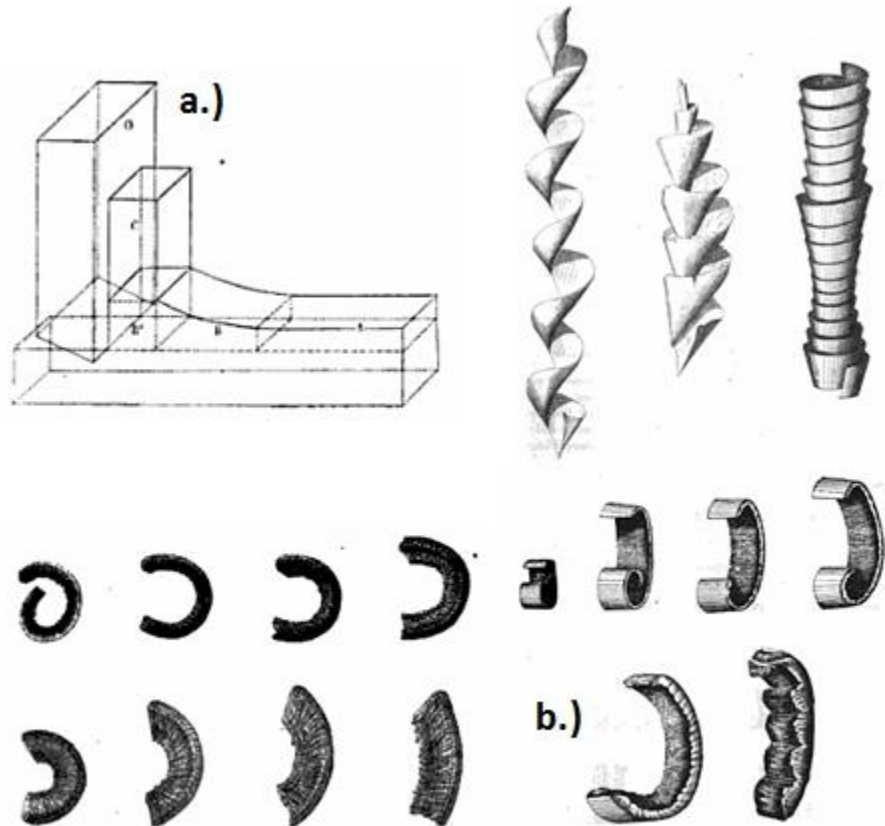


Figure 2: Illustrations from "Memoirs sur le Rabotage de Metaux" [7]. a.) a model of the chip formation process, b.) detailed illustrations of metallic chips, presumably formed by a variety of different metal cutting techniques.

Tresca's observations were published in the book "Memoirs sur le Rabotage de Metaux". The work contains hundreds of high quality illustrations of metal chips. Presumably, these illustrations were meant to serve as a qualitative guide when machining and often includes examples of correctly formed chips alongside poorly formed chips. Although an analytical model for the metal cutting process is not proposed in this work, these detailed observations would have been informative at the time. In addition, these intricate

illustrations underline the complexity and beauty of metal cutting, in all its various modes.

The shear plane model, which is the basis of modern analytical models of metal cutting and of this study, was first established by Mallock [8] in 1881. In his turning experiments, Mallock made hand drawings of the chip formation process in the course of their formation by means of a microscope mounted to the tool holder, see Figure 3.

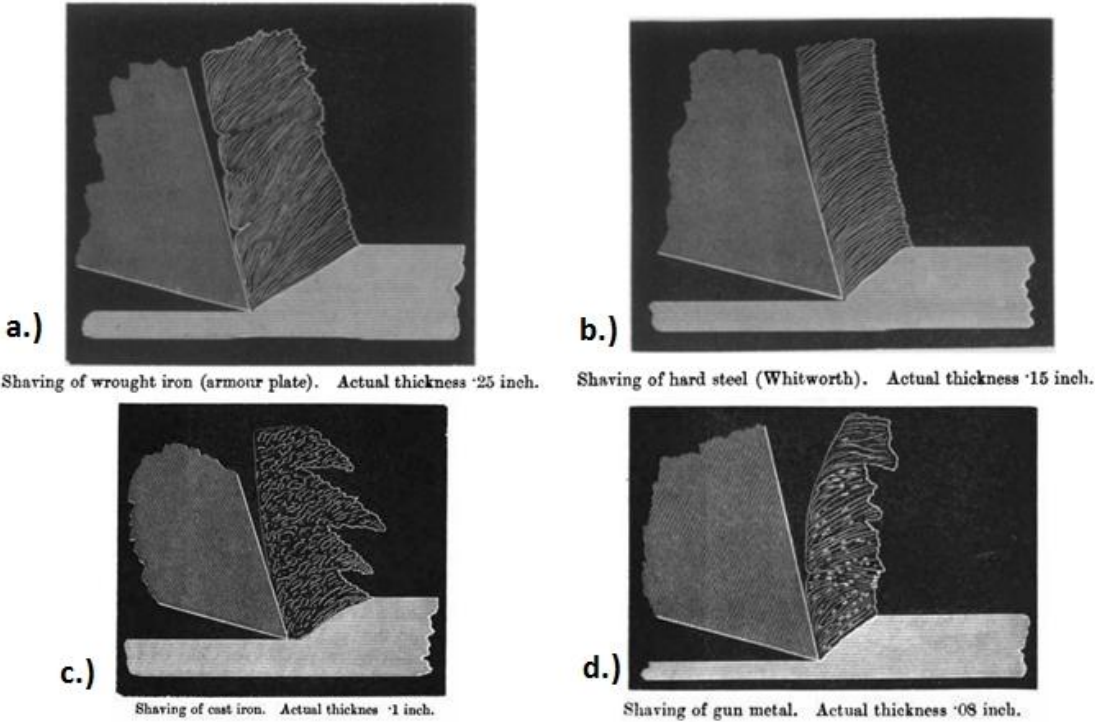


Figure 3: Illustration by Mallock [8] of the chip formation zone during a metal cutting process for a.) wrought iron, b.) hard stee, c.) cast iron and d.) gun metal. Note the contrast between the workpiece and chip, indicating the presence of a distinct ‘shear plane’.

Mallock remarked that the chip formation zones of the different workpieces appeared very similar and proposed that any difference in the ‘action’ of the tool would “depend on

the physical constants of the substance operated on". Mallock also suggests that the friction coefficient of the workpiece was a factor in chip formation. Mallock also used studied copper as the workpiece, see Figure 4.

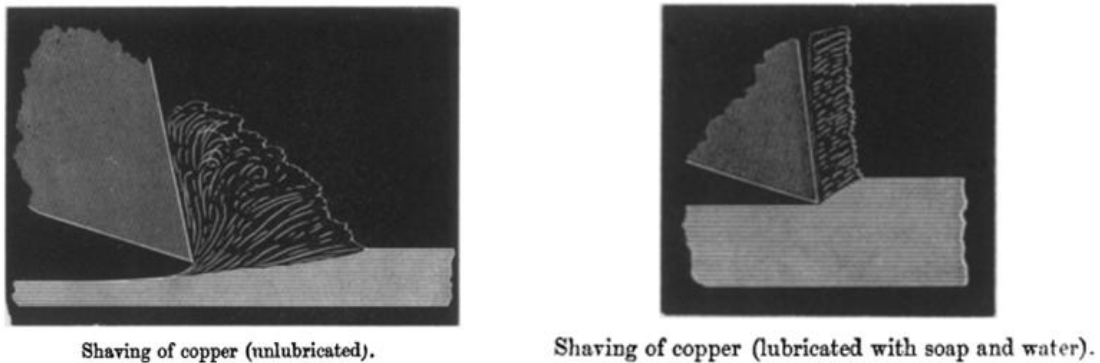


Figure 4: Illustrations by Mallock of the chip formation zone with copper as the workpiece. Of interest is the different configuration of the chip formation zone with and without the use of a lubricant.

In these experiments, Mallock observed the effect that lubrication had on chip formation. His observations of unlubricated cutting indicate a condition of buildup and possible seizure at the tool face. In contrast, when the copper workpiece is lubricated with a soap and water solution, Mallock observed the formation of a continuous chip, without buildup. This experiment with copper as the workpiece showed that friction was a significant factor in the chip formation process. As a result of his observations, Mallock presented a single model to describe chip formation for any material as the workpiece. This is the shear plane model as shown in Figure 5, which is the basis for modern studies in metal cutting.

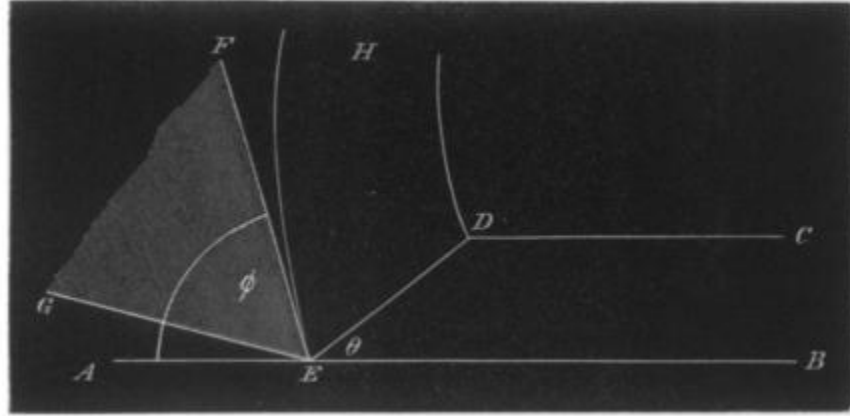


Figure 5: The shear plane model, as first proposed by Mallock in 1881[8].

With this model, Mallock correctly theorized that “the tools do not act, properly speaking, by cutting but by shearing”.

Further work in the field of metal cutting was performed by Merchant[9], applied the mechanics of solid bodies under applied loads by considering the chip in static equilibrium acted upon by two equal, opposite, and collinear forces—one acting on the shear plane and the other acting on the tool face. Shown in Figure 6 is an illustration of a condensed force diagram of the force components in the shear plane model.

MERCHANTS work was refined by Lee and Shaffer[10], Oxley [2] and by Trent [11] with the aim of improving the predictive capability of the shear plane model. At the end of the 1970’s the shear plane model was fully developed as a model capable of predicting the geometry of the metal cutting process and accompanying tool forces. By analyzing the plastic work done in the chip formation process, the temperatures of the cutting procedure could also be predicted.

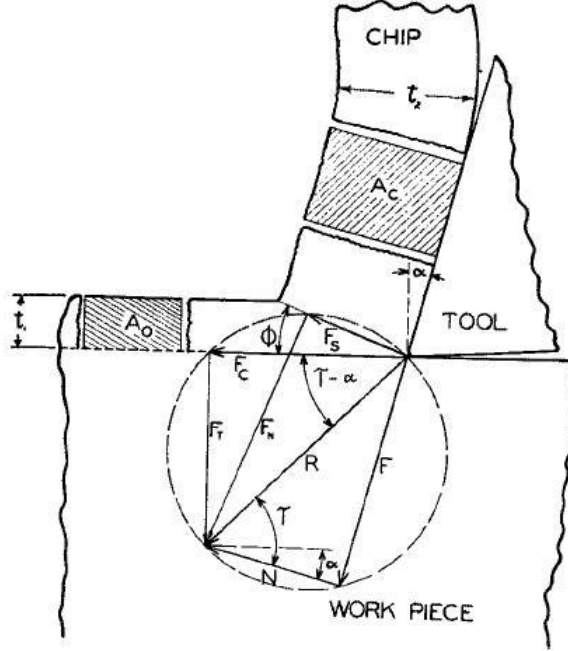


Figure 6: An illustration of the force equilibrium, as depicted by 'Merchant's Circle'[9].

Following the initial development of the shear plane model, additional research led to the alteration of the model to include other cutting conditions as well as certain modifications to make the simulation more realistic. Oxley [2] has developed a method of predicting cutting forces for oblique machining conditions, see Figure 7. Because it is common to use a tool with an oblique angle, this modification makes the shear plane model applicable to such metal cutting conditions.

The assumption of an infinitely sharp tool is unreasonable, since a tool with such a tip can be neither made nor maintained during normal operation. Additional research has been performed by N.Fang [12] to better simulate the tool as having a rounded tip, see Figure 8.

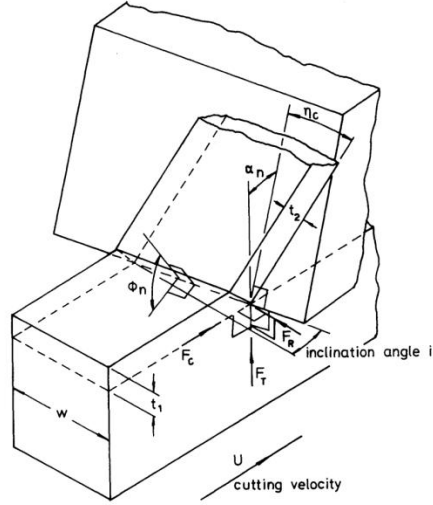


Figure 7: The shear plane model with the tool positioned at an oblique angle relative to the workpiece[2].

Fang's model still used the basic concepts of the original shear plane model, but further subdivides the chip formation zone to conform to the contours of the tool geometry. As such, this model has the ability to predict the additional heat and friction that would occur in a realistically shaped tool.

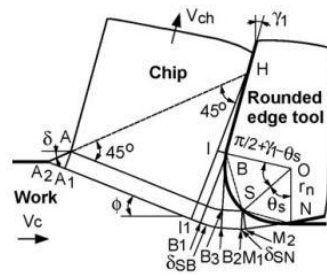


Figure 8: A depiction of the model derived by N.Fang to describe metal cutting using a tool with a rounded edge.

Beyond improvements to the shear plane, additional research in this area has expanded with the use of numerical methods to predict metal cutting performance. From

this research, computer programs running finite element code have been developed. Of note, a program called AdvantEdge, from the Third Wave company has been developed to predict metal cutting performance for turning, milling and drilling type cuts. This software combines a very simple user interface with a very sophisticated numerical solver which uses Adaptive Lagrangian-Eularian (ALE) meshing techniques. With adequate knowledge of the workings of this model, highly detailed simulations are possible, see Figure 9.

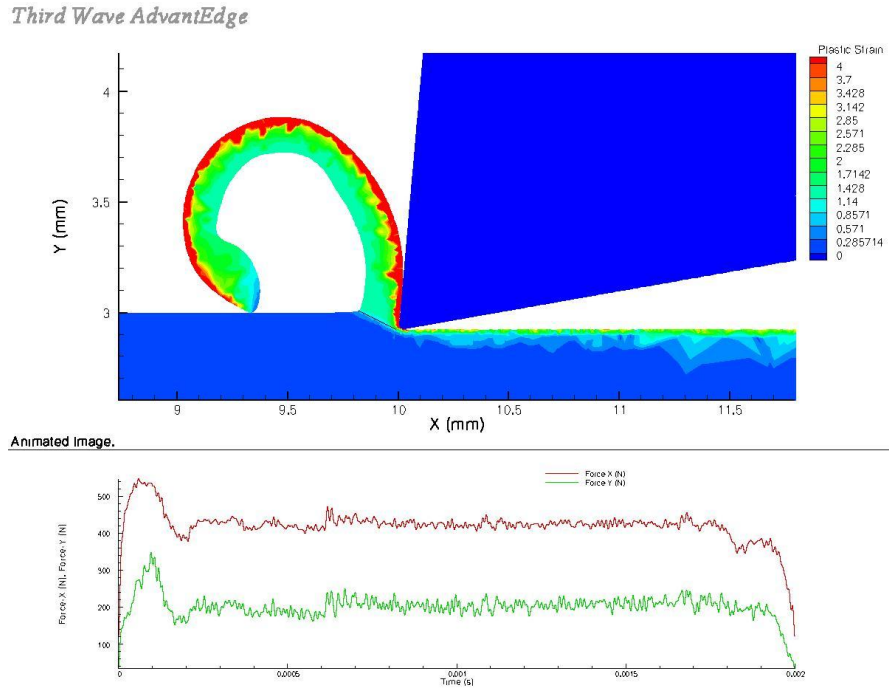


Figure 9: A example of simulation results from AdvantEdge software.

Results from AdvantEdge simulations include spatial information on stress, temperature, plastic deformation, etc. regarding not only the chip and chip formation zone, but also can predict the condition of the freshly cut surface of the workpiece.

The purpose of this study is not to work with the most advanced and realistic metal cutting model to date, as this would be a monumental academic achievement. Although the shear plane model remains the basis of current state-of-the-art work in metal cutting research, many modifications are possible which address realistic concerns. In order to understand any of the advanced topics, it is important to understand the basic shear plane model. Indeed, the shear plane model itself involves an understanding of plasticity and constitutive properties. The calculation procedure is involved. Thus, it is not sufficient to merely cite the early model; it must be understood and worked with if the more current advances are to be understood and applied. The shear plane model as presented by Oxley was chosen for study for a variety of reasons. It is nearly the same model presented by Mallock in 1881, yet it is the basis for modern metal cutting studies. By studying this model, modern approaches will be better understood and evaluated. It is simple, but not too simple to provide useful predictions of the metal cutting process. The predictions are bound by certain simplifications and this limits its usefulness. However it is expected that in future work, corrections can be made to the model to allow better predictions. In summary, this study is sought to be a fixture that future students can quickly read, gain some perspective and knowledge in order to take the next logical step of improving this model to enhance metal cutting predictions.

MODEL DESCRIPTION

Mathematical Concepts of Mechanics of Materials

The models used to describe the metal cutting process are based on fundamental principles of the mechanics of materials regarding plasticity. It is fitting to mention the basic models used in the metal cutting model.

Yield Criteria

The yield criteria is established with respect to two dimensional plane strain,

$$\frac{1}{4}(\sigma_x - \sigma_y)^2 + \tau_{xy}^2 = k^2 \quad (2)$$

where σ_x , σ_y and τ_{xy} are the normal stress in the x direction, normal stress in the y direction and shear stress in the xy plane, respectively. k is the maximum shear stress that results from a two dimensional load specified by σ_x , σ_y and τ_{xy} . Principal stresses can be defined as,

$$\sigma_1 = \sigma_m + k \quad (3)$$

$$\sigma_2 = \sigma_m - k \quad (4)$$

$$\sigma_3 = \sigma_m = \frac{1}{2}(\sigma_x + \sigma_y) \quad (5)$$

where σ_y , σ_1 , σ_2 are the normal yield stress and the normal stresses in the 1 and 2 principal directions, respectively. σ_m is the mean stress. According to the Von Mises criterion, the yield stress is,

$$\sigma_y = \frac{1}{2} \sqrt{\sigma_1 - \sigma_2}^2 + \sigma_2 - \sigma_3^2 + \sigma_3 - \sigma_1^2 \quad (7)$$

where σ_3 is the mean stress.

k , the yield shear stress criteria in a pure shear loading,

$$k = \frac{\sigma_y}{3} \quad (8)$$

In the predictive metal cutting calculations, the shear strain energy criterion will be used to evaluate the shear stress based on an available value of normal yield.

Eqilibrium Equations

The equilibrium equations state that the forces in the deforming material sum to zero.

In a differential form of stress, this results in the following equilibrium equations,

$$\frac{\partial \sigma_x}{\partial x} + \frac{\partial \tau_{xy}}{\partial y} = 0 \quad (9)$$

$$\frac{\partial \sigma_y}{\partial y} + \frac{\partial \tau_{xy}}{\partial x} = 0 \quad (10)$$

given a state of two dimensional plane strain. As will be seen later, the equilibrium equations are the basis of the slipline equations which describe the stress environment in the so called shear zone of the parallel plane model of the metal cutting process.

Constant Volume Condition

A constant volume condition is assumed for the workpiece. Ignoring elastic deformation, the following strain rate relationship holds,

$$\dot{\varepsilon}_x + \dot{\varepsilon}_y = 0 \quad (11)$$

where $\dot{\varepsilon}_x$ and $\dot{\varepsilon}_y$ are the normal strain rates in the x and y directions.

And, given that,

$$\dot{\varepsilon}_x = \frac{\partial V_x}{\partial x} \quad (12)$$

$$\dot{\varepsilon}_y = \frac{\partial V_y}{\partial y} \quad (13)$$

the constant volume condition can be expressed as,

$$\frac{\partial V_x}{\partial x} + \frac{\partial V_y}{\partial y} = 0 \quad (14)$$

where V_x and V_y are the velocities in the x and y directions, respectively.

The Isotropic Condition

If the workpiece is assumed to be an isotropic, perfectly plastic material that deforms according to the Levy-Mises relations, the following relationship holds for a three dimensional state of stress,

$$\frac{\dot{\varepsilon}_x}{\sigma'_x} = \frac{\dot{\varepsilon}_y}{\sigma'_y} = \frac{\dot{\varepsilon}_z}{\sigma'_z} = \frac{\dot{\gamma}_{xy}/2}{\tau_{xy}} = \frac{\dot{\gamma}_{yz}/2}{\tau_{yz}} = \frac{\dot{\gamma}_{zx}/2}{\tau_{zx}} \quad (15)$$

which describe the deformation of a viscous material. $\dot{\gamma}_{xy}$, $\dot{\gamma}_{yz}$ and $\dot{\gamma}_{zx}$ are the shear strain rates for a three dimensional stress state. τ_{xy} , τ_{yz} and τ_{zx} are the shear stresses for a three dimensional state. Prime notation denotes a condition of deviatoric stress. This assumption implies that the directions of maximum shear stress and maximum shear strain rate coincide.

The isotropic assumption implies that $\psi = \psi'$, where ψ and ψ' are the angular relationships of the stress and strain rate circle, respectively. Figure 6 shows the relationships between stress, strain-rate and the rotations according to maximum shear stress and maximum shear strain-rate.

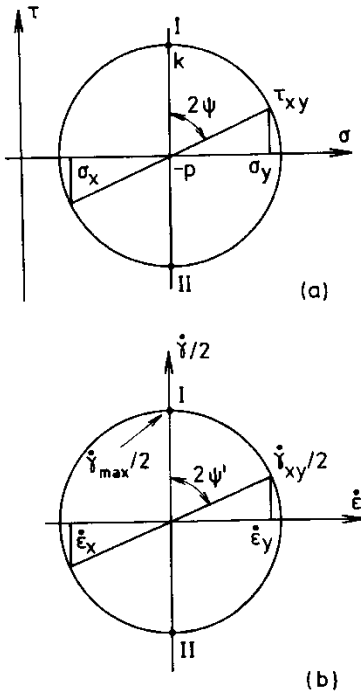


Figure 10: Mohr's circles for plane strain conditions: (a) stress circle; (b) strain-rate circle[2].

In terms of stress and strain rate components,

$$\tan(2\psi) = \frac{(\sigma_y - \sigma_x)}{2\tau_{xy}} \quad (16)$$

$$\tan(2\psi') = \frac{(\dot{\epsilon}_y - \dot{\epsilon}_x)}{\dot{\gamma}_{xy}} \quad (17)$$

The equations are equivalent according to the isotropic condition,

$$\frac{(\sigma_y - \sigma_x)}{2\tau_{xy}} = \frac{(\dot{\epsilon}_y - \dot{\epsilon}_x)}{\dot{\gamma}_{xy}} = \frac{\left(\frac{\partial V_y}{\partial y} - \frac{\partial V_x}{\partial x}\right)}{\left(\frac{\partial V_y}{\partial x} + \frac{\partial V_x}{\partial y}\right)} \quad (18)$$

which is the equation for the isotropic condition.

Metal Cutting Models

The yield criterion, equilibrium equations, constant volume condition and the isotropic condition in terms of σ_x , σ_y , τ_{xy} , V_x and V_y represent the basis for the solution of plane strain plasticity problems.

Before discussing the calculation procedure of the metal cutting process, it is beneficial to describe the models on which the calculation routine is based. These models include the shear plane model, parallel sided shear plane theory and the Johnson Cook constitutive equation. Note that the shear plane models will include elements of plane strain slipline field theory.

Slipline Field Theory

Slipline field theory is used to describe the stress environment of the 'chip formation zone' in the workpiece that is undergoing plastic deformation. This zone is located where the workpiece is being deformed into a chip. Sliplines consist of a set of two types of lines that intersect orthogonally.

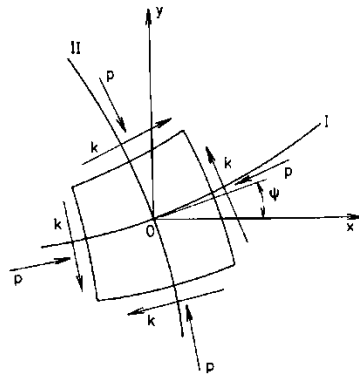


Figure 11: Curvilinear element bounded by sliplines showing stresses acting on sliplines[2].

These lines coincide with the directions of maximum shear stress and maximum shear strain rate. The shear stress on the sliplines is k and the normal stress on the sliplines is p , which is the mean stress. In this model, p is defined as,

$$p = -\frac{1}{2}(\sigma_x + \sigma_y) \quad (19)$$

A state of stress at a point on a slipline is completely defined by k and p .

σ_x , σ_y and τ_{xy} can be expressed in terms of p and k with the aid of the appropriate Mohr circle diagram and the following transformation equations can be expressed,

$$\sigma_x = -p - k \sin(2\psi) \quad (20)$$

$$\sigma_y = -p + k \sin(2\psi) \quad (21)$$

$$\tau_{xy} = k \cos(2\psi) \quad (22)$$

When substituting these transformation equations into the equilibrium equations (9), (10) and noting that s_1 , s_2 are analogous to the x , y axes in the equilibrium equation, the slipline equations can be written as,

$$\frac{\partial p}{\partial s_1} + 2k \frac{\partial \psi}{\partial s_1} - \frac{\partial k}{\partial s_2} = 0 \quad \text{along a I line} \quad (23)$$

$$\frac{\partial p}{\partial s_2} - 2k \frac{\partial \psi}{\partial s_2} - \frac{\partial k}{\partial s_1} = 0 \quad \text{along a II line} \quad (24)$$

The slipline equations can be interpreted as a manifestation of a force equilibrium in a deformed region that nonetheless allows summing of forces along curved lines.

The Shear Plane Model

The shear plane model is used to describe the process of 'steady state' chip formation in the metal cutting process where workpiece is modeled as perfectly plastic material. This allows for a velocity discontinuity at the shear plane which is contrary to experimental observations[1]. However, this model provides a correct description of the interaction of forces between the workpiece and the tool, see Figure 12. This model also describes the velocities and geometry correctly. The Parallel sided shear plane theory is an improvement on the basic shear plane model. This newer theory approximates the plastic deformation as a process that occurs in a spatial zone in the vicinity of the shear plane, rather than along a two dimensional shear plane. In this 'shear zone', workpiece velocity changes into chip velocity along smooth, geometrically identical lines, see Figure 8. In this way, the parallel sided shear plane theory is superior to the shear plane model. However, in some aspects the two models are identical. The calculation routine that is used to predict the outcomes of the metal cutting process uses elements of the simpler shear plane model but replaces outdated assumptions with newer assumptions that better fit experimental results.

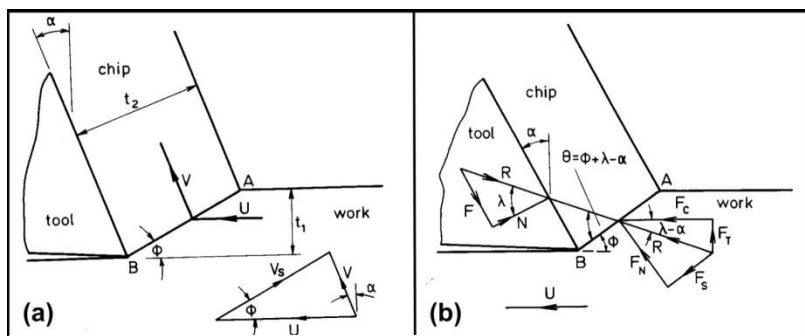


Figure 12: (a) The shear plane model. (b). forces associated with the shear plane model.

The workpiece is fed into the tool at a depth of t_1 with a cutting velocity U. The result is a continuous chip of thickness t_2 that is formed by plastic deformation along a 'shear plane' AB from the tip of the tool cutting edge to the surface of the workpiece. The position of the shear plane is defined by angle ϕ . The workpiece material is theorized to enter the shear plane AB with cutting velocity U and exit with a new chip velocity V. Because the shear plane has no thickness, this model states that there is a velocity discontinuity tangent to the shear plane denoted as V_s . This discontinuity creates a direction of maximum strain along the shear plane AB. This early model was used to describe the behavior of workpiece materials that were approximated as perfectly plastic. The workpiece is assumed to have no strain hardening behavior. Experimental observations [1] show that this approximation does not provide an accurate geometrical representation of the shear zone and predictions based on this model do not agree with experimental results. Specifically, this model fails to predict the correct value of the shear plane angle, which is descriptive of the entire process. However, useful relationships can be derived from this original model. The description of forces associated with the shear plane model was correct,

$$R = \frac{F_s}{\cos(\theta)} = \frac{k_{AB} L w}{\cos(\theta)} = \frac{k_{AB} t_1 w}{(\sin(\phi) \cos(\theta))} \quad (25)$$

$$F_c = R \cos(\lambda - \alpha) \quad (26)$$

$$F_t = R \sin(\lambda - \alpha) \quad (27)$$

$$F = R \sin(\lambda) \quad (28)$$

$$N = R \cos(\lambda) \quad (29)$$

where R , F_C , F_T , F_S , N , α , θ , λ and ϕ are described in fig.8. w is the width of the tool. L is the length of the shear plane. T_1 is the feed of the cutting process.

The relationships between the velocities are also valid and used in the metal cutting analysis.

$$v = \frac{U \sin(\phi)}{\cos(\phi - \alpha)} \quad \text{chip velocity} \quad (30)$$

$$v_s = \frac{U \cos(\alpha)}{\cos(\phi - \alpha)} \quad \text{velocity of the shear discontinuity} \quad (31)$$

$$v_n = U \sin(\phi) \quad \text{velocity normal to the shear plane} \quad (32)$$

These relationships are included in the improved shear plane theory, which is very similar to the shear plane model except to the way that the shear plane angle is calculated.

The Parallel Sided Shear Plane Model

The shear plane model is an updated version of the original shear plane model, based on observations from experiment[1]. Observations of experimental flow fields in the chip formation zone (13) show that the deformation process is not instantaneous at the shear plane. Rather, the deformation is a gradual process involving continuous changes in velocity and smooth streamlines. Instead of a shear plane, the plastic deformation is said to occur within a shear zone. This is because the workpiece exhibits strain hardening behavior. The parallel sided shear zone theory attempts to account for this strain hardening behavior of the workpiece by approximating the curved boundaries of the observed chip formation zone as if the zone were bounded by parallel planes CD and EF to form a shear zone of uniform thickness Δs_2 .

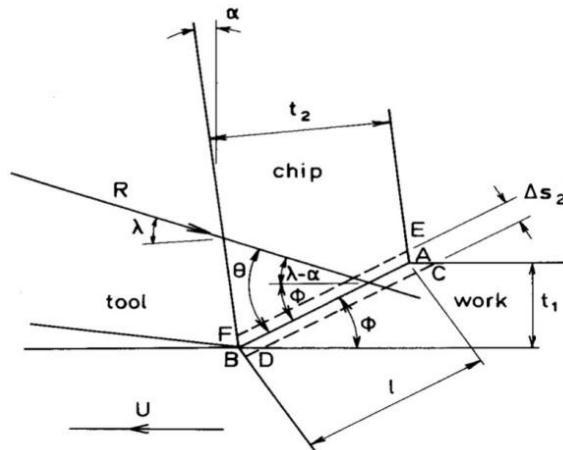


Figure 13: The shear plane model (9).

The parallel sided shear plane model does a better job describing the chip formation zone. However, many relationships from the earlier shear plane model are still functional and have remained a part of the model used in this study to predict the parameters of the metal cutting process.

The Johnson Cook Constitutive Model for Flow Stress

In order to calculate flow stress, the Johnson Cook constitutive model for flow stress was used in this study of the metal cutting process. In Oxley's original calculation scheme, the flow stress in the workpiece is calculated using data from an experiment using a 'velocity modified temperature' equation. These flow stress equations were specific to carbon steels. Because it was desirable to model a variety of workpiece materials, the use of a 'velocity modified temperature' method was replaced with the Johnson Cook constitutive equation to estimate Von Mises flow stress. This relationship was originally developed in 1983 by Johnson and Cook specifically to be used in

computations done by computer programs of the period. Although other models existed that gave better results, they were not as readily incorporated into the computer programs at that time. Rather a ‘dynamic flow stress’ that was readily calculated from strain, strain-rate and temperature was more often used and it is this parameter that Johnson and Cook studied for various metals as a function of strain, strain rate and temperature. At present, the Johnson Cook parameters for a variety of materials are known, allowing a comparison of different metals regarding metal cutting performance assuming that the concept of ‘dynamic flow stress’ is still relevant.

DESCRIPTION OF THE METAL CUTTING PROCESS CALCULATION

The Calculation Routine

A calculation routine was employed to predict the outcome of the metal cutting process as defined by the shear plane model. This routine is described by Oxley[2]. The calculation routine was broken up into component modules. Each module describes a major step in the analysis along with any other conclusions that can be made as a result of said calculation step. Figure 14 shows the description of each module, the order in which the modules are calculated and the outputs corresponding to each model.

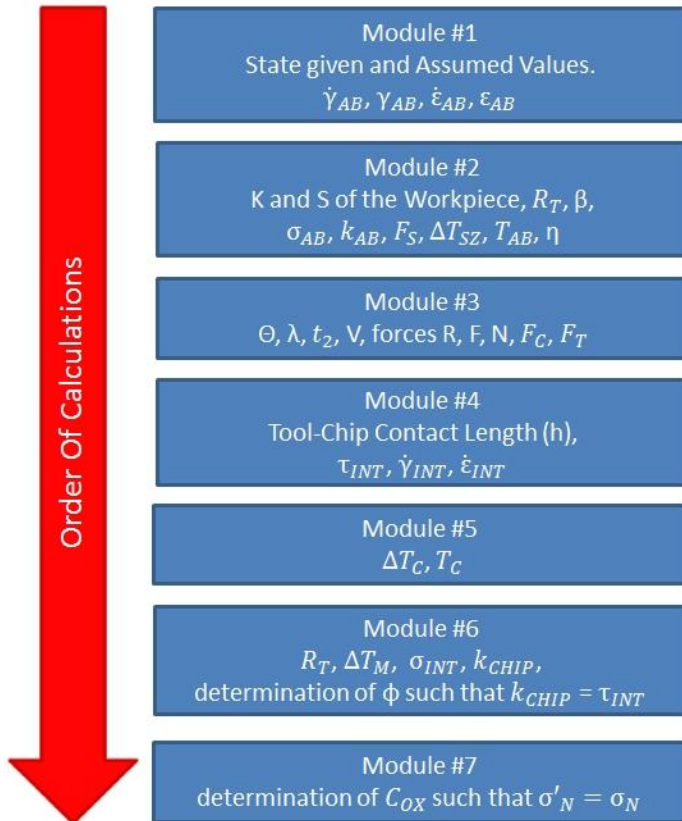


Figure 14: Flow chart of calculation routine.

Module #1

To begin with, several parameters may be defined as constants of the problem. In order to describe the constitutive response of the workpiece, constitutive material parameters must be known for every workpiece material under study.

Table 1: Johnson Cook parameters.

Johnson Cook parameters			$\sigma(\varepsilon, \dot{\varepsilon}, T) = [A + B\varepsilon^n] * [1 + C \ln(\varepsilon/\varepsilon_{ref})] * [1 - (T/T_m)^m]$					
material	Density (kg/m^3)	melting temperature (K)	A	B	n	C	m	ε_{ref}
OFE copper	8960	1356	90	292	0.310	0.0250	1.09	1
1006 steel	7890	1811	350	275	0.360	0.0220	1.00	1
6Al-4V Titanium	4428	1878	1098	1092	0.930	0.0140	1.10	1
2024-T3 aluminum	2770	775	265	426	0.340	0.0150	1.00	1

The Johnson-Cook (JC) model is defined as,

$$\sigma(\varepsilon, \dot{\varepsilon}, T) = A + B\varepsilon^n (1 + C \ln(\varepsilon/\varepsilon_0)) (1 - (T/T_m)^m) \quad (33)$$

where A, B, C, m and n are constants of the JC model. T_m is the melting point of the workpiece. ε_0 is the strain rate reference number which is taken as equal to one. The JC model is used to evaluate the flow stresses of the cutting process at locations where strain, strain-rate and temperature can be assessed. The parameters of this constitutive model are listed below. Constitutive properties of OFE copper and 1006 steel are from the original article describing the (JC) model[14]. Constitutive parameters of 6Al-4V Titanium and 2024-T3 aluminum are from a recent study sponsored by the Federal Aviation Administration[15]. Density and melting temperature are quoted along with the JC parameters.

In addition to these material properties, the cutting process as defined by the shear plane model must be specified by providing the rake angle α , cutting velocity V_C , feed t_1 , tool width w and the initial temperature of the work T_w . For this study, the tool rake angle was taken as 5° . Tool width is taken as 4mm. The initial temperature of the work piece was assumed to be $22^\circ C$. Results of this analysis are in terms of cutting velocity and feed. For each metal under study the tool forces, process temperatures and geometric configuration for feeds ranging from 0.01mm to 2mm and for cutting velocities ranging from 50 to 300 m/min. Preliminary calculations can be performed based on these given or assumed parameters. Shear plane length L_{AB} , shear velocity at the shear plane V_s and the velocity normal to the shear plane V_N , see Figure 15.

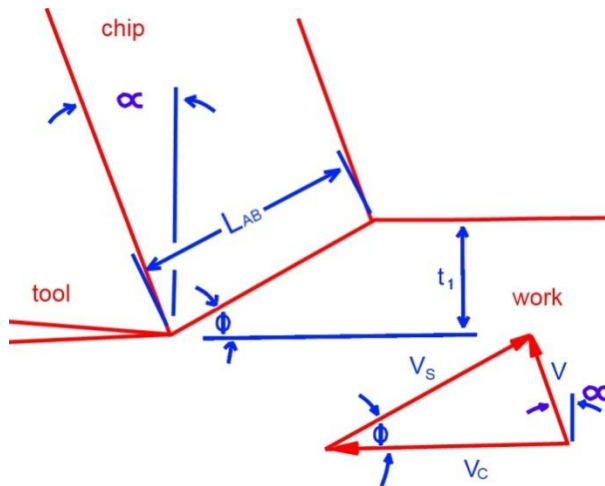


Figure 15: The shear plane model showing relevant parameters for preliminary calculations.

$$L_{AB} = t_1 / \sin \phi \quad (33)$$

$$V_s = V_C \cos(\alpha) / \cos(\phi - \alpha) \quad (34)$$

$$V_N = V_C \sin(\phi) \quad (35)$$

Note that V is the chip velocity as it moves along the tool surface.

A strain rate parameter C_{OX} and a shear plane angle ϕ will be assumed initially and then optimized to the correct value in an iterative fashion. The details of this optimization will be discussed at the end of this section. Other assumptions will be made as the analysis progresses; however these are the initial parameters and assumptions necessary to begin the analysis.

Shear strain rate γ_{AB} at the shear plane is found from an empirical relationship established by Stevenson and Oxley[1]. In this work, the flow field of a metal cutting process is preserved at an instant in time using an ‘explosive quick-stop’ device. Distortions of a ‘checkerboard’ pattern etched onto the workpiece are measured. From these measurements the maximum strain rate at the shear plane is derived for a variety of cutting velocities and feeds. The parameter C_{OX} relates γ_{AB} to the calculated shear velocity V_S and shear plane length L_{AB} . The value of C_{OX} is specific for a particular material.

Orthogonal machining experiments using an explosive quick stop device were performed to determine the influence of cutting speed and feed on the size of the chip formation zone and strain rates within the zone. Figure 16 shows a layout of the ‘turning’ type metal cutting experiment, including a detail of the specimen disc and orientation of the grid area.

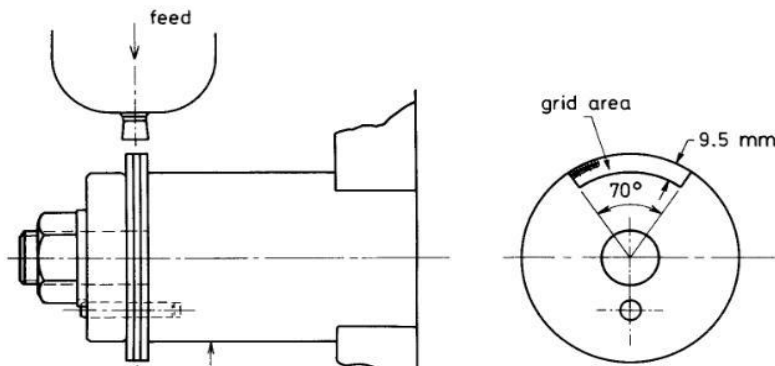


Figure 16: Layout of the orthogonal machining experiment used by Stevenson and Oxley (11).

Evidence of the shear strain rate distribution in the shear zone was recorded in the distortion of an etched copper checkerboard pattern on the side of the workpiece. Figure 17 shows a tracing of the observed chip formation zone indicating how the grid pattern records the distortion in the zone.

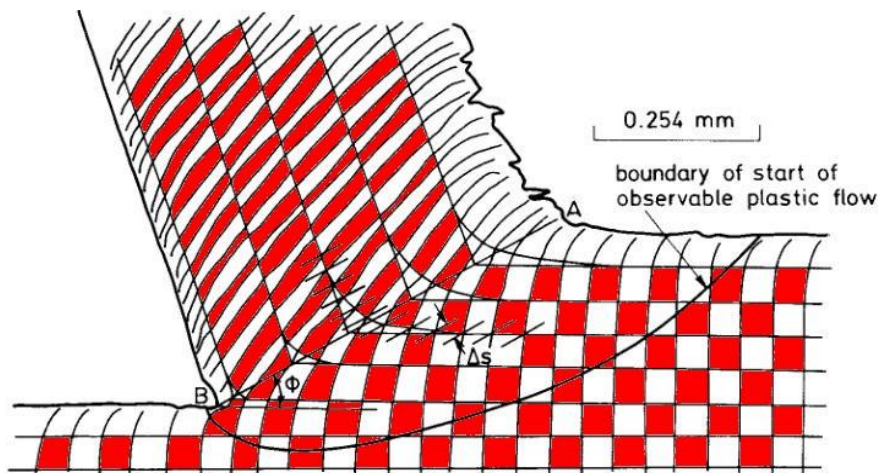


Figure 17: A typical observation of plastic deformation in the shear zone from experiments conducted by Stevenson and Oxley.

Shear strain rate was measured along parallel planes at varying distances from the classical location shear plane AB. This experiment was done for a range of feeds and speeds. From these observations, shear strain rate was calculated at the shear plane AB.

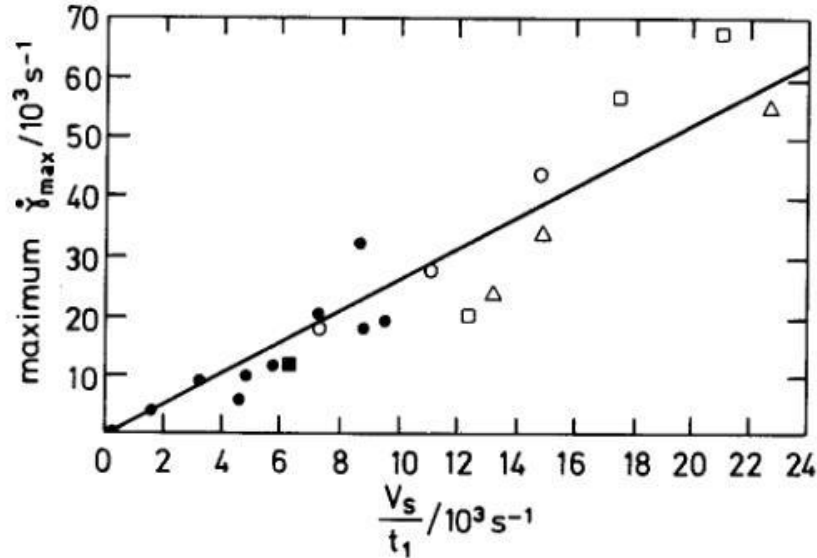


Figure 18: Shear strain-rate as a function of shear plane velocity and feed.

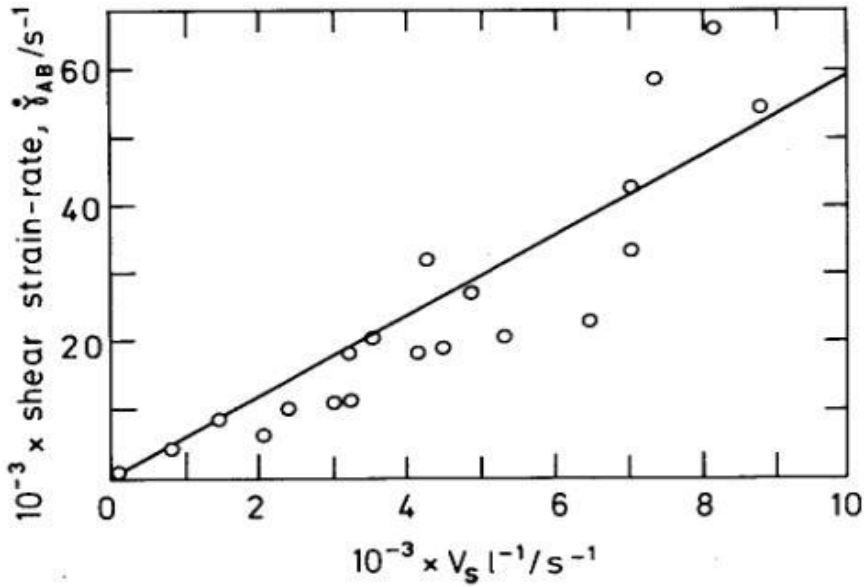
From this data a linear relationship was established between γ_{AB} , velocity of the shear plane and feed. The slope of this line is the value C_{OX} . In this way the experimental value of γ_{AB} for a given set of feed and cutting speed is given by,

$$\gamma_{AB} = C_{OX} V_s / t_1 \quad (36)$$

In later experiments, Stevenson and Oxley [16] used the expression,

$$\gamma_{AB} = C_{OX} V_s / L_{AB} \quad (37)$$

The expression uses L_{AB} rather than t_1 to estimate γ_{AB} because it was found to predict ϕ more accurately. Figure 19 shows a plot of experimental data modeled as a factor of L_{AB} . Note that initially C_{OX} is an assumed value. The true value of C_{OX} is determined by means of an energy minimization assumption as will be discussed later in module #7 of the calculation process.



Shear strain at the shear plane is given by the magnitude of the velocity of the discontinuity divided by the magnitude of the component of the velocity normal to the discontinuity[2]. If the discontinuity is taken to be at the shear plane, then the velocity of the discontinuity is the shear plane velocity and the velocity normal to the discontinuity is simply called the velocity normal to the shear plane. Figure 20 shows the orientation of shear plane velocity with respect to the velocity normal to the shear plane.

$$\gamma_{AB} = V_S \cdot V_N \quad (38)$$

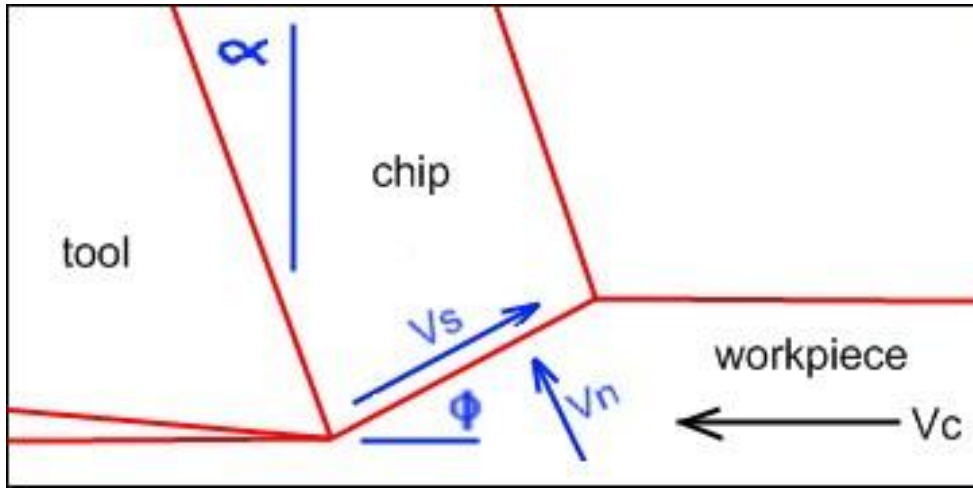


Figure 20: The shear plane model showing the relationship between the shear plane velocity (V_s) and the velocity component normal the the shear plane (V_n).

This expression of γ_{AB} is from the original shear plane model which states that all shear occurs upon the shear plane, resulting in a velocity discontinuity. This simplification results in an unrealistic situation that is contrary to experimental observations[2]. The parallel sided shear zone theory more realistically describes shear of the metal cutting process as occurring in a zone near the shear plane AB. According to the parallel sided shear zone theory, the shear zone is defined by planes CD, AB and EF.

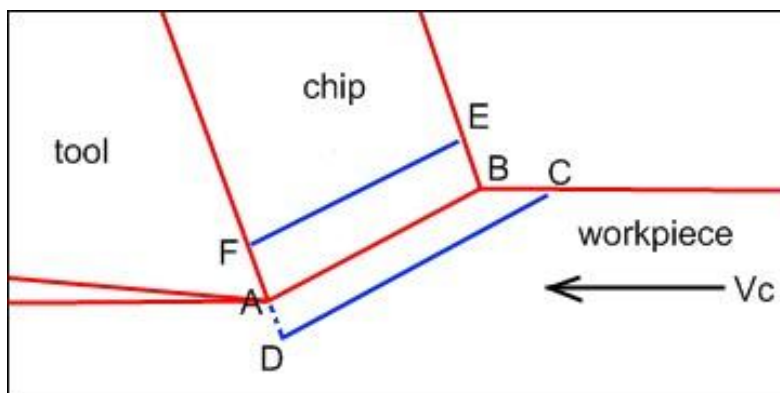


Figure 21: The parallel sided shear plane model. The chip formation zone is approximately bounded by planes CD and EF, which are parallel to the shear plane.

EF is assumed to be a slipline along which shear strain is constant. Shearing of the process is assumed to be zero at plane CD and a maximum at plane EF. At AB the workpiece is assumed to have undergone approximately half of the total strain in the process of chip formation. The parallel sided shear zone theory is in better agreement with experimental observations[1]. Therefore, γ_{AB} can be more realistically calculated by,

$$\gamma_{AB} = \frac{1}{2} V_S V_N \quad (39)$$

Effective strain-rate is defined as,

$$\dot{\varepsilon}_{eff} = \frac{\sqrt{2}}{3} [(\dot{\varepsilon}_1 - \dot{\varepsilon}_2)^2 + (\dot{\varepsilon}_2 - \dot{\varepsilon}_3)^2 + (\dot{\varepsilon}_3 - \dot{\varepsilon}_1)^2]^{\frac{1}{2}} \quad (40)$$

Assuming a state of uni-axial stress, the normal strain and normal strain rate at the shear plane can be calculated.

Noting that the principal strains are defined as,

$$\varepsilon_{1,2} = \varepsilon_{AB} = \frac{\varepsilon_x + \varepsilon_y}{2} \pm \sqrt{-\frac{\varepsilon_x - \varepsilon_y}{2}^2 + \varepsilon_{xy}^2} = \varepsilon_3 \pm \frac{\gamma_{MAX}}{2} = \varepsilon_3 \pm \frac{\gamma_{AB}}{2} \quad (41)$$

ε_{AB} can be expressed in terms of γ_{AB} ,

$$\dot{\varepsilon}_{AB} = \frac{\dot{\gamma}_{AB}}{\sqrt{3}} \quad (42)$$

Similarly, ε_{AB} can be expressed in terms of γ_{AB} ,

$$\varepsilon_{AB} = \frac{\gamma_{AB}}{\sqrt{3}} \quad (43)$$

Module #2

Thermal conductivity and specific heat for the materials as functions of temperature were necessary for the steps involving temperature calculation. Although thermal conductivity and specific can be approximated as constants of the material, it is possible that the temperatures involved in the metal cutting process could be very high, requiring thermal properties to be calculated at the temperature required. Further, since thermal data exists for a number of engineering materials, it is a simple task to evaluate the workpiece thermal properties as a function of process temperatures. The formulas for copper and steel were used as referenced[2],[17]. The formulas for 2024 aluminum and 6Al-4V titanium were taken from[18]. Original data for the behavior of Ti and Al were ‘digitized’ from the original published graphs and fit to a polynomial equation. Shown in Figure 22 is a graph of thermal conductivity as a function of temperature for the workpiece materials under study. The thermal conductivity equations for the alloys under study are,

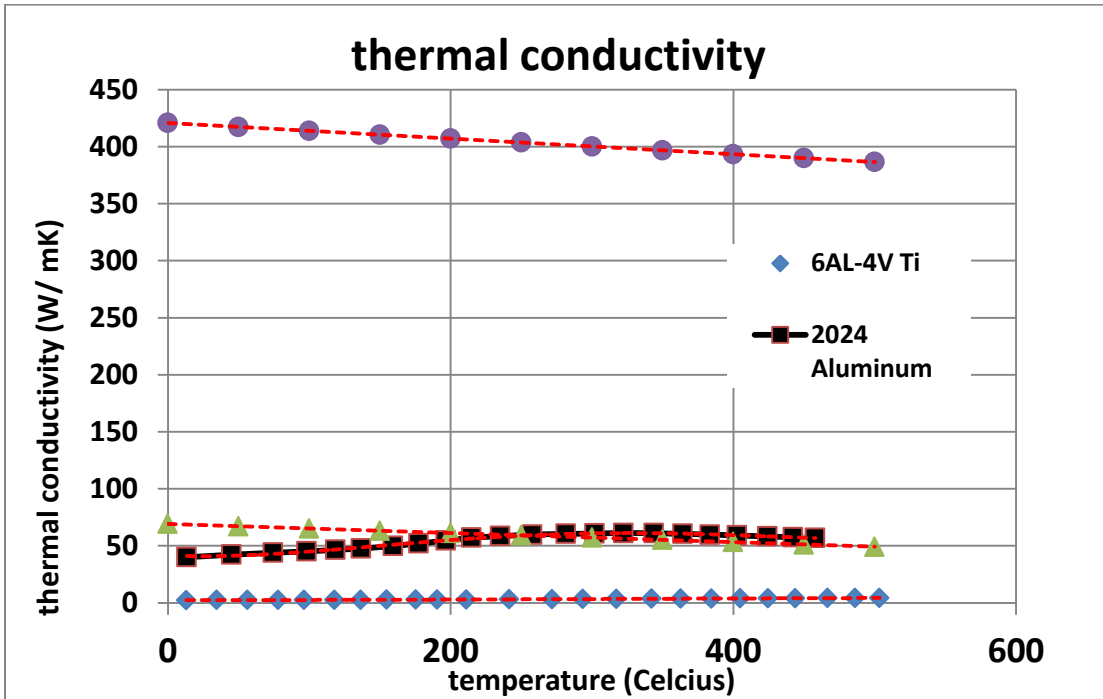


Figure 22: Thermal conductivity as a function of temperature for the workpiece materials under study.

$$K_{Cu} = -0.068 T + 420.750 \text{ W/mK} \quad (44)$$

$$K_{STEEL} = -0.040 T + 69.239 \text{ W/mK} \quad (45)$$

$$K_{Al} = 0.0000000032 T^4 - 0.0000036980 T^3 + 0.0012165603 T^2 - 0.0533275400 T + 41.5756570469 \text{ W/mK} \quad (46)$$

$$K_{Ti} = -0.0000000130 T^3 + 0.0000134430 T^2 + 0.0003659000 T + 2.4068608526 \text{ W/mK} \quad (47)$$

The specific heat equations for the alloys under study are graphed in Figure 23 and corresponding equations are displayed below.

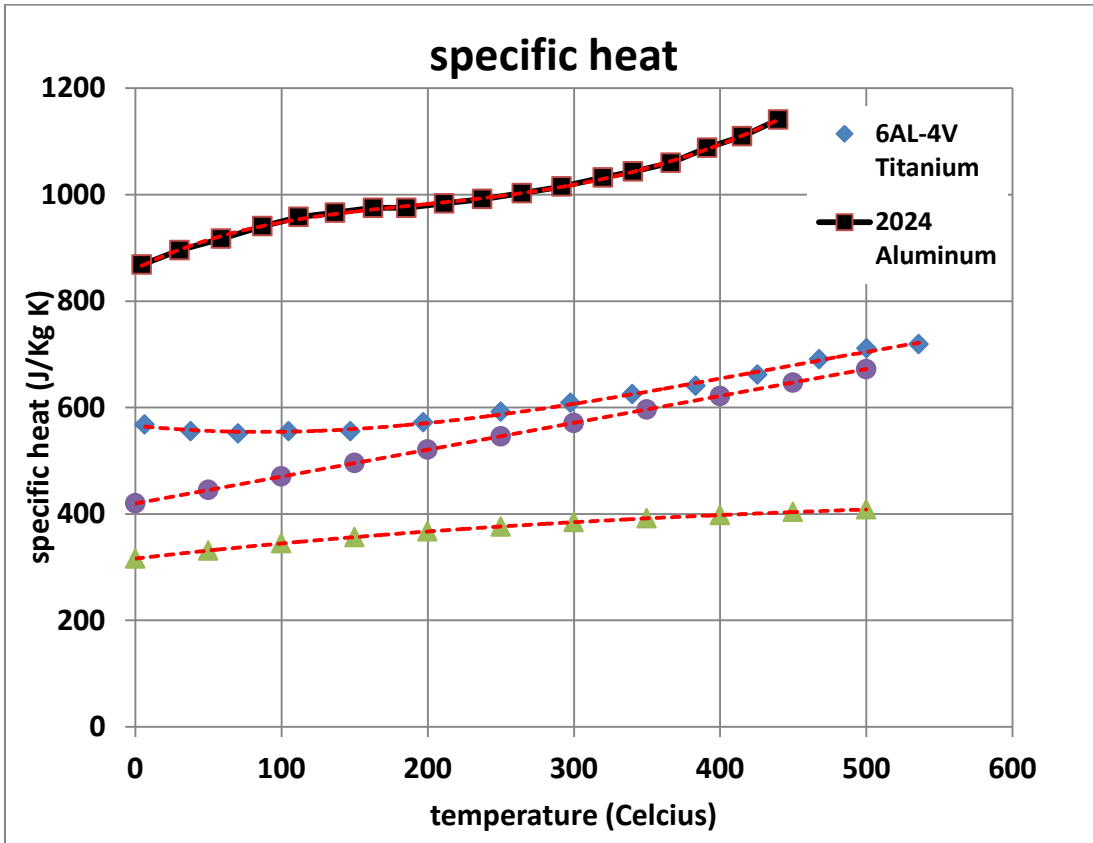


Figure 23: Specific heat as a function of temperatures for the workpiece materials under study.

$$s_{Cu} = 0.0000001660 T^3 - 0.0003493600 T^2 + 0.3177000000 T + 316.2100000000 \text{ J/KgK} \quad (48)$$

$$s_{steel} = 0.504 T + 420.000 \text{ J/Kg K} \quad (49)$$

$$s_{Al} = -0.0000013992 T^3 + 0.0018210211 T^2 - 0.2836376890 T + 565.9713904505 \text{ J/Kg K} \quad (50)$$

$$s_{Ti} = -0.0000000071 T^4 + 0.0000134133 T^3 - 0.0061882742 T^2 + 1.3678173719 T + 860.6021438354 \text{ J/Kg K} \quad (51)$$

With these expressions, the thermal properties of the workpiece can be calculated at the shear plane AB and at the tool-chip interface, which are at different temperatures.

R_T is referred to as the 'dimensionless thermal number',

$$R_T = \frac{\rho S U t_1}{K} \quad (52)$$

R_T combines relevant material properties and process parameters to describe how well heat can be conducted into the workpiece, for a given metal and cutting speed and feed.

Beta is defined as the fraction of the plastic work done in the shear zone that is converted into heat[2]. Note that beta is a function of R_T and ϕ , the shear plane angle, (52).

Various attempts have been made to determine beta theoretically and experimentally. The most widely accepted and used method for estimating β are based on experimental observations[19],[20]. Note that although these experiments involved carbon steel and brass only, it is reasonable to assume that the relationship will hold for other metals, since beta is in terms of the thermal number. The thermal number is a factor of density, specific heat and thermal conductivity and it is reasonable to assume that β will scale according to these basic material parameters, see Figure 24.

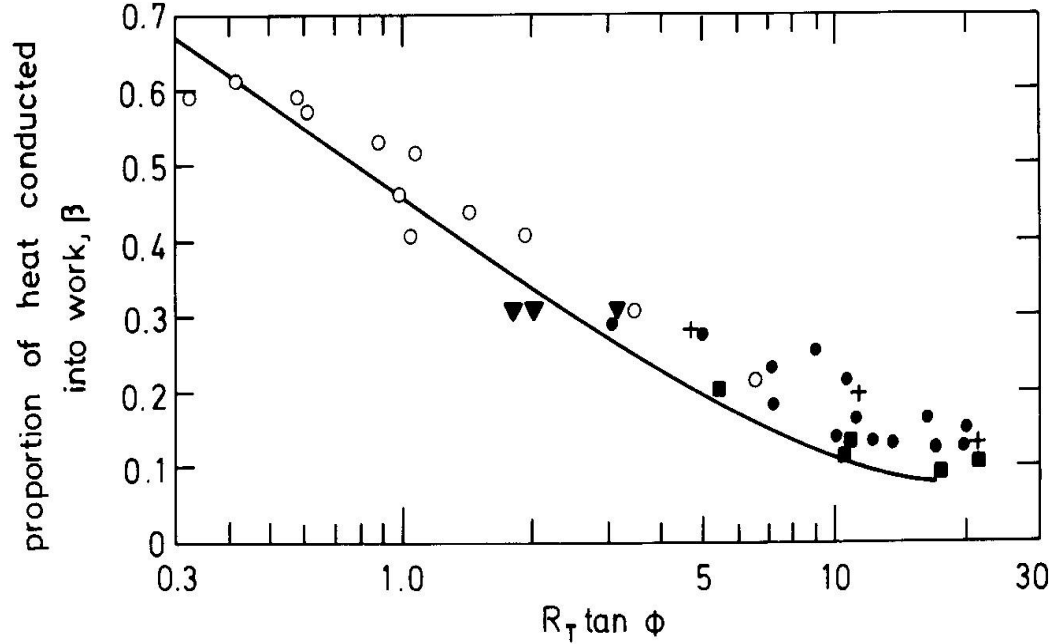


Figure 24: Theoretical and experimental results for beta: line represents Weiner's theoretical results; open circle represents Nakayama's experimental results; closed triangle, closed square and closed circle represent boothroyd's results, '+' symbol represents results calclated by Tay et al. using finite element method[2].

The following empirical equation is a result of a linear fit of the linearized data from Figure 24,

$$\beta = 0.5 - 0.35 \log(R_T \tan \phi) \quad \text{for } 0.04 \leq R_T \tan \phi \quad (53)$$

$$\beta = 0.3 - 0.15 \log(R_T \tan \phi) \quad \text{for } R_T \tan \phi > 10.0 \quad (54)$$

The method of calculating the average temperature rise in the shear zone is involves the consideration of the plastic work done in the shear zone. The average enthalpy of the material leaving the shear zone is given by[20],

$$H_{SZ} = \frac{1 - \beta}{\rho V t_2 w} q_s \quad (55)$$

where q_s is defined as the heat generated in the shear zone. Given that,

$$t_2 = \frac{t_1 \cos(\phi - \alpha)}{\sin \phi} \quad (56)$$

$$V = \frac{U \sin \phi}{\cos(\phi - \alpha)} \quad (57)$$

$$q_S = \frac{F_S U \cos \alpha}{\cos(\phi - \alpha)} \quad (58)$$

enthalpy of the shear zone can be expressed in terms of physical machining parameters β , ϕ , α , t_1 , w and F_S ,

$$H_{SZ} = \frac{1 - \beta}{\rho w t_1} \frac{F_S \cos \alpha}{\cos(\phi - \alpha)} \quad (59)$$

If enthalpy can be redefined as,

$$H_{SZ} = \Delta T_{SZ} S \quad (60)$$

then the temperature rise in the shear zone can be expressed as,

$$\Delta T_{SZ} = \frac{1 - \beta}{\rho w t_1} \frac{F_S \cos \alpha}{\cos(\phi - \alpha)} \quad (61)$$

The average temperature along AB is then,

$$T_{AB} = T_W + \eta \Delta T_{SZ} \quad (62)$$

Note that η is a factor ($0 \leq \eta \leq 1$) which accounts for the situation where not all of the plastic work of chip formation that occurs in the plastic zone will occur at the shear plane AB. In the calculation routine, η is given the value of one since experiments or analytical arguments to estimate η have not been attempted as of yet.

Using the Von Mises criteria (41) shear stress at the shear plane, k_{AB} is defined as,

$$k_{AB} = \sigma_{AB} \quad \frac{1}{3} \quad (63)$$

where sigma is the one dimensional flow stress as defined by the Johnson Cook constitutive model. In addition, the force normal to the shear plane, F_S can be calculated,

$$F_S = \frac{k_{AB}}{L_{AB}w} \quad (64)$$

Module #3

θ is the angle made by the resultant force R with the shear plane AB. In the calculation routine theta, along with an assumed value of ϕ , is used in determining R, the resultant force of the tool on the work and vice versa. The determination of θ is based on the parallel sided shear zone theory.

Temperature variations are neglected along AB and shear stress is assumed constant at the shear plane. Further, AB is approximated as a straight line, which simplifies the corresponding I slipline equation for the shear plane AB,

$$\partial p = \frac{\partial k}{\partial s_2} \partial s_1 \quad (65)$$

which can be replaced with the finite difference version,

$$\Delta p = \frac{\Delta k}{\Delta s_2} \Delta s_1 \quad (66)$$

Noting that,

$$\frac{\Delta k}{\Delta s_2} = (k_{EF} - k_{CD}) \Delta s_1 \quad (67)$$

$$\Delta p = p_A - p_B \quad (68)$$

$$\Delta s_1 = L_{AB} \quad (69)$$

the slipline equation can then be written as,

$$p_A - p_B = (k_{EF} - k_{CD}) \Delta s_2 L_{AB} \quad (70)$$

With this form of the I slipline equation applied to AB, p_B can be written in terms of p_A ,

$$p_B = p_A - (k_{EF} - k_{CD})\Delta s_2 L_{AB} \quad (71)$$

Normal force and shear force on the shear plane AB are given by,

$$F_N = \text{average stress}_{AB} * \text{area}_{AB} = \frac{(p_A + p_B)}{2} L_{AB} w \quad (72)$$

$$F_S = \text{shear stress}_{AB} * \text{area}_{AB} = k_{AB} L_{AB} w \quad (73)$$

Then, a relationship for theta can be written,

$$\tan\theta = \frac{F_N}{F_S} = \frac{(p_A - p_B) 2 k_{AB}}{(p_A + p_B)} \quad (74)$$

Substituting p_B in terms of p_A ,

$$\tan\theta = \frac{p_A}{k_{AB}} - \frac{k_{EF} - k_{CD}}{\Delta s_2} \frac{L_{AB}}{2 k_{AB}} \quad (75)$$

The theta equation can be further simplified by considering the state of stress at point A, which is on the free surface of the workpiece. At the free surface, normal stress and shear stress are zero, as visualized by the appropriate Mohr circle diagram, see Figure 25.

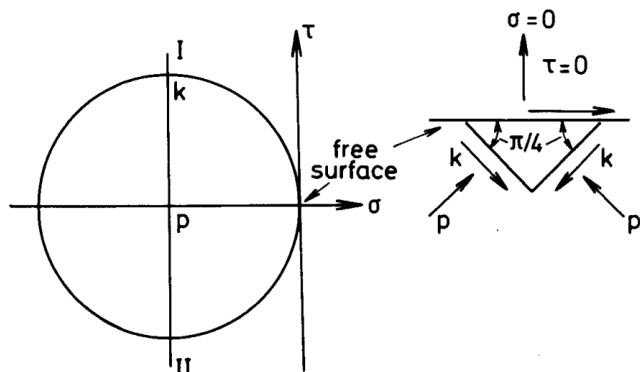


Figure 25

Figure 25: Mohr's stress circle and slipline field element showing stress-free surface condition[2].

This stress condition at the surface can only be satisfied if AB, which is a I slipline, meets the surface at a 45 degree angle. In fact, all splines must meet this condition at the surface. Note that there is no requirement that this rotation occur in a given distance. Hence, this rotation can occur in a very small, negligible distance. This requirement at the surface acts as a boundary condition at point A, where it is assumed that,

$$p = k_{AB} \quad (76)$$

$$\psi = \pi/4 - \phi \quad (77)$$

where ψ is the required rotation of the AB slipline to an orientation 45 degrees from the free surface.

Substituting p and ψ into the I slipline equation,

$$\frac{p_A}{k_{AB}} = 1 + 2 \pi/4 - \phi \quad (78)$$

To further simplify the expression for finding theta, $\Delta k / \Delta s_2$ can be redefined using experimental results [16] which improves on certain assumptions made in the original shear plane model. In general, shear stress is a function of strain, strain rate and temperature,

$$\frac{\partial k}{\partial s_2} = \frac{\partial k}{\partial \gamma} \frac{\partial \gamma}{\partial s_2} + \frac{\partial k}{\partial \gamma} \frac{\partial \gamma}{\partial s_2} + \frac{\partial k}{\partial T} \frac{\partial T}{\partial s_2} \quad (79)$$

At plane AB, the strain rate term vanishes, since the value of strain rate goes through a maximum at the shear plane. If temperature variations along the shear plane are neglected, k simplifies to a function of strain rate only,

$$\frac{\partial k}{\partial s_2} = \frac{\partial k}{\partial \gamma} \frac{\partial \gamma}{\partial t} \frac{\partial t}{\partial s_2} \quad (80)$$

The $\partial t / \partial s_2$ term is the inverse of the cutting velocity normal to the shear plane,

$$\frac{\partial t}{\partial s_2} = 1 \quad U \sin\phi \quad (81)$$

The $\frac{\partial \gamma}{\partial t}$ term is equal to γ_{AB} and can be defined as,

$$\gamma_{AB} = C_{OX} V_S L_{AB} = C_{OX} L_{AB} U \cos\alpha \cos(\phi - \alpha) \quad (82)$$

with V_S as the velocity of the shear plane in the direction of maximum strain rate.

Approximating the workpiece as a power law strain hardening material,

$$\sigma_{FLOW} = \sigma \varepsilon^n \quad (83)$$

then at the shear plane AB,

$$\frac{\partial \sigma}{\partial \varepsilon} = n \sigma_{AB} \varepsilon_{AB} \quad (84)$$

$$\frac{\partial k}{\partial \gamma} = n k_{AB} \gamma_{AB} \quad (85)$$

Considering the redefinition of these three terms, $\frac{\partial k}{\partial s_2}$ can be redefined as,

$$\frac{\partial k}{\partial s_2} = \frac{\partial k}{\partial \gamma} \frac{\partial \gamma}{\partial t} \frac{\partial t}{\partial s_2} = n k_{AB} \gamma_{AB} * U \cos\alpha C_{OX} L_{AB} \cos \phi - \alpha * 1 \quad U \sin\phi \quad (86)$$

Substituting in previously defined values,

$$\gamma_{AB} = \frac{1}{2} \frac{\cos\alpha}{\sin\phi \cos(\phi-\alpha)} \quad (87)$$

$$\frac{\partial k}{\partial s_2} = 2 C_{OX} n k_{AB} L_{AB} \quad (88)$$

Yields an expression that can be solved for θ ,

$$\tan\theta = 1 + 2 \pi/4 - \phi - C_{OX} n \quad (89)$$

Once θ is determined, several parameters according to the shear plane model may be calculated. Specifically, all the forces of the model, including the tool forces, may be determined.

λ , the angle between the tool face and the resultant force is,

$$\lambda = \theta + \alpha - \phi \quad (90)$$

At this point, a number of parameters of the shear plane can be solved for.

R the resultant force between the tool face and the shear plane is,

$$R = F_s / \cos(\theta) = k_{AB} L w / \cos(\theta) = k_{AB} t_1 w / (\sin(\phi) \cos(\theta)) \quad (91)$$

F_C and F_T are the tool cutting force and tool thrust force, respectively,

$$F_C = R \cos(\lambda - \alpha) \quad (92)$$

$$F_T = R \sin(\lambda - \alpha) \quad (93)$$

F, the friction force is,

$$F = R \sin(\lambda) \quad (94)$$

N, the force normal to the tool face is,

$$N = R \cos(\lambda) \quad (95)$$

t_2 is the chip thickness,

$$t_2 = t_1 \cos \phi - \alpha \sin \phi \quad (96)$$

V is the velocity of the chip along the tool face,

$$V = U \sin(\phi) / \cos(\phi - \alpha) \quad (97)$$

Module #4

Tool-chip contact length is the distance that the chip travels down the tool face while in a fully 'adhered' state. In this state, the chip and tool are interlocked; work material is forced up against the tool at such a pressure that the workpiece material is seen to penetrate all irregularities of the workpiece[11]. Calculation of the tool-contact length is

necessary to determine the value of shear stress and average temperature at the tool-chip interface. An expression for h was obtained in the following way[21]. Taking moments of the normal stress on AB about point B, it can be shown that the resultant force R intersects the tool chip interface at a distance x ,

$$x = \frac{2t_1 \sin \theta}{\cos \lambda \sin \phi} * \frac{\frac{1}{3}p_A + \frac{1}{6}p_B}{p_A + p_B} \quad (98)$$

Assuming that for a uniform distribution of normal stress at the interface, R intersects the tool face at a distance $x = h/2$ from point B, and given that p_A and p_B are defined as,

$$p_A = 2C_{ox}nk_{AB} + p_B \quad (99)$$

$$p_B = k_{AB} \left[1 + 2 \left(\frac{\pi}{2} - \theta \right) - 2C_{ox}n \right] \quad (100)$$

the tool-chip contact length can be established,

$$h = \frac{t_1 \sin \theta}{\cos \lambda \sin \phi} \left\{ 1 + \frac{C_{ox}n}{3 \left[1 + 2 \left(\frac{1}{4}\pi - \phi \right) - C_{ox}n \right]} \right\} \quad (101)$$

With a calculated value of h , shear force at the tool chip interface can be calculated as,

$$\tau_{INT} = \frac{F}{hw} \quad (102)$$

where F is the tool-chip friction force from the shear plane model and w is the width of the tool. Shear strain rate and normal strain rate at the interface is descriptive of a thin layer of high shear in the chip material that is closest to the tool. The thickness of this layer is described as a ratio of this high shear layer thickness to the thickness of the chip. This value is known as δ ; the shear thickness ratio. Shear strain rate at the interface is approximated as,

$$\dot{\gamma}_{INT} = \frac{v_{CHIP}}{\delta t_2} \quad (103)$$

And from the definition of effective strain in uniaxial conditions,

$$\dot{\varepsilon}_{INT} = \dot{\gamma}_{INT} / \sqrt{3} \quad (104)$$

For the purpose of calculating the flow stress at the interface, the normal strain is given a value of one. Machining results [16] show that above normal strains larger than one have little influence on the flow stress at the interface.

The relationship of shear strain rate at the interface assumes that the sliding velocity at the cutting face is zero, implying that seizure has occurred in the tool-chip contact region. This is consistent with experimental findings [11]. Examinations of the tool-chip interface using optical and electron microscopy reveal that the tool and chip are interlocked at the surface with adhering metal penetrating all irregularities of the tool surface. However, according to the steady state shear plane model, the chip must leave the interface region with a velocity equal to the chip velocity as previously calculated. The sliding velocity of the chip material cannot be zero everywhere, since even the chip material at the tool surface must eventually move away from the tool-chip contact region. It is reasonable to assume that the chip velocity at the tool surface may be estimated as the chip velocity, however in reality the chip material may be moving somewhat slower because of the nature of the tool-chip adhesion. Therefore the calculated value of $\dot{\gamma}_{INT}$ represents an upper bound on the shear strain rate at the interface.

Module #5

The temperature at the interface is assumed to be[2],

$$T_{INT} = T_W + \Delta T_{SZ} + \psi \Delta T_M \quad (105)$$

where ΔT_M is the maximum temperature rise within the chip at the interface. ψ is a factor which accounts for the variation in temperature along the interface. ΔT_M is calculated using numerical methods [20] to test several theoretical distributions of heat generation within the newly formed chip along the tool-chip interface. Specifically, a rectangular and a triangular heat generation zone were postulated, see Figure 26.

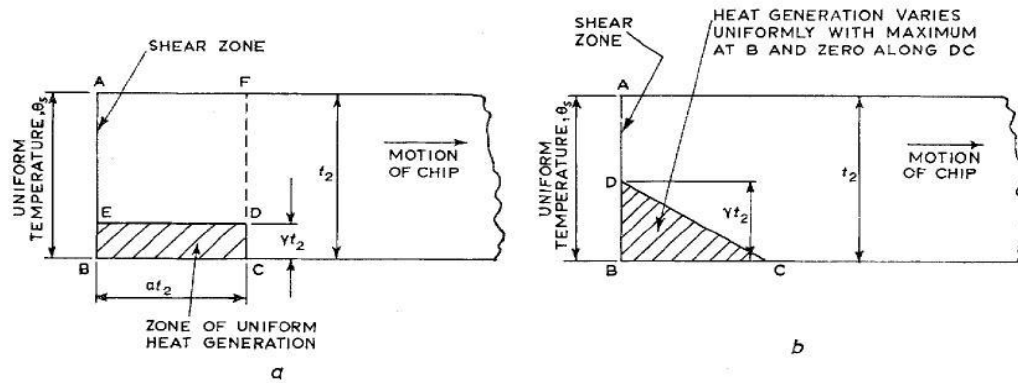


Figure 26: Heat Generation models considered in the numerical method used to evaluate the maximum temperature rise at the chip interface[1].

The results of this numerical simulation, when compared to experimental observations of the temperature distribution at the interface region, suggest that the triangular region of heat generation is the more realistic of the two models, see Figure 27.

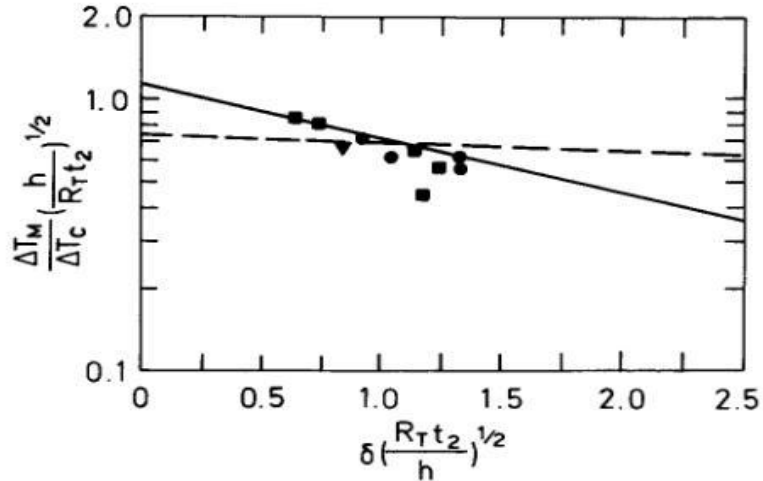


Figure 27: Calculated and experimental tool-chip interface results: full line represents numerical results assuming rectangular plastic zone and broken line represents numerical results assuming triangular plastic zone; symbols represent experimental results.

It is then shown that the relation of $\Delta T_M / \Delta T_C$ to the relevant material and process parameters could be expressed in equation form,

$$\log \frac{T_M}{T_C} = 0.06 - 0.195 \frac{1}{2} \delta R_T t_2 h + 0.5 \log R_T t_2 h \quad (106)$$

with,

$$T_C = \frac{F \sin \phi}{\rho S t_1 \cos(\phi - \alpha)} \quad (107)$$

T_C is calculated by considering the plastic work done in the chip adjacent to the tool chip interface[2].

Module #6

Shear Stress at the interface (τ_{INT}) is calculated by considering the friction force along the tool surface divided by the contact area between the tool and chip,

$$\tau_{INT} = \frac{F}{h w} \quad (108)$$

Shear stress in the chip (k_{CHIP}) is determined according to the definition of effective stress in uniaxial conditions,

$$k_{CHIP} = \frac{\sigma_{INT}}{3} \quad (109)$$

where σ_{INT} is the flow stress of the chip material at the tool-chip interface as calculated by the Johnson Cook constitutive equation. k_{CHIP} defined as the shear stress in the region of the chip that is in contact with the tool. In order to maintain a force equilibrium, k_{CHIP} must equal τ_{INT} . This equilibrium corresponds to the correct value of ϕ according to the shear plane model. To find the correct value of ϕ , the program initially assumes a low value of ϕ , performs all of the previously described calculations and determines if k_{CHIP} and τ_{INT} are equal. If so, the calculation proceeds to the next step. If not, the value of ϕ is increased by a predetermined increment and the calculations are repeated.

Module #7

The boundary condition at B, the tool tip, can be used to determine C_{OX} . This is especially helpful, since C_{OX} is an empirically derived parameter that is specific for a given alloy. An analytical derivation of C_{OX} within this calculation procedure, on the basis of a force balance, negates the experiments that would otherwise be required to define it. The I slipline equation can be simplified as previously mentioned,

$$\partial p = \frac{\partial k}{\partial s_2} \partial s_1 \quad (110)$$

Given from previous discussions,

$$\partial p = p_A - p_B \quad (111)$$

$$\frac{\partial k}{\partial s_2} = 2 C_{OX} n k_{AB} \quad (112)$$

$$\partial s_1 = L_{AB} \quad (113)$$

The slipline equation can be rewritten as,

$$p_A - p_B = 2 C_{OX} n k_{AB} L_{AB} \quad (114)$$

And, given that,

$$p_A = k_{AB} + 2 k_{AB} \frac{\pi}{4} + \phi \quad (115)$$

p_B can be expressed in terms of the normal stress and shear stress at point B if slipline AB meets the tool face without changing direction.

$$\sigma'_N = p_B + k_{AB} \sin 2(\phi - \alpha) \quad (116)$$

However, if the slipline AB meets the tool face at a 90 degree angle, then the expression simplifies to,

$$\sigma'_N = p_B + k_{AB} 2(\phi - \alpha) \quad (117)$$

Now, given the previous definition of p_B ,

$$p_B = k_{AB} 1 + 2 \frac{\pi}{2} - \theta - 2 C_{OX} n \quad (118)$$

the uniform normal stress on the tool face can be defined as,

$$\sigma'_N = k_{AB} 1 + \frac{\pi}{2} - 2\alpha - 2 C_{OX} n \quad (119)$$

But, the uniform normal stress on the tool face can alternatively be defined as,

$$\sigma_N = \frac{N}{h w} \quad (120)$$

By imposing the condition that $\sigma'_N = \sigma_N$ it is assumed that the normal stress at the shear plane, as defined by the slipline equations, must equal the average normal stress on the shear plane. In the calculation routine, the simulation starts the calculations at a low

value of C_{OX} , runs through the entire calculation procedure and evaluates the expression, $\sigma'_N = \sigma_N$. If the equality is not below 0.1%, the value of C_{OX} is incremented, the calculations are reinitiated with this new value until the error criteria is met.

Modifications to the Calculation Routine

Recall that δ , the shear thickness ratio, is defined as the thickness of the high shear region in the workpiece which lies up against the tool face in the tool-chip interface region. In the calculation routine outlined by Oxley, the determination of δ is found by use of an iterative calculation. The calculation procedure is performed for a range of δ values. The correct value of δ is assumed to be that which results in the lowest total work rate which also coincides with the lowest shear flow stress in the chip[2]. This method proved to be excessively time consuming and a faster way to determine δ was needed to perform the required simulations in a reasonable way. An alternative to finding δ by running the entire calculation process many times is to find δ as a function of V_c and t_1 . This would allow δ to be calculated as a function of initial, constant values. To achieve this, a number of calculations were carried out using the calculation routine as described to manually find the value of δ corresponding to the value of minimum work rate for a specific workpiece and a specific set of process parameters, see Figure 28. These process parameters include the rake angle, tool width, feed, and speed desired. The result is a function of delta as a function of feed and speed, but only for the process parameters so specified. Hundreds of plots were created to determine the relationship of total work rate

and delta as a function of feed and cutting speed. For brevity, they are not displayed in this work.

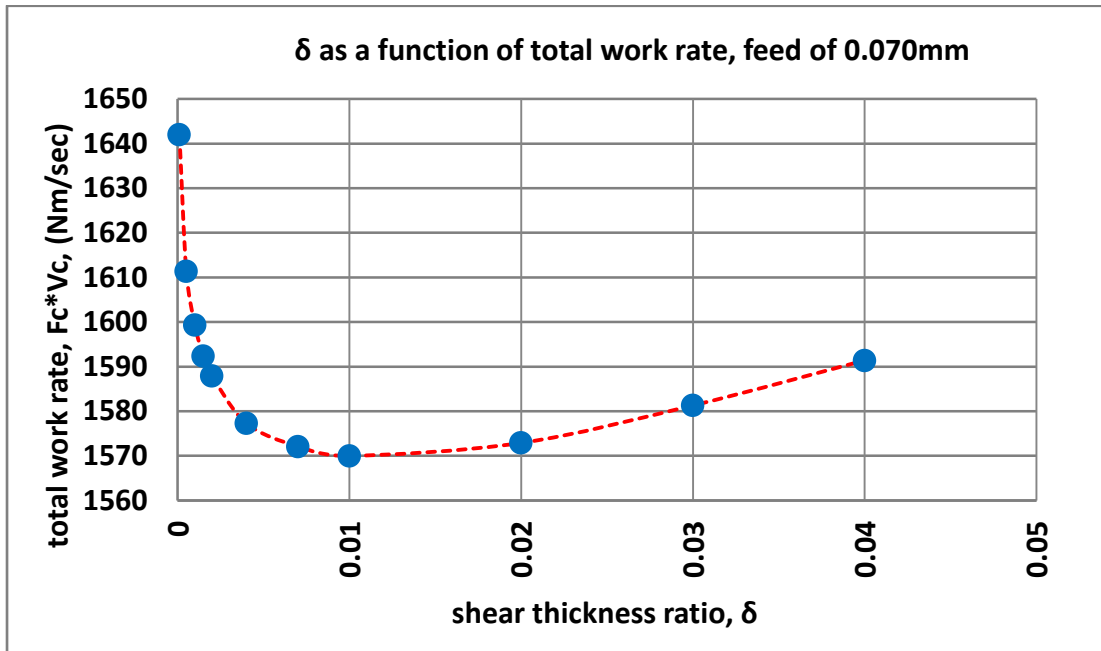


Figure 28: A sample plot of total work rate as a function of shear thickness ratio, with $\alpha = 5^\circ$, $w=3\text{mm}$, $t_1 = 0.07\text{mm}$, $V_C = 200 \text{ m/min}$.

In this way δ was found as a function of feed for cutting velocities of 50, 100, 200 and 300 m/min. As an example, see Figure 29 for an example plot relating δ as a function of feed and cutting speed with 1006 steel as the workpiece. Similar plots for the other workpieces under study can be found in the appendix.

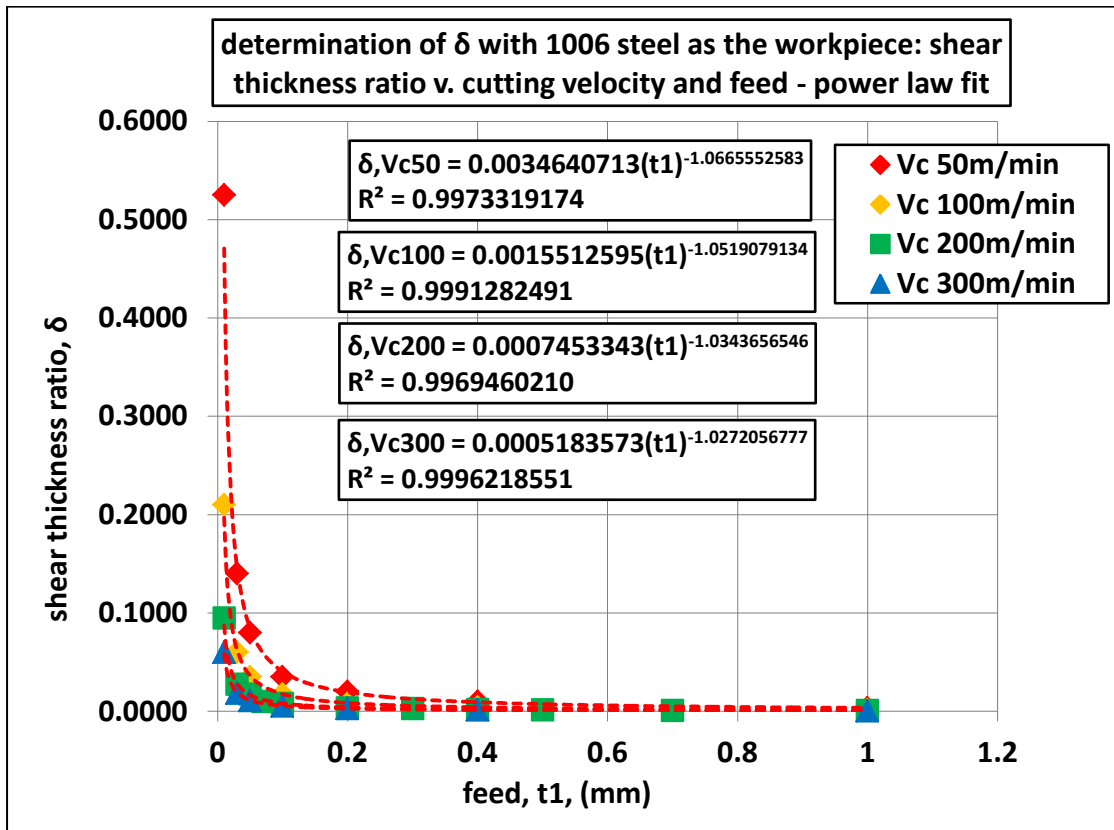


Figure 29: A sample plot of the determination of δ with 1006 steel as the workpiece.

By plotting the shear thickness values in this way, a power law fit of form,

$$y = Ax^n \quad (121)$$

was used to quantify the relationship of δ to cutting velocity, rake angle and tool width as a function of feed. A power law curve was observed as the best fit in this case compared to a polynomial, logarithmic or exponential fit. Constants of the power law fits, A and n , can also be modeled as functions of cutting velocity, see Figure 30 and Figure 31.

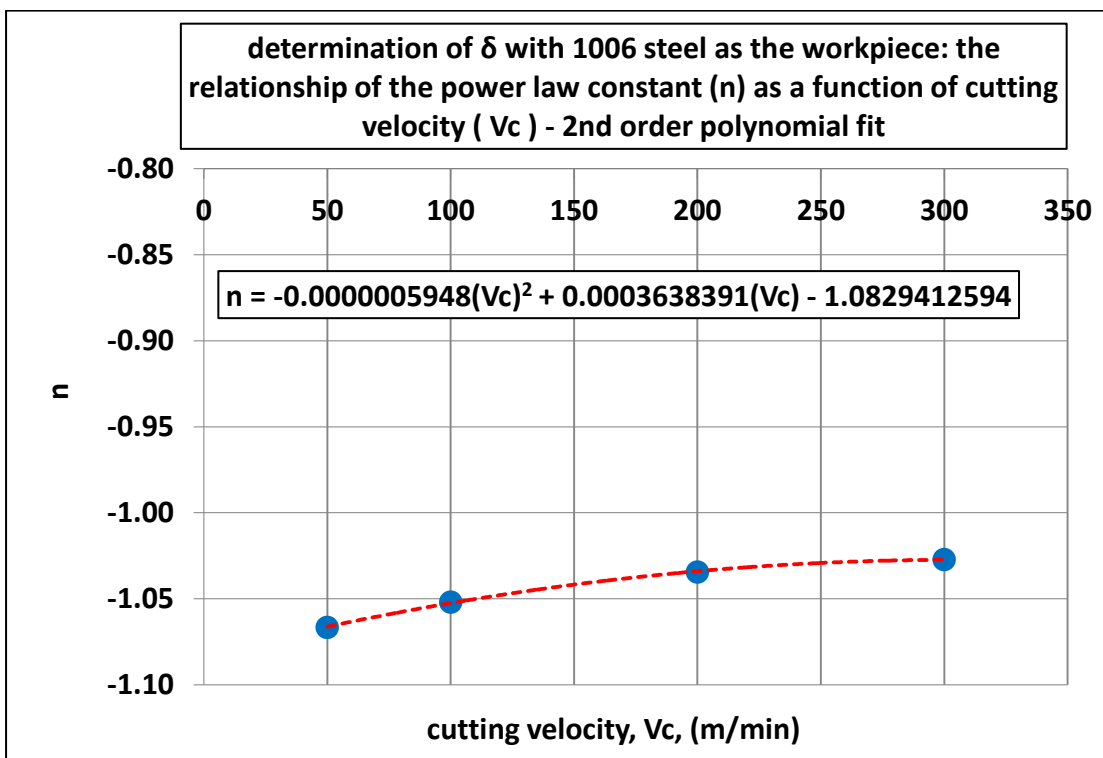


Figure 30: Determination of δ with 1006 steel as the workpiece: the relationship of the power law constant (n) as a function of cutting velocity (Vc).

Here it can be seen that n can be predicted with a second order polynomial function of cutting velocity. The power law constant, A, can also be expressed as a function of cutting velocity.

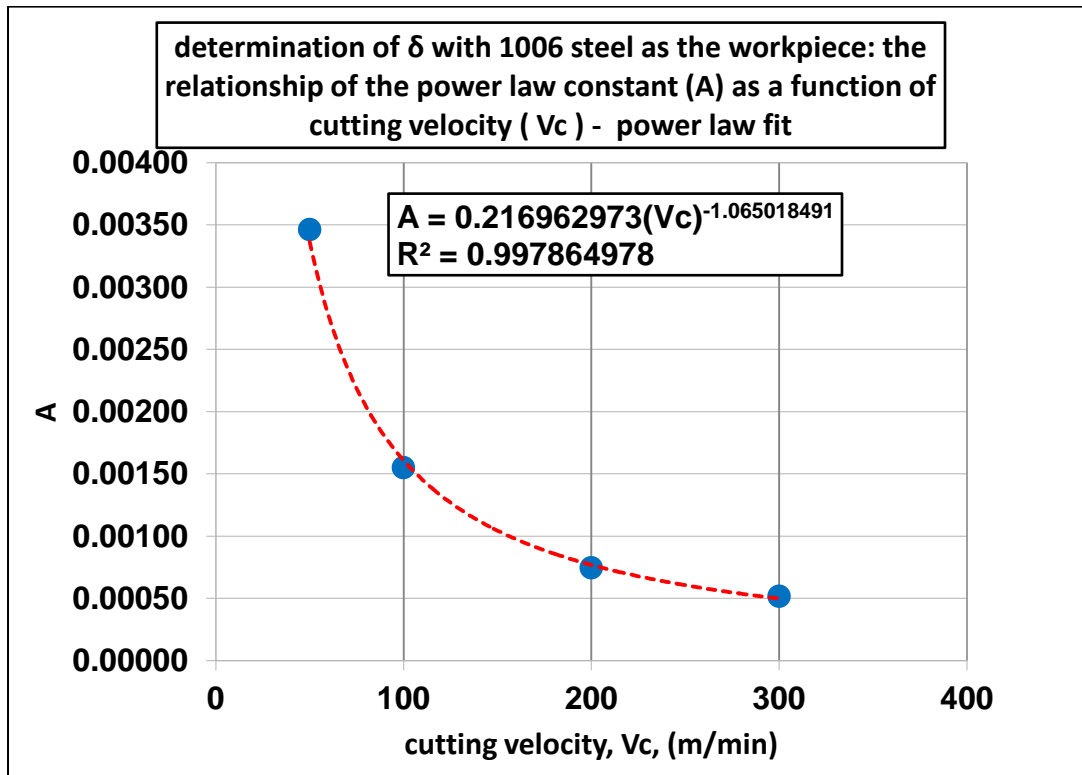


Figure 31: Determination of δ with 1006 steel as the workpiece: the relationship of the power law constant (A) as a function of cutting velocity (Vc).

Using 1006 steel as an example, δ can be expressed as a function of feed and cutting speed,

$$\delta_{steel} = 0.216962973 V_C^{-1.065018491} * t_1^{-0.0000005948V_C^2 + 0.0003638391V_C - 1.0829412594} \quad (122)$$

This δ relationship was established for the other workpieces under study with the same method used to find δ_{steel} ,

$$\delta_{titanium} = 0.018168545 V_C^{-1.081694245} * t_1^{0.0000161703V_C^2 - 0.0053328744V_C - 0.8706011366} \quad (123)$$

$$\delta_{copper} = 9.712002782 V_C^{-1.188833533} * t_1^{-0.0000037819V_C^2 + 0.0019687171V_C - 1.3850784387}$$

(124)

$$\delta_{aluminum} = 0.170942382 V_C^{-0.995048359} * t_1^{0.0000007697V_C^2 - 0.0001237521V_C - 1.0213847315}$$

(125)

However it must be emphasized that this δ function only applies to cases where $\alpha = 5^\circ$, $w=4$ mm and workpiece alloy as described by JC constitutive parameters. This means that the delta function must be recalculated for every different scenario. δ was calculated for 1006 steel, 6Al-4V titanium, 2024-T3 aluminum and OFE copper in for a metal cutting process as specified. To analyze metal cutting data from other groups, which involved a different set of process parameters, the values of δ were recalculated and will be specified in the relevant section.

PARAMETRIC STUDY OF THE SIMULATION

The metal cutting process was simulated with 6Al-4V titanium, 1006 steel, 2024-T3 aluminum and OFE copper as the workpiece in order to observe how the parameters of the metal cutting process changed as a function of feed, cutting speed and choice of workpiece. These simulations were appropriate as the first step in evaluating this model in order to characterize how the model worked and what kind of behavior it predicted. These initial predictions serve as a baseline which from which the model could be improved with data from future experiments.

All simulations were carried out with a 5° rake angle, 3 mm tool width and an initial workpiece temperature of 22° C. JC constitutive parameters from table 1 were used in this simulation.

Cutting Force

Cutting force is the largest component force on the tool and is directly proportional to the total work rate of the process. Depending on the rigidity of the tool post and of the metal cutting machine in general, a maximum force on the tool may apply. In addition, excessive forces on the tool may destroy the tool edge itself. In these cases, a maximum allowable force would restrict the process to an upper limit of feed and speed. Cutting force for the four workpieces as a function of feed and cutting speed were calculated and plotted, see Figure 32.

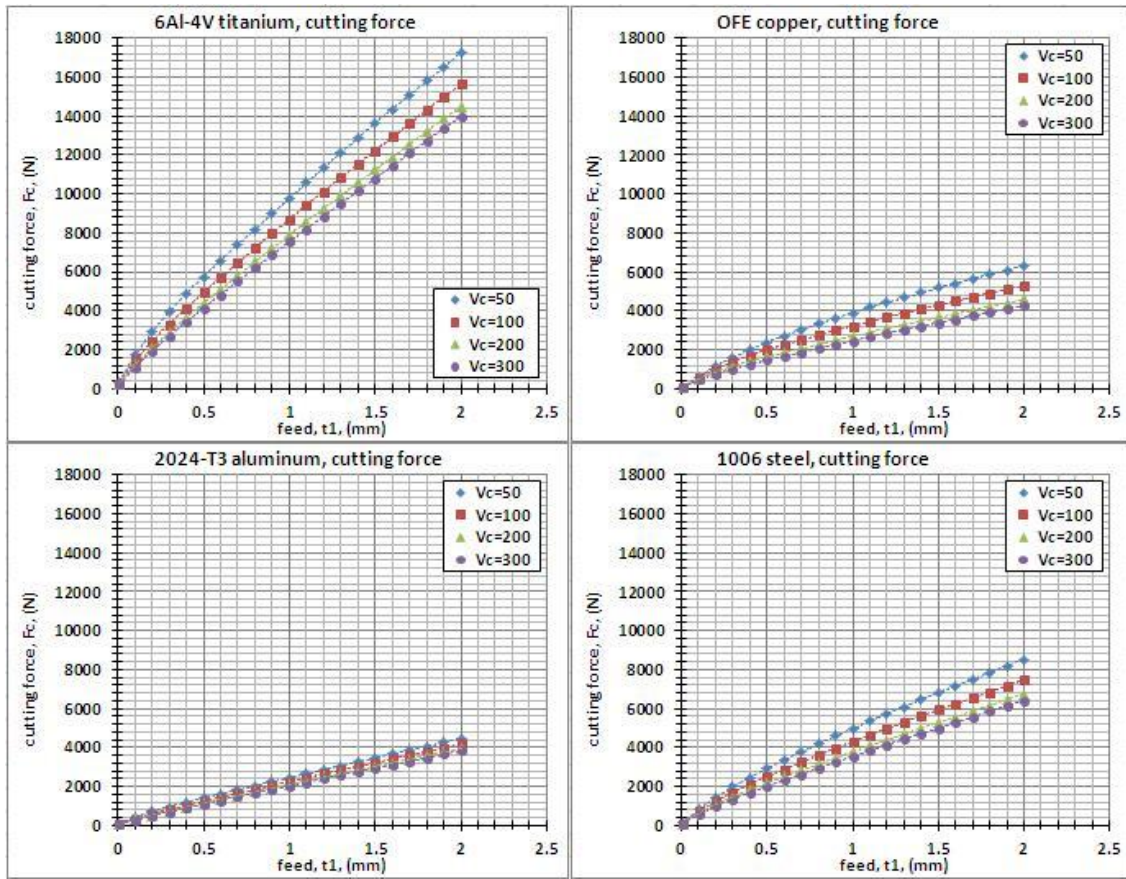


Figure 32: Predicted cutting force as a function of cutting speed and feed.

Titanium is predicted to have the highest cutting forces for a given feed and cutting speed, followed by steel, copper and aluminum. It is interesting to note that although the 2024-T3 aluminum alloy has a larger yield stress than copper or steel, it has the lowest predicted cutting forces. Thermal softening, which is a factor on the JC constitutive law, may have a large role in reducing the shear flow stress, which is a factor required in determining the cutting force. The titanium alloy has the largest required cutting forces of all the materials under simulation. This is due to its high yield strength and strain hardening. In addition, the titanium alloy has the highest melting point of all the metals

studied, making it the least susceptible to thermal softening. The steel and copper alloys have similar values of cutting forces, with those of the steel alloy being slightly higher.

For a given value of cutting velocity, cutting force increases with increasing feed. For feeds of up to 1mm, and for all metals under study, the behavior takes on a curved 'power law' shape. For feeds greater than 1mm, the relationship of cutting force to feed becomes linear.

For a given value of feed the highest cutting force for a given value of feed coincides with cutting speed of 50 m/sec, which is the slowest cutting speed simulated. Although slower cutting speeds were not simulated, it is expected that the cutting force will continue to rise, for a given feed, as the cutting speed is further decreased. When the cutting velocity is increased, the cutting force is predicted to decrease. This effect is limited to some upper limit of cutting velocity beyond which no increase in cutting force will accompany an increase in cutting velocity. In other words, the cutting force will eventually 'plateau' as higher and higher cutting velocities are selected. This holds for all metals studied. This effect predicts obvious benefits for high speed machining which involves very high cutting velocities; metal may be removed at very high speed without creating a situation where the cutting force is also proportionately very high.

Thrust Force

Thrust force is the component of force on the tool that is normal to the cutting force. Typically, the thrust force pushes the tool away from the workpiece in a direction perpendicular to the workpiece. Highest thrust forces are predicted for titanium, followed

by steel, copper and aluminum. Thrust force, as shown in Figure 33, seems to exhibit the same power law type relationship as seen in the cutting force, only the curvature is more pronounced in the thrust force behavior. For a given feed, the thrust force decreases with increasing cutting velocity until some upper limit is reached, after which the thrust force remains constant.

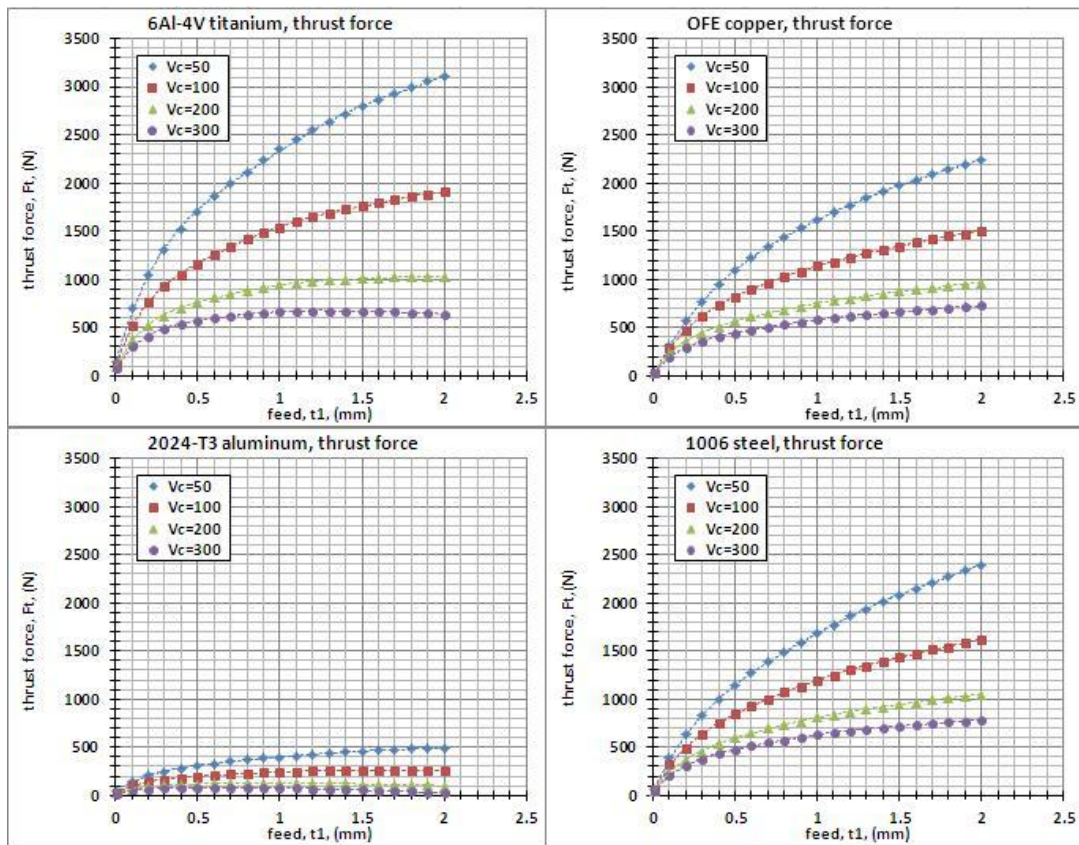


Figure 33: Predicted thrust force as a function of cutting speed and feed.

It is interesting to note that for a cutting velocity of 300 m/min, the thrust forces of titanium and aluminum decrease at higher feeds, suggesting the possibility of negative thrust forces at even higher feeds or cutting velocities beyond 300 m/min. A negative thrust force would push the tool face into the workpiece. Although there does not seem

anything prohibitive about negative thrust forces, they have not been mentioned in any of the literature encountered thus far, suggesting a fault of the model. However there is no information to indicate the possibility or impossibility of negative thrust forces, or of decreasing thrust forces with feed and cutting speed.

Shear Plane Temperature

Shear plane temperature is the temperature of the workpiece as it moves through the shear plane in the region known as the chip formation zone. The shear plane is geometrically located at an angle ϕ away from the cutting direction and extends from the tool tip to the free surface of the workpiece. The maximum shear strain rate in the chip formation zone occurs at the shear plane[1]. According to the parallel sided shear plane model, approximately half of the plastic deformation that occurs in the chip formation zone has occurred by the time the workpiece material passes through the shear plane. As such, the average temperature of the chip formation zone, T_{AB} , as defined by the parallel sided shear plane theory, is assumed to be equal to the temperature at the shear plane. T_{AB} is a factor in the flow shear stress at the shear plane, which determines the shear force, F_S , at the shear plane. Further, F_S is used to calculate the resultant force which is a factor in all the forces of the problem. T_{AB} is an important factor in the calculation that can be used to trouble-shoot the model if tool forces predicted are undesirably high.

The highest values of T_{AB} are predicted for 6Al-4V titanium, followed by 1006 steel, 2024-T3 aluminum and OFE copper. These temperatures are a function of the plastic work done. Titanium has the highest yield shear stress of the metals studied and it

follows that the highest shear plane temperatures would arise from the plastic deformation of this material relative to the other metals.

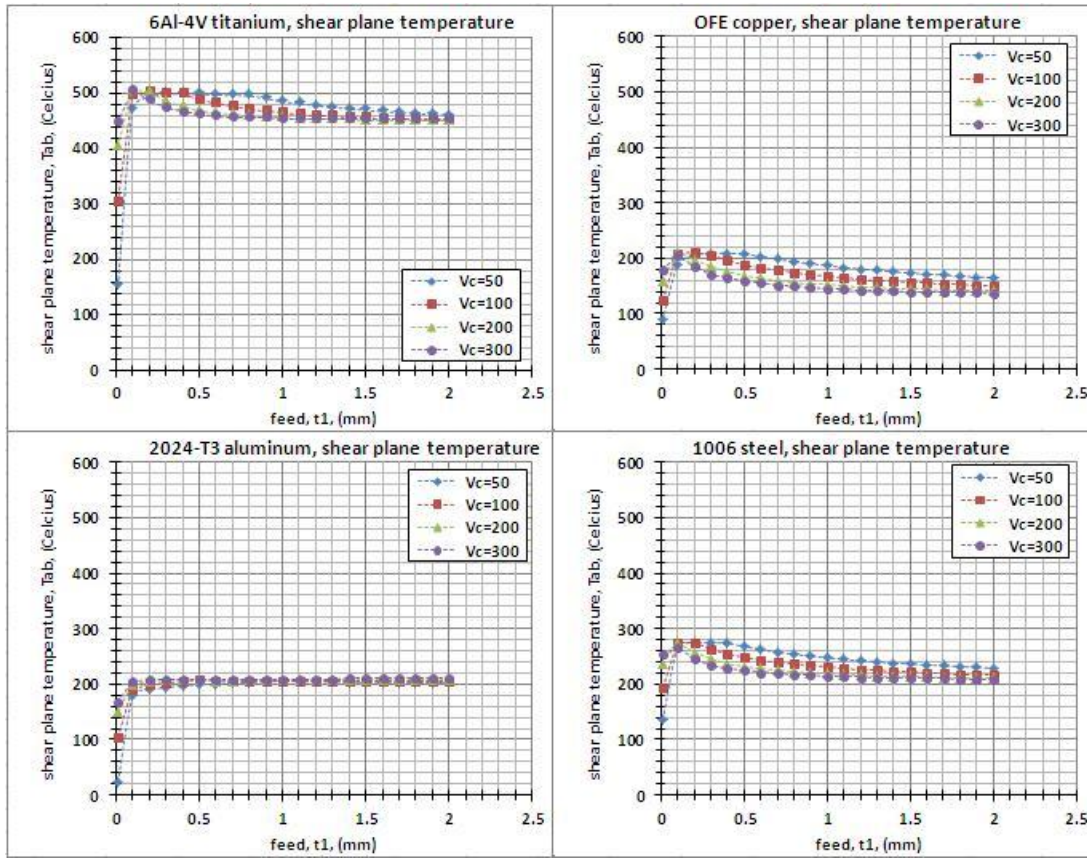


Figure 34: Predicted shear plane temperature as a function of cutting speed and feed.

It is observed that the shear plane temperature rises rapidly with increasing cutting speed at low feeds. This is because the heat partition coefficient is also changing rapidly. At higher cutting speeds, a decreased amount of heat is conducted into the workpiece and the shear plane temperature becomes approximately constant. 2024-T3 aluminum is not predicted to have this type of behavior, as seen by the similarity in shear plane

temperatures for the range of cutting velocities from 50-300 m/min. Another mechanism must be compensating for this effect.

Average Chip Temperature

Unlike the shear plane and the tool-chip interface, the chip is visible during metal cutting and not buried or hidden from view. As such, the tool chip temperature may be monitored by means of an IR camera or similar device to allow indirect temperature measurement, see Figure 35.

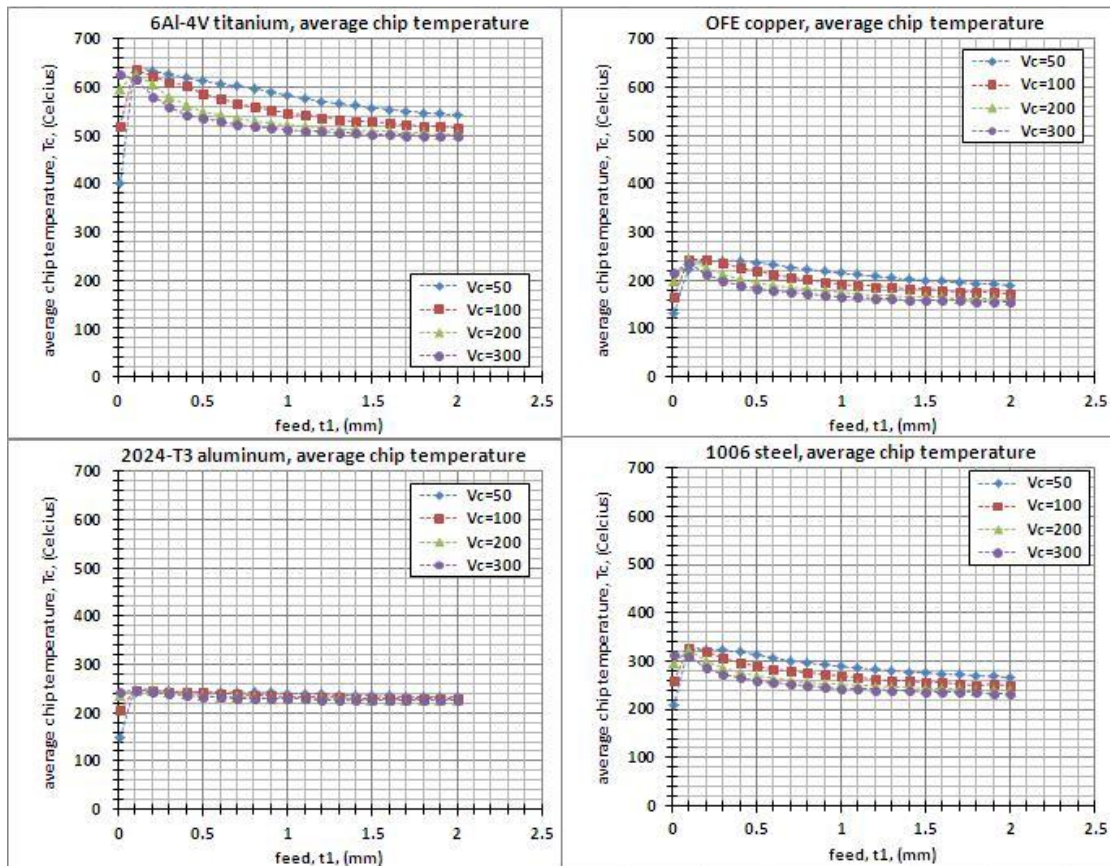


Figure 35: Average chip temperature as a function of cutting speed and feed.

The highest chip temperatures are predicted for titanium, followed by steel, copper and aluminum. The predicted temperatures suggest some maximum chip temperature with sufficiently high feed and cutting speed. This is due to a decreased amount of heat being conducted into the chip, resulting in a subtle decrease in chip temperatures as feeds and cutting speeds are increased.

Tool-Chip Interface Temperature

Recall that the tool-chip interface is the region where the chip is pressed up against the tool face in what is described as intimate contact under a condition of high hydrostatic pressure. Additional heat is generated by plastic deformation in a region of high shear in the chip adjacent to the tool face and defined by the shear thickness ratio delta. The highest temperatures of the metal cutting process occur at the tool-chip interface. Temperatures in this region are predicted to reach substantial fractions of the melting temperature. The tool-chip interface temperatures are highest for titanium, followed by steel, copper and aluminum, see Figure 36.

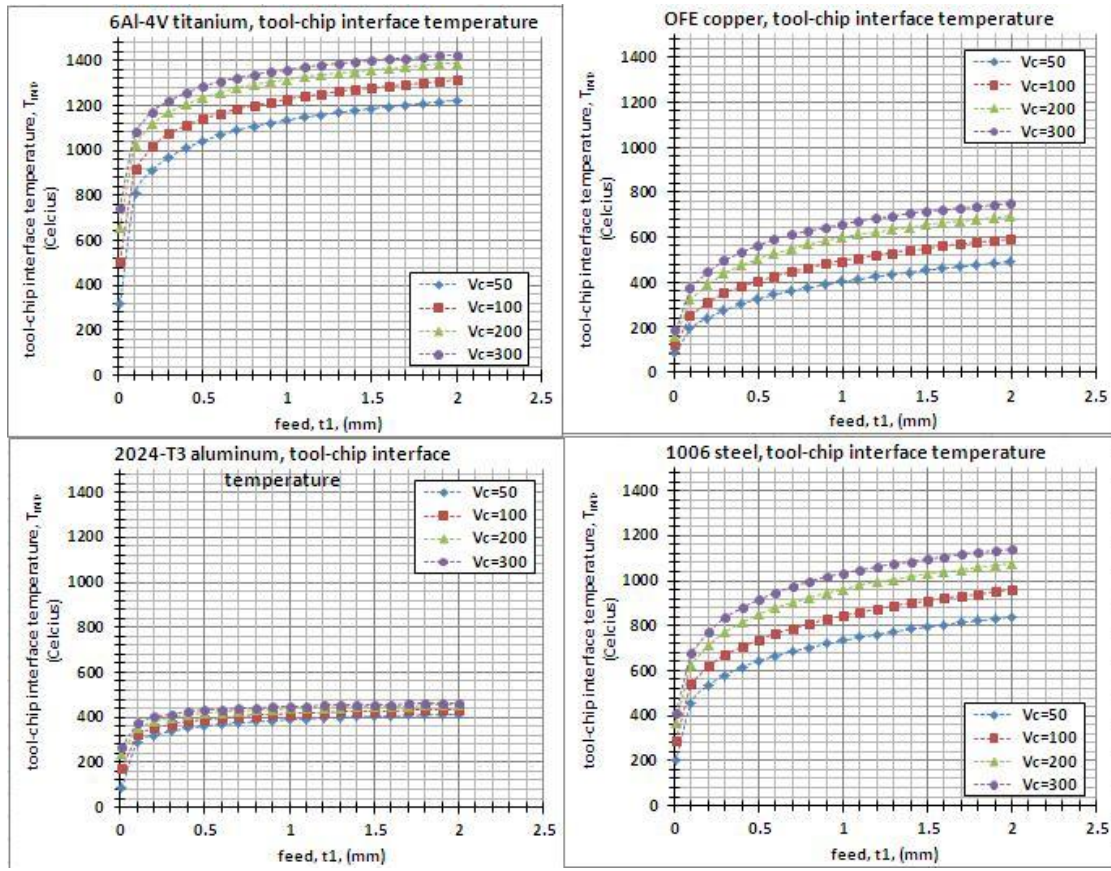


Figure 36: Tool-chip interface temperature as a function of cutting speed and feed.

For a constant cutting velocity, there exists a power law relationship between feed and tool-chip interface temperature where increasing feed increases the tool-chip interface temperature. For a constant feed, tool-chip interface temperature increases with increasing cutting velocity. To add, the simulations predict that for all the metals there is some cutting velocity beyond which the tool-chip interface temperature will remain constant with increasing cutting velocity. Recall that this tool chip interface temperature is the sum of T_{AB} and some fraction of the maximum temperature rise, ΔT_M , in the chip. This fraction is defined by ψ which accounts for temperature non-uniformities in the

chip. In the absence of knowledge of these inconsistencies, ψ is given a value of 1. This may be a source of error, as it may not be realistic to assume that the average temperature of the chip can be applied to the entire interface region. ΔT_M is calculated from experimental data with steel as the workpiece. It is assumed that the expression for ΔT_M applies not only to steel alloys, but also for titanium, aluminum and copper alloys. If the predicted tool forces are smaller than shown by experiment, then one possible explanation would be that the predicted temperatures were too high. These high predicted temperatures would lead to an overestimation of thermal softening in the flow stress model, leading to lower predicted forces than would actually be the case. Therefore, tool-chip interface temperature is important as an indicator in order to verify the correctness of the predictive metal cutting model, and suggests how to modify the model if the prediction is incorrect.

Shear Plane Angle

The shear plane angle is indicative of the geometry of the metal cutting process in general. The shear plane angle is a fundamental parameter that factors into all of the forces of the process as well as the temperature calculations. The simulation predicts the highest shear plane angles for titanium, followed by aluminum, steel and copper, see Figure 37.

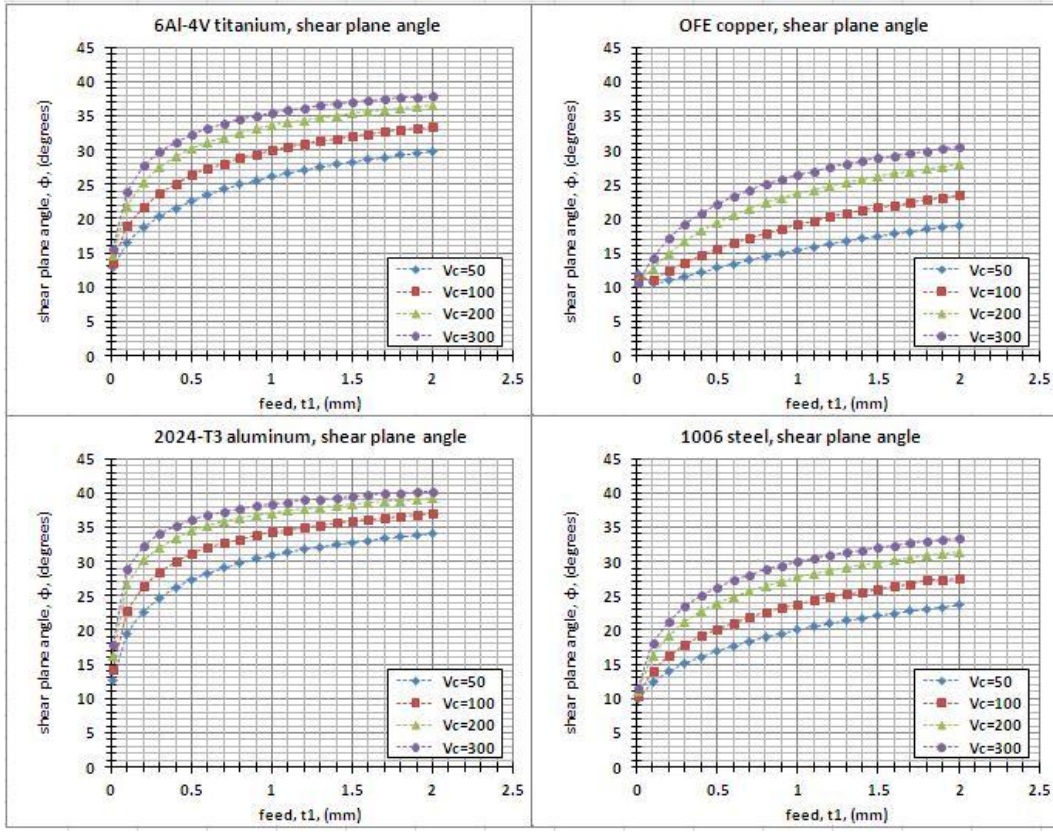


Figure 37: Shear plane angle as a function of cutting speed and feed.

As in much of the previous predictions, a power law behavior is deduced for feed as a function of shear plane angle and cutting force as a function of shear plane angle. Φ is observed to have the same dependency of feed and speed as do the predicted forces and temperatures. Large changes in ϕ are predicted for changes in feed and speed for feeds less than 0.5 mm and cutting speeds less than 200 m/min. For feeds and speeds above this, the behavior seems to plateau. This is simply the nature of the solution which is a form of force equilibrium solution. It should be noted that for a tool rake angle of 5 degrees, the shear plane angle never rises above 45 degrees, but this is not necessarily the case for larger tool rake angles.

Chip Thickness

Chip thickness is another readily accessible factor that can be readily monitored in the machine shop. The chip thickness is a function of the shear plane angle, feed and the rake angle. Since for a given simulation the feed and rake angle are constant, the chip thickness is then merely an extension of the shear plane angle. However the chip thickness is readily measurable, while the shear plane angle requires very special and novel experimental procedures such as slow motion cinematography or a 'quick stop' mechanism[1]. The metal cutting simulation reveals that chip thickness is a function of feed cutting speed and the workpiece selected, see Figure 38.

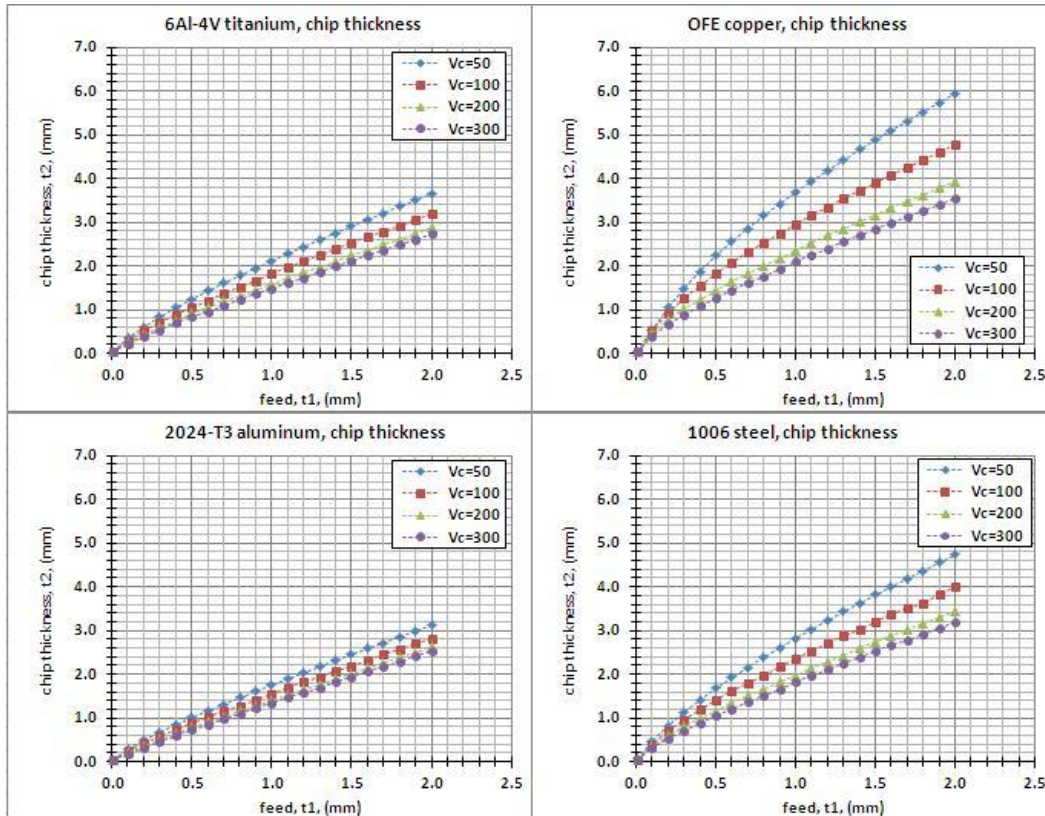


Figure 38: Chip thickness as a function of cutting speed and feed.

A power law relationship is deduced between feed and chip thickness between feed and also for cutting speed and chip thickness. The thickest chip thicknesses are predicted for copper, followed by steel, titanium and aluminum.

Shear Strain Rate at the Shear Plane

Shear strain rate at the shear plane is a maximum at the shear plane. Recall that the shear strain rate at the shear plane, γ_{AB} , is a function of cutting velocity and feed,

$$\gamma_{AB} = \frac{C_{OX} V_s}{L_{AB}} = \frac{C_{OX} V_c \cos \varphi - \alpha}{L_{AB}} = \frac{C_{OX} V_c \sin \varphi \cos \varphi - \alpha}{t_1} \quad (126)$$

This function shows that γ_{AB} increases with increasing V_c and decreases with increasing t_1 . γ_{AB} is also a function of C_{OX} and φ which are functions of the flow stress and of the JC constitutive properties of the material. The prediction of γ_{AB} simply shows that the shear plane model is able to describe the difference in γ_{AB} for different workpiece materials, see Figure 39.

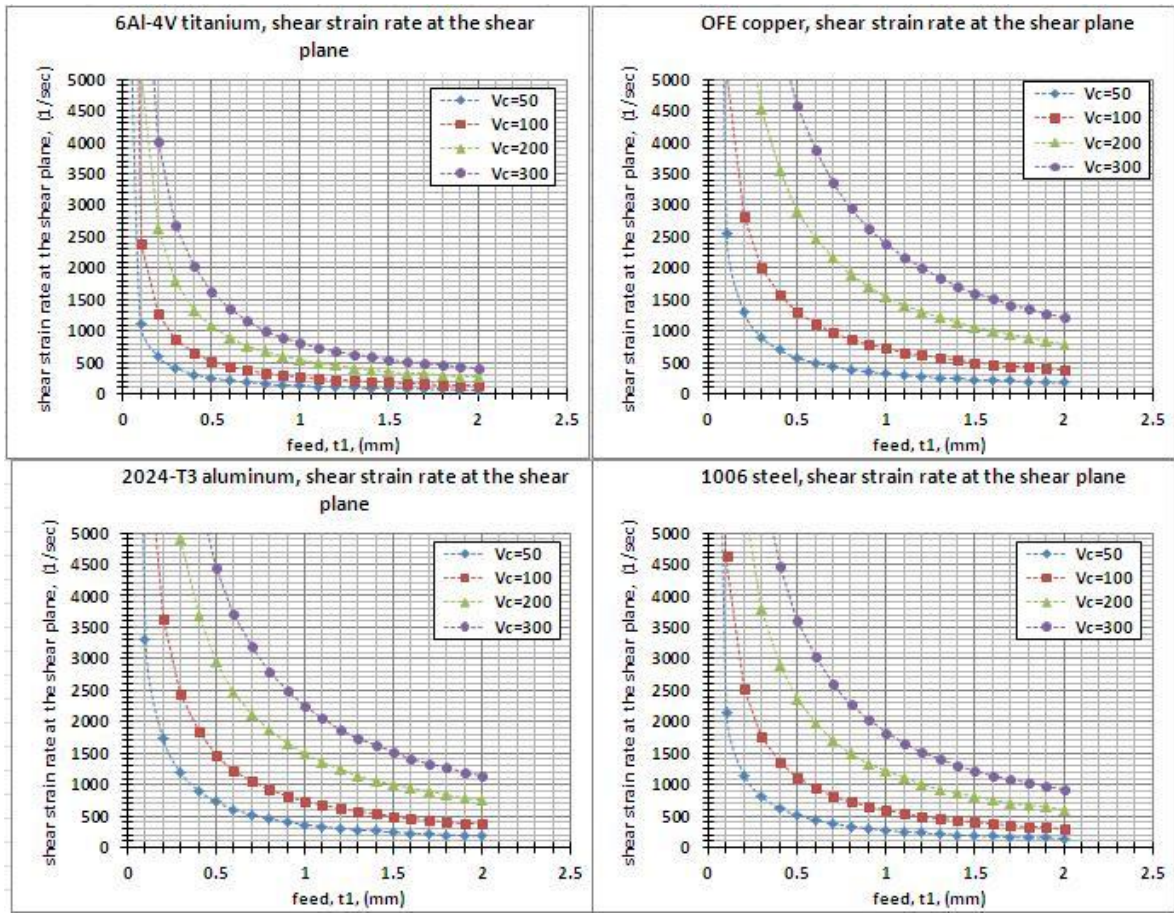


Figure 39: Shear strain rate as a function of cutting speed and feed.

Shear strain rate at the shear plane, γ_{AB} , increases with increasing cutting velocity and decreases with increasing feed.

Friction Force

The friction force is calculated such that it satisfies a force balance required by the steady state assumption. In this way, the coefficient of friction never comes into play. This method of calculating the friction force simplifies calculation of an ill-defined

process. Because of this, it is worth examining the predictions of the metal cutting model in order to gain insight to the friction force, see Figure 40.

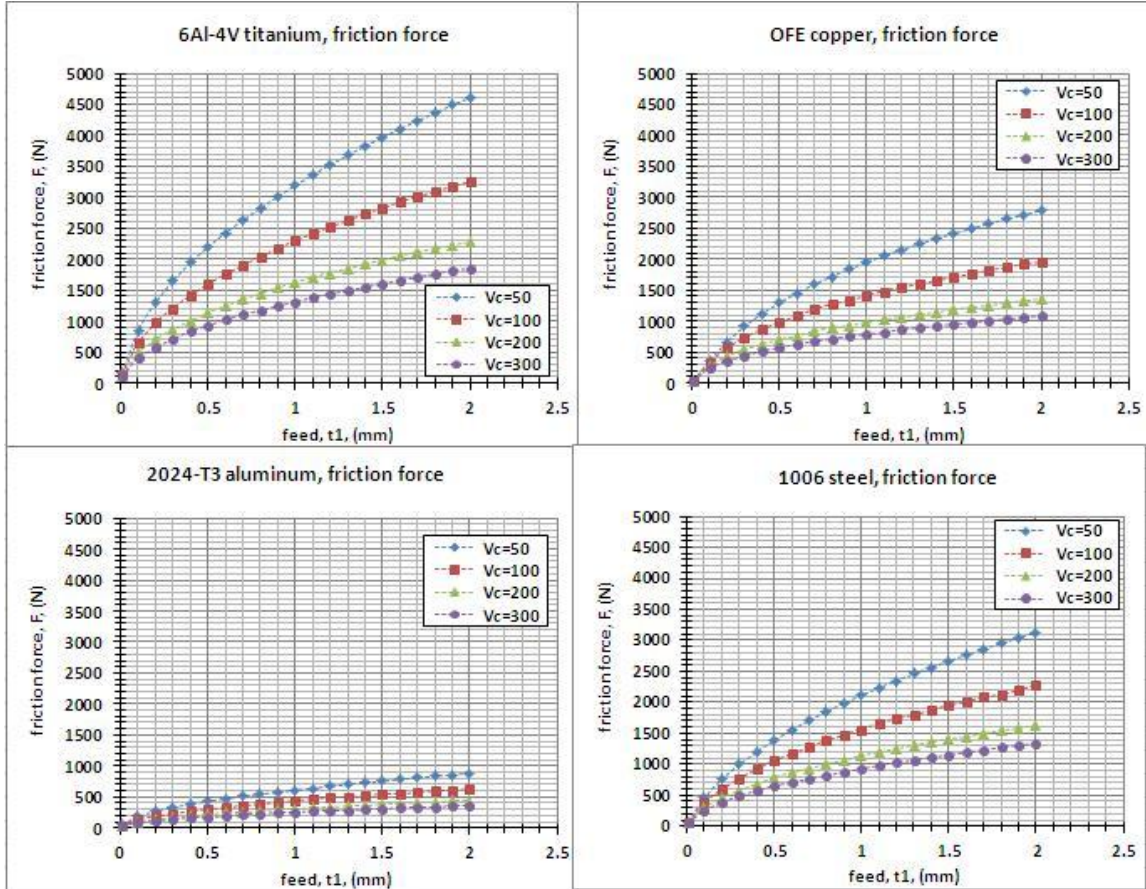


Figure 40: Predicted friction force.

The friction force decreases with increasing cutting velocity and increases with increasing feed. Friction force was highest for 6Al-4V titanium, followed by 1006 steel, OFE copper and 2024-T3 aluminum.

Shear Stress at the Tool-Chip Interface

The chip moves along the surface of the tool as the cutting is performed. Shear stress at the tool interface is created as a result of friction between the chip and the tool. The simulation predicts different values of τ_{INT} depending on the workpiece simulated, see Figure 41.

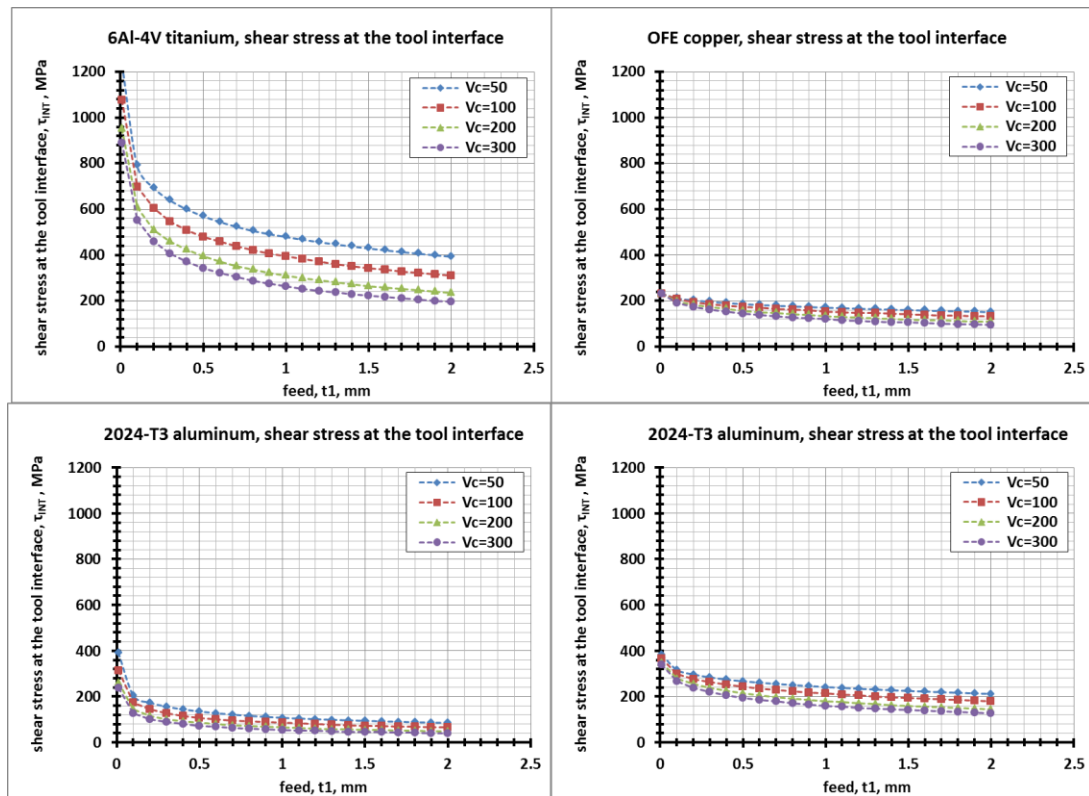


Figure 41: Shear stress at the tool-chip interface.

The highest values were predicted for the titanium alloy and the lowest values were predicted for the aluminum alloy.

Shear Stress at the Shear Plane

Shear stress at the shear plane is required to find the correct value of φ . It may also serve to indicate the amount of shear stress required to form the chip. Titanium is predicted to have the highest shear stress at the shear plane while aluminum and copper have the lowest predicted shear stress at the shear plane, see Figure 42. This is related to the yield stress qualities of the particular workpiece, as defined by the Johnson Cook constitutive parameters.

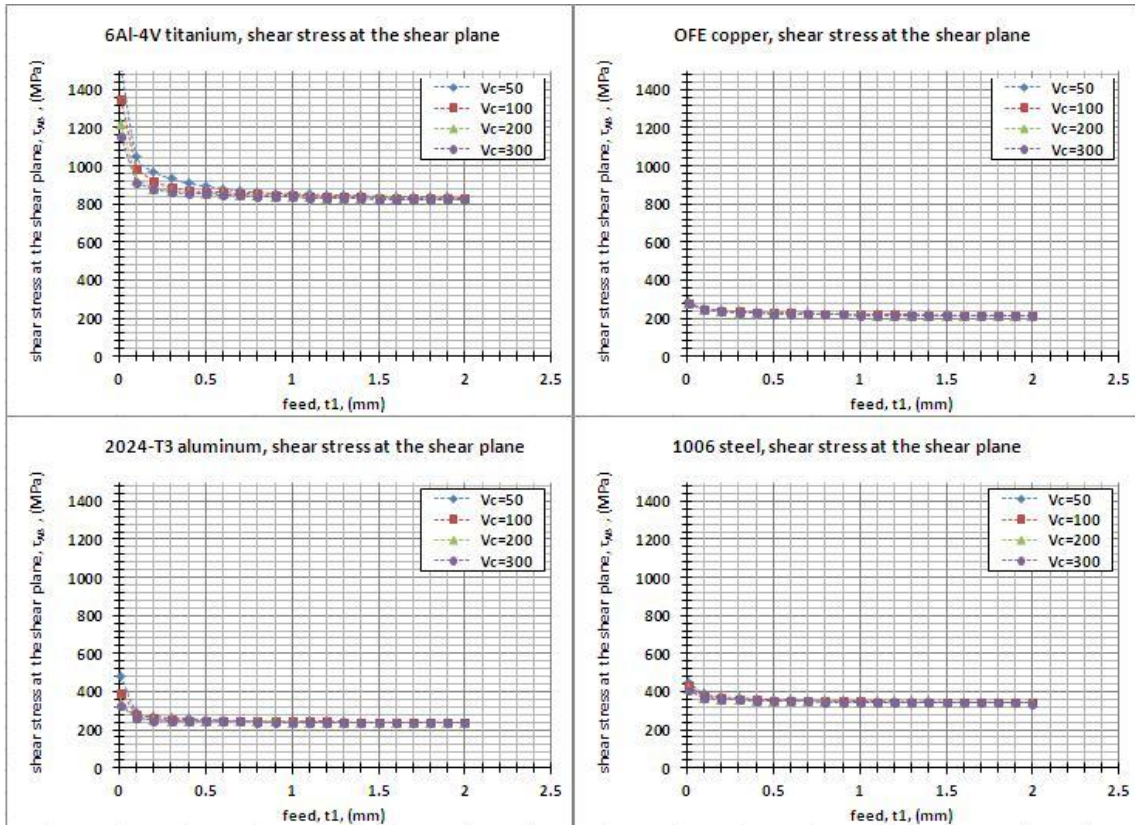


Figure 42: Shear stress at the shear plane.

This analysis seeks to address how tool forces, process temperatures and geometrical orientation of the cutting process change as a function of feed and cutting speed. The

feed, t_1 , and cutting speed, V_c , are two process parameters that the machinist has direct control over. Often, the most efficient cutting results when the cutting process is performed at the highest allowable temperatures and tool forces specified by the coolant, choice of tool and choice of workpiece material. If the tool forces are too great, the tool cutting edge may wear down prematurely or chip and break away all together. In addition, because the machine tool is not perfectly rigid, excessive tool forces will push the tool away from the workpiece in the event of a very forceful cut. This results in unpredictable cutting where the material removed is a function of the dynamic interaction of the tool and workpiece. If the temperatures of the process are too great, the tool will wear down or break prematurely. High temperatures can cause the cutting fluid to burn, removing any effect of lubrication or coolant that the cutting fluid may have originally provided. If the temperatures are sufficiently high, the workpiece will undergo thermal expansion, which effectively leads to deeper cuts than would be made at cooler temperatures. Defining the various temperatures and tool forces as a function of feed and cutting speed allows the machinist to better control the cutting process and to make the most efficient use of time and energy.

COMPARISON OF METAL CUTTING PREDICTIONS WITH EXPERIMENT

Experimental data was used to evaluate the metal cutting model of this study. The available published metal cutting experiments were sufficient to serve as a comparison to predicted tool forces and chip thicknesses. Although it would be beneficial to examine the conditions of the shear plane and of the tool-chip interface, the case studies are limited to the data published. Experimentally determined temperatures, parameters of the chip formation zone and parameters of the tool-chip interface are difficult and costly to measure. As such, only tool forces and chip thicknesses were analyzed because these represent the measurable parameters of the metal cutting process that are most commonly published.

Case Study of 1006 Steel

Data from metal cutting experiments was acquired [2] and used to compare the cutting force predicted by the metal cutting model, see Figure 43.

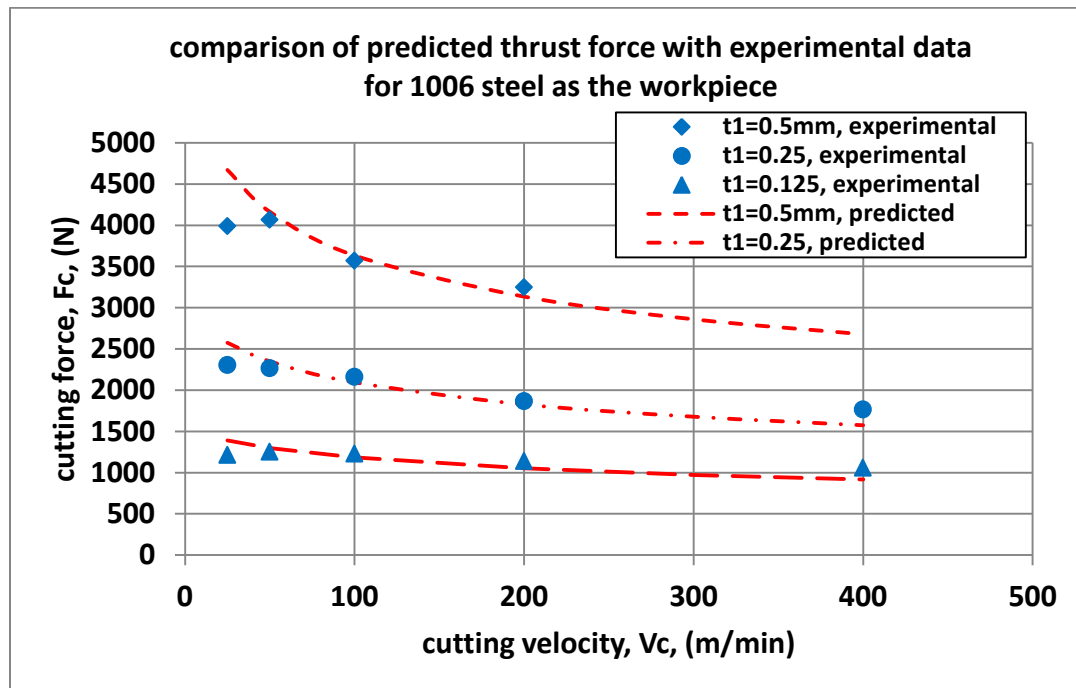


Figure 43: Comparison of cutting forces from experiment and from simulation.

Metal cutting experiments were carried out for low carbon steel (0.38% carbon content) similar in composition to 1006 steel. Experiments were made on a Heidenreich and Harbech Gildemeister M530 lathe. Cutting forces were measured using a Kistler type 9257-A three component piezoelectric dynamometer. The cutting tools used were tungsten carbide ‘throwaway’ tips with a rake angle of 5° , a clearance angle of 6° and a width of 4mm. Cutting force was measured for a range of cutting velocities and feeds.

At the lowest tested cutting velocity of 25 m/min, the cutting force observed is significantly lower than predicted. The lower cutting forces were caused by the formation of a ‘built-up edge’ on the tool face which is theorized to have effectively lowered the rake angle of the tool. Such a modification to the tool would correspond to lower cutting force in this case. For the cutting velocity range of 50-400 m/min, the predicted cutting forces were in good agreement with experimental results. Note that Oxley’s metal cutting model, which is the basis of the model used in the present study, was designed to specifically predict the outcome of metal cutting with low carbon steel. The experiments done to find relationships of β and ΔT_M were done only with low carbon steels. The verification of this model with experiments with low carbon steel as the workpiece suggests that the model is functioning properly. Comparison of prediction and experiment with other alloys will indicate if it is suitable to use this model for other workpiece materials without modification.

Case Study of 6Al-4V Titanium

Tool forces and chip formation have been observed[22] with 6Al-4V titanium as the workpiece. In this empirical study, a ‘turning’ type of cut was done on a 3.5 HP Hafco Metal Master lathe with a CNMX1204A2-SMH13A tool from Sandvik. The rake angle was +15 degrees and the angle of inclination was -6 degrees. Note that the model developed for the metal cutting process is specific for an inclination angle of 0 degrees. However, since the angle of inclination is small, it will be neglected for this comparison. Cutting experiments were done with a cutting velocity of 75 m/min and a tool width of

1.5 mm. Tool forces were measured for a series of feeds, see Figure 44. In addition, the average chip thickness of 0.13mm was observed for a feed of 0.122mm. Chip thickness was only recorded for this one value of feed.

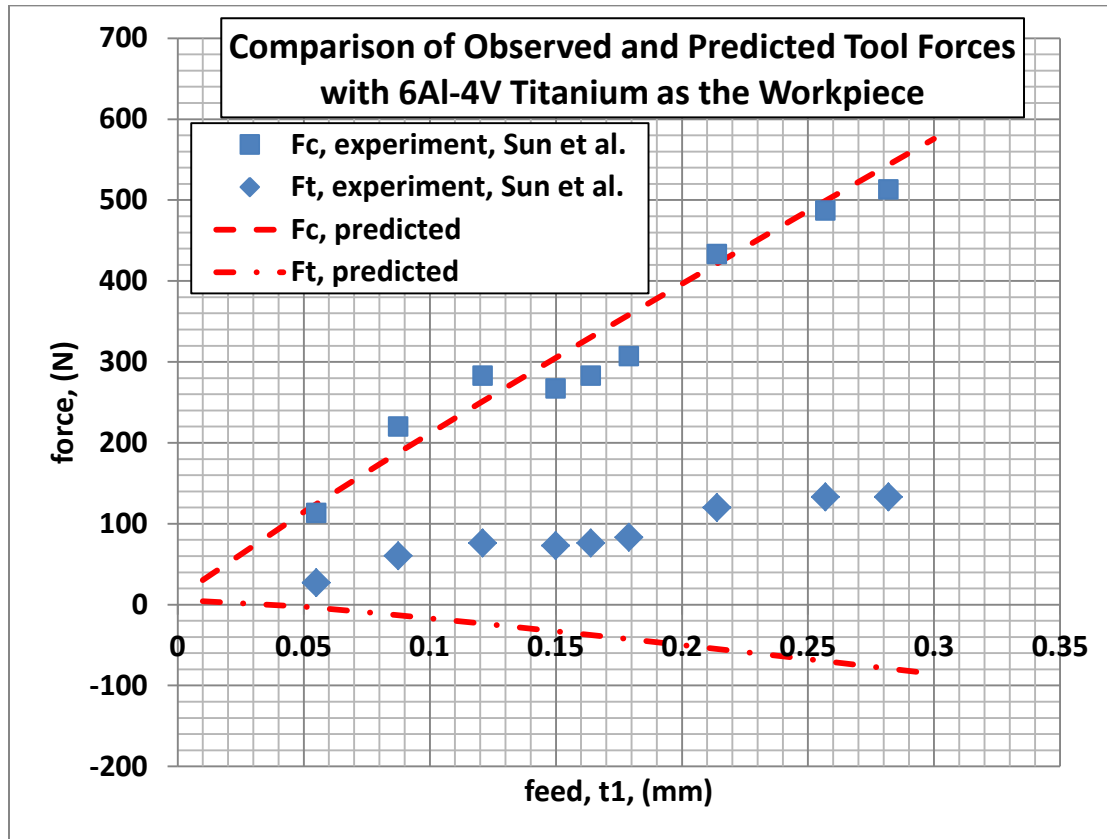


Figure 44: Comparison of observed and predicted tool forces with 6Al-4V titanium as the workpiece.

The empirical study encountered vibrational phenomena that impacted the tool forces. For small feeds below 0.15mm were accompanied by vibrations in the workpiece and in the machine. This vibrational load is cited as the cause of higher tool forces in this region of feed settings. Cutting force was observed to be higher than the thrust force, with an approximate ratio of cutting force to thrust force of 5:1. The predicted cutting force

agrees well with the empirical values, capturing the overall relationship between feed and cutting force. However it does not account for the effects that vibration have on tool forces. For a feed of 0.12 mm the predicted chip thickness was 0.132 mm, which is the same chip thickness observed in experiment. The predicted thrust force does not agree well with the experimental results. Negative thrust forces are predicted for feeds greater than 0.05 mm. This is most likely a fault of the model, which was designed to calculate for relatively small rake angles on the order of 5 degrees; not 15 degrees. Although this difference may appear small, it can have a dramatic effect when considering workpiece materials of high strength, such as titanium alloys. Although the predicted thrust forces are not in agreement with experiment, the predicted chip thickness agrees well with experiment. Given the limited data presented in this experimental study due to the vibrational effects, it is difficult to say definitively if the model accurately predicts the metal cutting process of titanium. There is evidence that the predictions are appropriate, but a more comprehensive study on the machinability of titanium is required in order to gauge the fitness of the model and make corrections. Note that the prediction of the cutting force is in good agreement with experiment. Nevertheless there are features in the experimental results caused by vibrational effects. Such vibration effects are not accounted for in the model and this is apparent in the comparison. A smooth relationship is predicted between tool force and cutting velocity, whereas a stepped profile is observed in experiment.

Case Study of 2024-T3 Aluminum as the Workpiece

Tool forces and chip formation have been observed[23] with 2024-T3 aluminum as the workpiece. The experiments were done with a tool with a 0° rake angle, and a width of 4.7 mm. Although the predicted cutting and thrust forces are lower than is seen in the experiment, similarities exist regarding the predicted and experimental tool forces. For a given feed, tool forces decrease with increasing cutting speed, see Figure 45 and Figure 46.

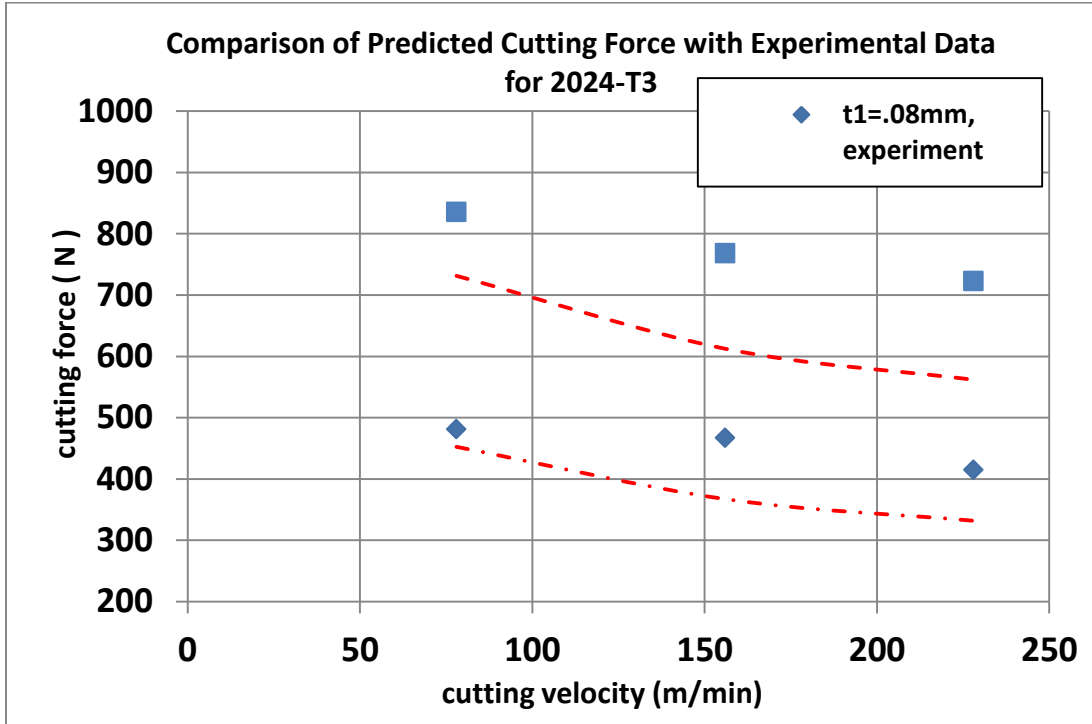


Figure 45: Comparison of predicted cutting force with experimental data for 2024-T3.

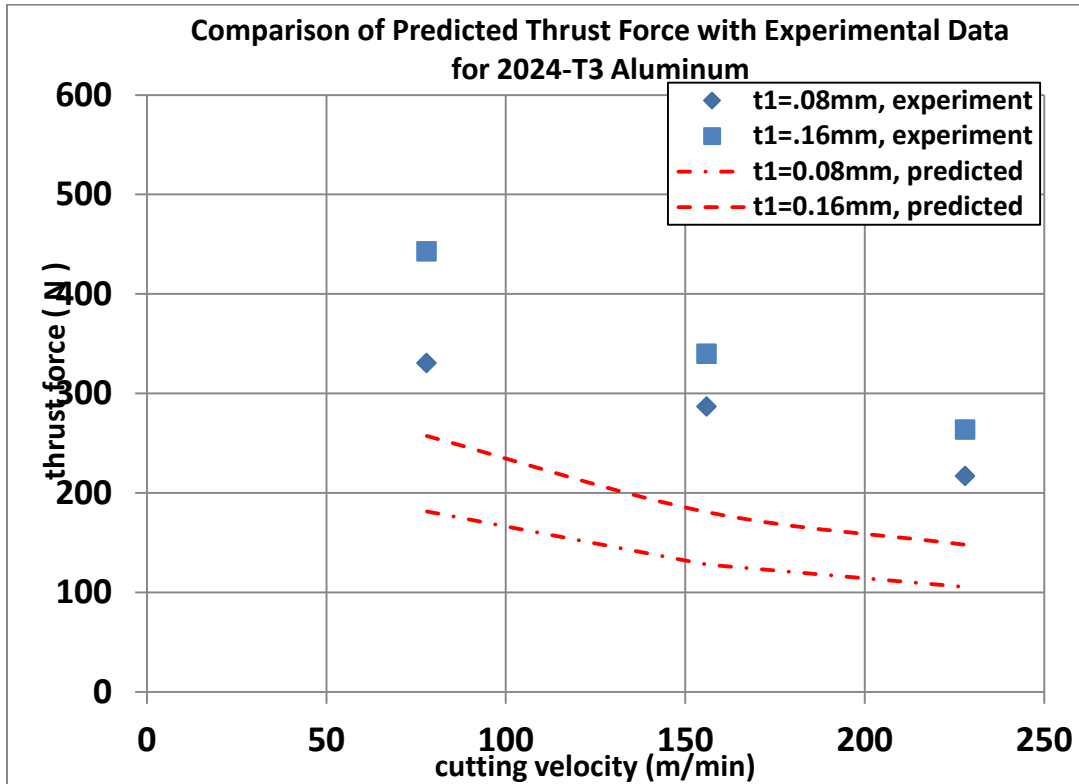


Figure 46: Comparison of predicted thrust force with experimental data for 2024-T3.

This suggests that the model is operating correctly, except for some offset within the calculations. For example, if the predicted temperatures are higher than they actually would be, then the excessive thermal softening of the workpiece / chip material would serve to lower the resulting tool forces.

The predicted tool forces do approximate the tool forces anticipated, but the model will have to be modified if it is to accurately predict the metal cutting process with 2024-T3 aluminum.

The predicted chip thickness is higher than is seen in experiment for feeds of 0.08 mm and 0.16 mm. However the trend of decreasing chip thickness with increasing cutting velocity is present in both the predicted and experimental results, see Figure 47.

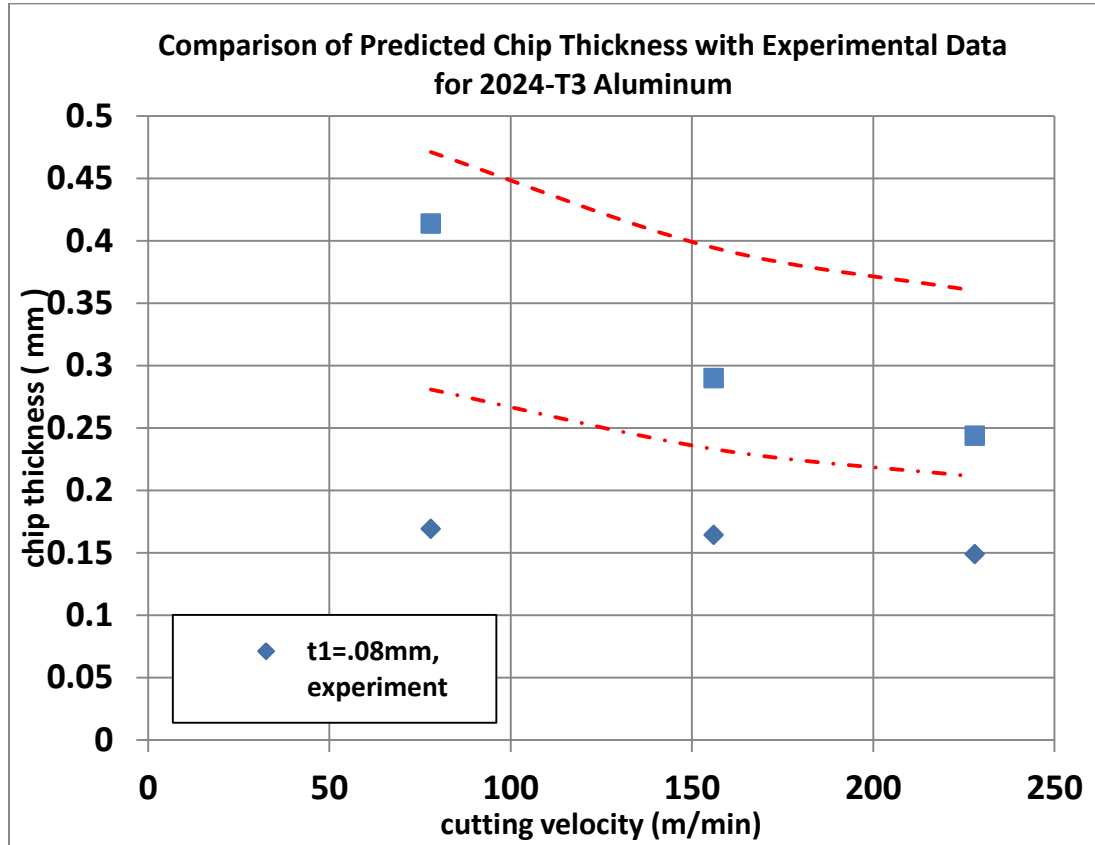


Figure 47: Comparison of predicted chip thickness with experimental data for 2024-T3.

An explanation for the relationship between chip thickness and cutting velocity can be visualized by considering the equation for chip thickness, [55]. Chip thickness is a function of the shear plane angle. By plotting chip thickness as a function of shear plane angle, with $\alpha = 0^\circ$ and $t_1 = 0.08 \text{ mm}$, it is apparent that an increase in shear plane angle leads to a decrease in chip thickness, see Figure 49. The temperatures of the metal cutting process indirectly impact the geometry of the chip formation zone. Tool-chip

interface temperature is a factor of the shear stress in the chip and it is this shear stress at the interface region is what determines the correct value of the shear plane angle. All of the forces of the metal cutting process, including the chip thickness are functions of the shear plane angle and the geometry of the process in general. Hence, tool forces and chip thickness are subject to the temperatures of the metal cutting process.

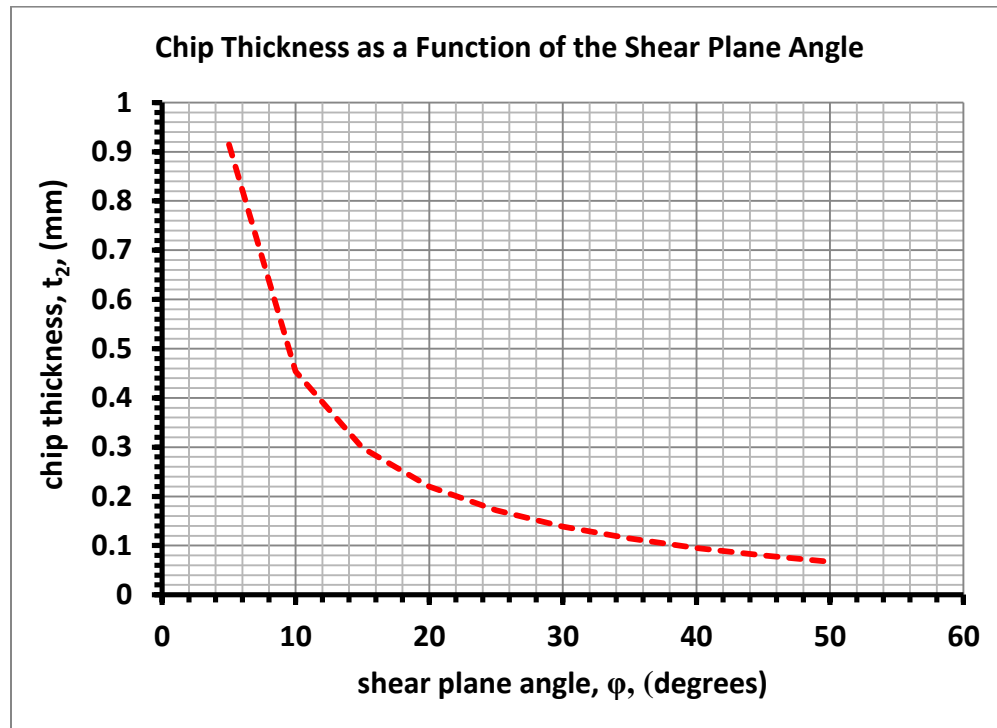


Figure 48: Chip thickness as a function of shear plane angle with $a = 0^\circ$ and $t_1 = 0.08\text{mm}$.

In the case study of 2024-T3 aluminum, the underestimate of tool forces and the overestimate of chip thickness can be explained by an overestimation of shear plane temperature, tool-chip interface temperature, or both.

Case Study with OFE Copper as the Workpiece

Tool forces have been observed[24] with OFE copper as the workpiece. The experiments were done with a tool with an 8° rake angle, and a width of 1.17 mm. Although the predicted cutting and thrust forces are lower than is seen in the experiment, similarities exist regarding the predicted and experimental tool forces. For a given feed, tool forces decrease with increasing cutting speed, see Figure 49 and Figure 50.

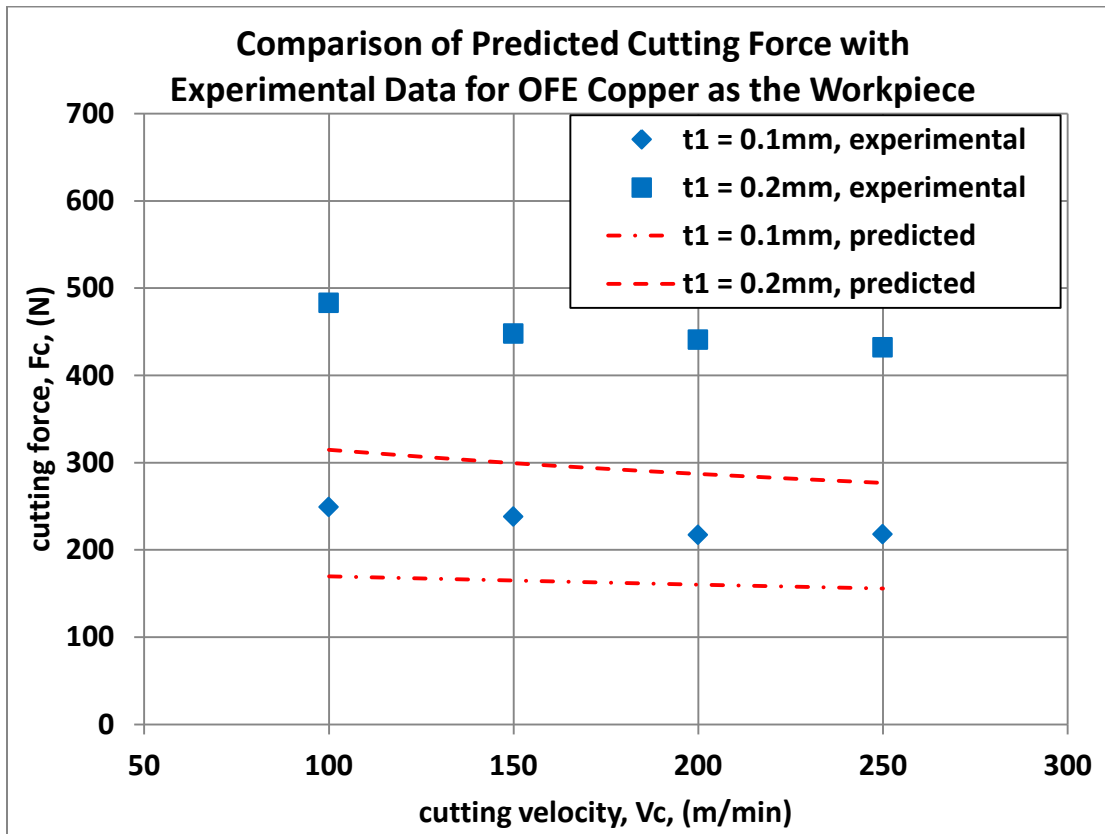


Figure 49: Comparison of predicted cutting force with experimental data for OFE copper as the workpiece.

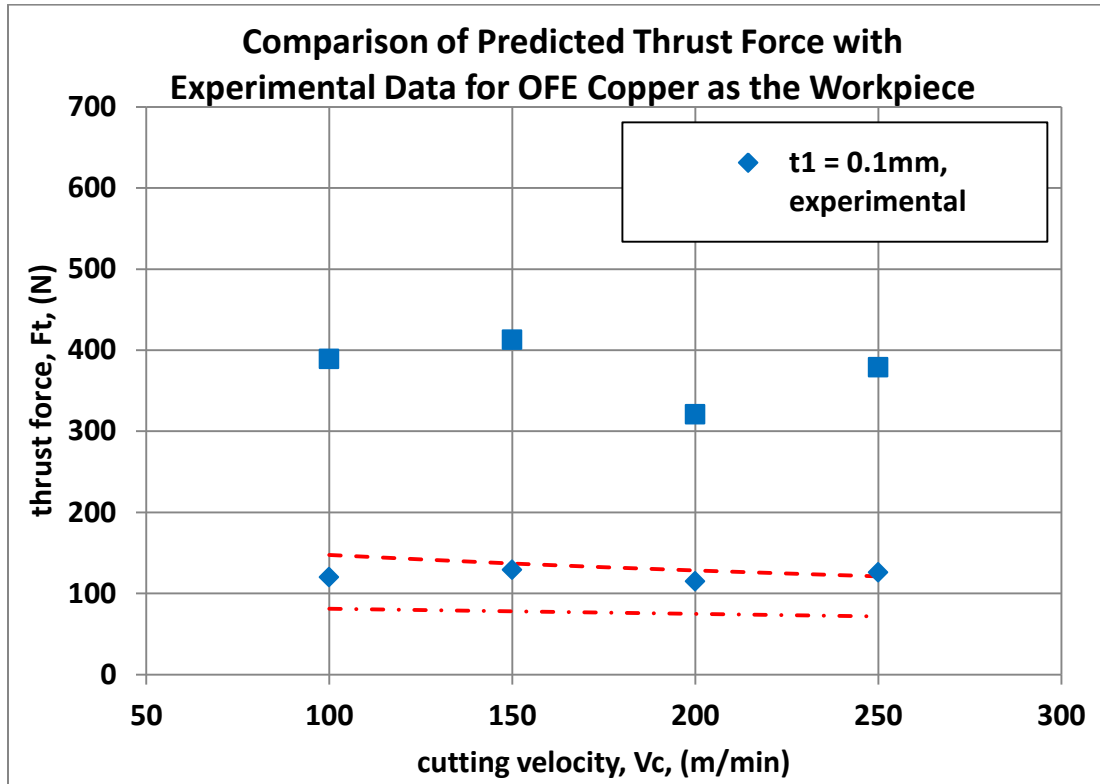


Figure 50: Comparison of predicted thrust force with experimental data for OFE copper as the workpiece.

The simulated results are in better agreement for the 0.1mm feed compared to the 0.2mm feed, however the predicted tool forces for both feeds were underestimated compared to experimental results. The prediction for OFE copper was very similar to the prediction for 2024-T3 aluminum. For both workpiece materials, the tool forces are predicted to be lower than in experiment, indicating a trend in the performance of the metal cutting model.

CONCLUSION

The parametric study of the shear plane metal cutting model, revealed the usefulness of the model to adequately describe the metal cutting process. With minimal input parameters, the process temperatures, forces, velocities, stresses, etc. can be determined on the assumption of a minimal energy solution. Although the model has the greatest success in predicting the metal cutting process for steels, the model does not perform as well for metal cutting processes with other materials such as titanium, aluminum or copper alloys. For materials other than steel, tool forces are underestimated and chip thicknesses are overestimated. The root cause of this may be due to an overestimation of process temperatures made with models based on experiments done with steel. New models or techniques for estimating process temperatures are required for the proper modeling of the metal cutting process with alloys other than steel. Despite this problem of temperature calculation, the predictions of the metal cutting model contain trends similar to what is seen in experiment. Although predicted and experimental tool forces and chip thickness are not in agreement, the essential behavior is captured by the prediction. Tool forces and chip thicknesses have been the focus of the comparison of the model with experimental results. This is because tool forces and chip thicknesses are the most commonly reported outputs of the metal cutting experiments. To refine the model, more experiments need to be done for a wider range of feeds and cutting speeds. In addition, more parameters of the metal cutting process need to be monitored. These additional parameters include process temperatures and the shear plane angle. If these parameters could be monitored along with the tool forces and chip thicknesses, then the

model could be better evaluated for its ability to predict the metal cutting process. A overestimation of tool forces could be correlated with predicted temperatures. The temperature models themselves could be evaluated against experimental results.

The majority of this study was to research the best model of metal cutting available in literature, to write a program to perform the necessary calculations and then to test the model. Although this metal cutting model is well known and its performance well documented[2], it is not sufficient to merely cite the previous work and proceed with the study of metal cutting models employing FEA techniques. These FEA programs represent the most advanced form of metal cutting analysis available today. But without practical knowledge of the analytical models that preceded it, FEA studies can be difficult to analyze and interpret. By committing to a study of the basis of metal cutting models, it is possible to grasp the metal cutting process on simple terms as a problem of plasticity. It is expected that more complex efforts will be made upon the conclusion of this preliminary work.

REFERENCES CITED

- [1] Stevenson, M. G., and Oxley, P.L.B., 1969, "An experimental investigation of the influence of speed and scale on the strain-rate in a zone of intense plastic deformation," Proceedings of the Institute of Mechanical Engineering, 184, pp. 561-576.
- [2] Oxley, P. L. B., 1989, *The Mechanics on Machining: an analytical approach to assessing machinability*, Ellis Horwood Limited, Chichester.
- [3] Finnie, A., 1956, "Review of Metal Cutting of the Past Hundred Years," *Mechanical Engineering*, 78(8), pp. 715-720.
- [4] Cocquilhat, M., 1851, "Experiences sur la Resistance Utile Produites dans le Forage," *Annales des Travaux Publics en Belgique*, 10, p. 199.
- [5] Wiebe, H., 1861, *Handbuch der Maschinen - Kunde*, Berlagstuhndlung von Carl Raden, Stuttgart.
- [6] Hartig, W., 1873, *Handbuch der Maschinen*.
- [7] Tresca, H., 1873, "Memiors sur le Rabotage de Metaux," *Bulletin de la Societe d'Encouragement pour L'industrie Nationale*, p. 585 and 685.
- [8] Mallock, 1881-1882, "The Action of Cutting Tools," *Proceedings of the Royal Society of London*, p. 127.
- [9] Merchant, M., 1945, "Mechanics of the Metal Cutting Process. I. Orthogonal Cutting and a Type 2 Chip," *Journal of Applied Physics* Cincinnati, Ohio, pp. 267-275.
- [10] Lee E.H., S. B. W., 1951, "The Theory of Plasticity Applied to a problem of Machining," *Transactions of the ASME, Journal of Applied Mechanics*, 18, pp. 405-413.
- [11] Trent, E. M., 1977, *Metal Cutting*, Butterworths, Guildford.
- [12] N. Fang, G. F., 2007, "Theoretical and experimental investigations of finish machining with a rounded edge tool," *Journal of Materials Processing Technology*, 191, pp. 331-334.

- [13] Palmer, W. B., and Oxley, P.L.B., "Mechanics of Metal Cutting," Proc. Proceedings of the Institute of Mechanical Engineering, pp. 623-654.
- [14] Johnson, G. R. a. C., W.H., "A Constitutive Model and Data for Metals Subjected to Large Strains, High Strain Rates and High Temperatures."
- [15] Lesuer, D., 2000, "Experimental Investigation of Material Models for Ti-6Al-4V Titanium and 2024-T3 Aluminum," Lawrence Livermore National Laboratory, Livermore, CA.
- [16] Stevenson, M. G. a. O., P.L.B., 1970, "An experimental investigation of the influence of strain-rate temperature on the flow stress properties of a low carbon steel using a machine test."
- [17] White, G. K. a. S. J. C., 1984, "Heat Capacity of Reference Materials: Cu and W," J. Phys. Chem. Ref. Data, Sydney, Australia, pp. 1251-1257.
- [18] 2003, Military Handbook - MIL-HDBK-5H: Metallic Materials and Elements for Aerospace Vehicle Structures (Knovel Interactive Edition), U.S. Department of Defense.
- [19] Nakayama, K., 1956, "Temperature rise of workpiece during metal cutting," Bull. Fac. Eng. Yokohama Nat. Univ., pp. 1-10.
- [20] Boothroyd, G., 1963, "Temperatures in Orthogonal Metal Cutting," Proceedings of the Institute of Mechanical Engineering, pp. 789-802.
- [21] Oxley, P. L. B., 1966, "Introducing strain-rate dependent work material properties into the analysis of orthogonal metal cutting," CIRP Annals, pp. 127-138.
- [22] S. Sun, M. B., M.S. Dargusch, 2009, "Characteristics of cutting forces and chip formation in machining of titanium alloys," International Journal of Machine Tools & Manufacture, pp. 561-568.
- [23] Samuel, T., 2000, "Investigation of the Effectiveness of Tool Coatings in Dry Turning of Aluminum Alloys," MS theisi, Wichita.

- [24] Balasubramanian, S., 2001, "The Investigation of Tool-Chip Interface Conditions Using Carbide and Saphire Tools," MS thesis, Wichita.

APPENDICES

APPENDIX A

CALCULATION METHOD

The metal cutting predictions were made using a program written in OCTAVE, which is similar to MATLAB. A great majority of the commands used in this routine are compatible with MATLAB, however some OCTAVE commands are slightly different and may require modification in order to run properly in MATLAB. Specifically, the ‘write to file’ portion of the program may differ from that seem in MATLAB.

What follows below is the body of the calculation routine:

```

function OJCD_AL_Vc200_fRange
%constants
%format long e
%input file name
filename=("OJCD_AL_Vc192_fR0p08_0p16mm")
pie=3.14159265
alpha=0*0.0174532925
% Vc range [ 78 117 156 192 228 ]
Vc=192/60
Coxinput=.70
philOWinput=17
wid=4.7/1000
Tw=22+273
TwCEL=Tw-273
Tm=775%kelvin
rho=2770
Ajc=265
Bjc=426
Cjc=0.015
mjc=1.00
njc=0.34
% [ 0.08 0.09 0.10 0.11 0.12 0.13 0.14 0.15 ]
t1array=[ 0.08 0.16 ]%in mm
t1arraylength=length(t1array)
t1DATA=zeros(54,t1arraylength);
for t1Loop = 1:1:t1arraylength
t1=t1array(1,t1Loop) %in mm
%the following equation for delta, the thickness ratio, only holds for,
%alpha=5, wid=4mm, Tw=22c, and JC parameters for 1006 steel.

```

```
%the delta equation is only good for varying t1 and seeing how it impacts the
forces, temps etc.
%%%%%
Vcd=Vc*60;
delta=(0.1709423846*Vcd^(-0.9950483618))*t1^(0.0000007697*Vcd^2 -
0.0001237507*Vcd - 1.0213848672);
t1=t1/1000; % convert feed to meter units for the rest of the calculation
%%%%%
%DeltaCount=0
%deltaStep=.0001
%TWRstore=zeros(1,2)
%DELTAsstore=zeros(1,2)
%Slopestore=zeros(1,2)
%SlopestoreCount=0
%while(1);
%DeltaCount=DeltaCount+1
%delta=delta+deltaStep
% if rem (DeltaCount,2)~=0
% disp("Odd delta.")
% DELTAsstore(1,1)=delta
% end
% if rem (DeltaCount,2)==0
% disp("Even delta.")
% DELTAsstore(1,2)=delta
% end
%Cox loop
eaCox=10
CoxStep=0.05;
Cox=Coxinput
while (1);
%variable step size to increase calculation speed
if eaCox < 4
CoxStep=0.01;
end
if eaCox < 1
CoxStep=0.001;
end
Cox=Cox+CoxStep;
%phi loop
phiLOW=phiLOWinput
phiHI=45
step=0.002;
%result collection matrix
P=zeros(3,((phiHI-phiLOW)/step)+1);
[PRow PColumn]=size(P);
```

```

mark=0;
for p=phiLOW:step:phiHI;
phi=p*0.0174532925;
mark=mark+1;
P(1,mark)=phi/0.0174532925;
%%%%%%%%%%%%%%%
% Start Basic Calculation Loop
%%%%%%%%%%%%%%%
%preliminary calculations
Lab=t1/sin(phi);
Vs=Vc*cos(phi-alpha);
SSrAB=Cox*Vs/Lab;
SSAB=0.5*(cos(alpha)/(sin(phi)*cos(phi-alpha)));
NSrAB=SSrAB/sqrt(3);
NSAB=SSAB/sqrt(3);
NSrREF=1;
%find equilibrium Temp at AB
TabOld=Tw;
TempLoopIterations=0;
while(1)
TempLoopIterations=TempLoopIterations+1 ;
%S and k
S=875; %J/KgK
k=121; %W/mK
Rt=rho*S*Vc*t1/k;
if Rt*tan(phi) < 10.0;
beta=0.5-0.35*log10(Rt*tan(phi));
else
beta=0.3-0.15*log10(Rt*tan(phi)) ;
end
sigma1AB=(Ajc+Bjc*NSAB^njc)*(1+Cjc*log(NSrAB/NSrREF))*(1-((TabOld-
Tw)/(Tm-Tw))^mjc);
sigma1AB=sigma1AB*1e6; %convert MPa to Pa
kAB=sigma1AB/sqrt(3);
areaAB=Lab*wid;
Fs=kAB*areaAB;
deltaTsz=((1-beta)*Fs*cos(alpha))/(rho*S*t1*wid*cos(phi-alpha));
eta=1;
TabNew=Tw+eta*deltaTsz;
ea=((TabNew-TabOld) / TabNew)*100;
if abs(ea) < 0.1;
Tab=TabNew ;
break
else
TabOld=TabNew ;

```

```

end
end
%Fs=Fs;
%beta=beta;
TabCEL=Tab-273;
deltaTszCEL=deltaTsz-273;
kab=k;
Sab=S;
%calculate theta, false position method
thL=20*0.0174532925 ;
thU=45*0.0174532925;
ThetaLoopIterations=0;
while(1);
ThetaLoopIterations=ThetaLoopIterations+1;
fU=1+2*((pie/4)-thU)-Cox*njc*tan(thU);
fL=1+2*((pie/4)-thL)-Cox*njc*tan(thL);
thR=thU - (fU*(thL-thU)/(fL-fU));
fR=1+2*((pie/4)-thR)-Cox*njc*tan(thR);
eval=fU*fR;
ea=((thR-thL)/thR)*100;
if eval < 0;
thL=thR;
else
thU=thR;
end
if abs(ea) < 0.01;
break
end
end
theta=thR;
thetaDEG=theta/0.0174532925;
% calculate forces and chip thicknesses
lambda=theta+alpha-phi;
lambdaDEG=lambda/0.0174532925;
R=Fs/cos(theta);
F=R*sin(lambda);
N=R*cos(lambda);
Fc=R*cos(lambda-alpha);
Ft=R*sin(lambda-alpha);
%calculate for tool-chip interface
t2=t1*cos(phi-alpha)/sin(phi);
ChipRatio=t2/t1;
V=Vc*sin(phi)/cos(phi-alpha);
h1=(t1*sin(theta))/(cos(lambda)*sin(phi));
h2=1+(Cox*njc)/ (3*(1+2*(pie/4-phi)-Cox*njc));

```

```

h=h1*h2; %tool-chip contact length
TauInt= F/(h*wid); %resolved shear stress at the tool
TauIntMPa=TauInt/1e6;
P(2,mark)=TauIntMPa;
SSrInt=V/(delta*t2); %Shear strain rate at interface
NSrInt=SSrInt/sqrt(3);% normal strain rate at interface
NSInt=1; %an approximation, oxley text pg. 103
%calculate a new Tc,
TcOld=Tw+deltaTsz;
TcLoopIterations=0;
while (1);
TcLoopIterations=TcLoopIterations+1;
%S and k
S=875; %J/KgK
k=121; %W/mK
deltaTc=F*sin(phi)/(rho*S*t1*wid*cos(phi-alpha));
TcNew=Tw+deltaTsz+deltaTc;
ea=((TcNew-TcOld) / TcNew)*100;
if abs(ea) < 0.01;
Tc=TcNew;
break
else
TcOld=TcNew ;
end
end
TcCEL=Tc-273;
deltaTcCEL=deltaTc;%-273;
kC=k;
SC=S;
%calculate for tool - chip interface,
Rt=rho*S*Vc*t1/k;
exponent=0.06-0.195*delta*(Rt*t2/h)^0.5+0.5*log10(Rt*t2/h);
deltaTm=deltaTc*10^exponent;
deltaTmCEL=deltaTm;%-273;
Templnt=Tw+deltaTsz+deltaTm;
TemplntCEL=Templnt-273;
%calculate the normal stress at interface region, JC model
sigma1chipMPa=(Ajc+Bjc*NSInt^njc)*(1+Cjc*log(NSrInt/NSrREF))*(1-((Templnt-Tw)/(Tm-Tw))^mjc); %MPa
sigma1chip=sigma1chipMPa*1e6; %convert MPa to Pa
kchip=sigma1chip/sqrt(3); %in Pa, shear stress in the chip at the interface
kchipMPa=kchip/1e6; %with thickness delta.
P(3,mark)=kchipMPa;
%%%%%%%%%%%%%%%
% End Basic Calculation Loop

```

```
%$$$$$$$$$$$$$$$$$$$$$$$$$$$$$$$$$$$$$$$$$$$$$$$$$$$$$$$$$$$$$$$$$$$$$$$$
eashear=abs(((TauInt-kchip)/TauInt)*100);
if abs(eashear) < 0.2
t1DATA(1,t1Loop)=t1;
phiSelect=phi;
phiDEG=phi/0.0174532925
eashear;
%report
%givens
format long e
t1DATA(2,t1Loop)=alpha;
t1DATA(3,t1Loop)=Vc;
t1DATA(4,t1Loop)=TwCEL;
t1DATA(5,t1Loop)=rho;
t1DATA(6,t1Loop)=Ajc;
t1DATA(7,t1Loop)=Bjc;
t1DATA(8,t1Loop)=Cjc;
t1DATA(9,t1Loop)=mjc;
t1DATA(10,t1Loop)=njc;
t1DATA(11,t1Loop)=Lab;
t1DATA(12,t1Loop)=Vs;
t1DATA(13,t1Loop)=SSrAB;
t1DATA(14,t1Loop)=SSAB;
t1DATA(15,t1Loop)=NSrAB;
t1DATA(16,t1Loop)=NSAB;
t1DATA(17,t1Loop)=NSrREF;
t1DATA(18,t1Loop)=TabCEL;
t1DATA(19,t1Loop)=deltaTsz;
t1DATA(20,t1Loop)=kab;
t1DATA(21,t1Loop)=Sab;
t1DATA(22,t1Loop)=phiDEG;
t1DATA(23,t1Loop)=thetaDEG;
t1DATA(24,t1Loop)=lambdaDEG;
t1DATA(25,t1Loop)=R;
t1DATA(26,t1Loop)=F;
t1DATA(27,t1Loop)=N;
t1DATA(28,t1Loop)=Fc;
t1DATA(29,t1Loop)=Ft;
t1DATA(30,t1Loop)=t2;
t1DATA(31,t1Loop)=ChipRatio;
t1DATA(32,t1Loop)=V;
t1DATA(33,t1Loop)=h;
t1DATA(34,t1Loop)=TauIntMPa;
t1DATA(35,t1Loop)=SSrlnt;
t1DATA(36,t1Loop)=NSrlnt;
```

```

t1DATA(37,t1Loop)=NSInt;
t1DATA(38,t1Loop)=TcCEL;
t1DATA(39,t1Loop)=deltaTcCEL;
t1DATA(40,t1Loop)=kC;
t1DATA(41,t1Loop)=SC;
t1DATA(42,t1Loop)=deltaTmCEL;
t1DATA(43,t1Loop)=TemplntCEL;
t1DATA(44,t1Loop)=sigma1chipMPa;
t1DATA(45,t1Loop)=kchipMPa;
TotalWorkRate=Fc*Vc;
FrictionWorkRate=F*V;
t1DATA(46,t1Loop)=TotalWorkRate;
t1DATA(47,t1Loop)=FrictionWorkRate;
t1DATA(48,t1Loop)=kAB;
t1DATA(49,t1Loop)=Fs;
t1DATA(50,t1Loop)=Cox;
t1DATA(51,t1Loop)=sigma1AB;
t1DATA(52,t1Loop)=delta;
t1DATA(53,t1Loop)=TotalWorkRate;
t1DATA(54,t1Loop)=FrictionWorkRate;
fopen([filename],'w')
s=('metal cutting results')
fdisp([filename],s)
fdisp([filename],t1DATA)
fclose([filename])
format short
break
end
%useful from phi loop
%Z
end%phi
%phi=phiSelect;
%Cox equilibrium criteria
SigmaNp=kAB*(1+pie/2-2*alpha-2*Cox*njc);
SigmaN=N/(h*wid);
eaCox=((SigmaNp-SigmaN)/SigmaNp)*100
if abs(eaCox) < 0.2;
break
end
end%Cox
%%%%%%%%%%%%%
%if rem (DeltaCount,2)~=0
% disp("Select TWRstore(1,1).")
%TWRstore(1,1)=TotalWorkRate

```

```

%end
%%%%
%if rem (DeltaCount,2)==0
disp("Select TWRstore(1,2).")
%TWRstore(1,2)=TotalWorkRate
%SlopeStoreCount=SlopeStoreCount+1
%DeltaSlope = (TWRstore(1,2)-TWRstore(1,1))/ (DELTAsstore(1,2) -
DELTAsstore(1,1))
% if rem (SlopeStoreCount,2)~=0
% disp("Select SlopeStore(1,1).")
% SlopeStore(1,1)=DeltaSlope
% end
% if rem (SlopeStoreCount,2)==0
% disp("Select SlopeStore(1,2).")
% SlopeStore(1,2)=DeltaSlope
% SlopeChange = SlopeStore(1,2) - SlopeStore(1,1)
%%%%
% if abs(SlopeChange) > 5000
% deltaStep= 0.0001
%delta=delta+deltaStep
% end
% if abs(SlopeChange) < 5000
% deltaStep= 0.005
%delta=delta+deltaStep
% end
%%%%
% end
%Delta selection condition
% if DeltaSlope > 0
%disp("Delta overshoot. Possible equilibrium solution.")
% break
% end
%end
%%%%
end%delta loop
format long e
fopen([filename],'w')
s='metal cutting results'
fdisp([filename],s)
fdisp([filename],t1DATA)
fclose([filename])
t1DATA
disp("end of calculations")
%delta
%TotalWorkRate

```

```
%FrictionWorkRate
%kchipMPaselect
%t1
%Fcselect
%Ftselect
%TabCELselect
%TcCELselect
%TemplntCELselect
%t2select
%phiDEG
%Cox
%hold on
%plot and display "Curves of Shear Stress at Tool-Chip Interface", displaying the
phi solution.
%P
%plot(P(1,:),P(2,:))
%plot(P(1,:),P(3,:))
%xlabel("shear plane angle, degrees")
%ylabel("interface shear stress, Taulnt (MPa), kchip (MPa)")
%title("Curves of Shear Stress at Tool-Chip Interface")
```

APPENDIX B

DEFINING THE SHEAR THICKNESS RATIO

The shear thickness ratio, δ , was calculated as a function of feed and cutting speed for the 1006 steel, 6Al-4V titanium, 2024-T3 aluminum and OFE copper, see Figure 51.

Note that these relationships are specific to a rake angle of 5° and a tool width of 3mm.

For predictions of a different rake angle or tool width, the calculation for shear thickness ratio must be made anew. Power law fits from the simulations shown in Figure 51 show that feed and cutting velocity are factors of δ . For each metal under study, the power law constants of the fits were each themselves fit as functions of feed and cutting velocity.

The result of this modeling is an expression for δ as a function of feed and cutting speed, relative to the aforementioned tool parameters. Shown below are all the fits to the simulated δ values that were used in determining the expressions for delta.

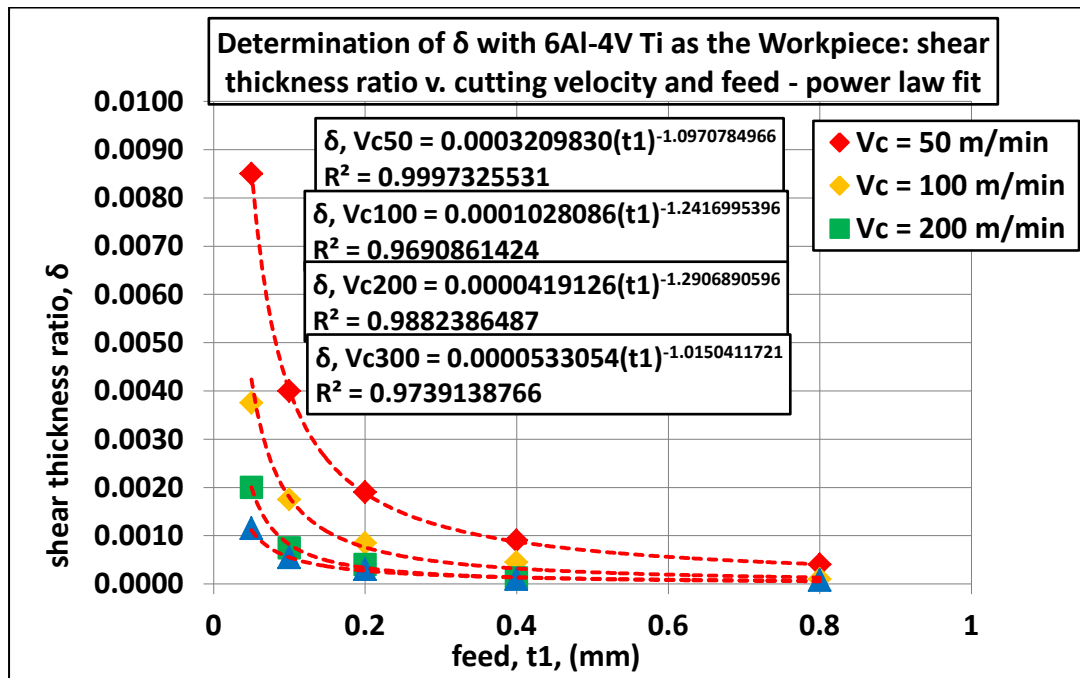


Figure 51:Determination of δ with 6Al-4V Ti as the workpiece: shear thickness ratio v. cutting velocity and feed - power law fit.

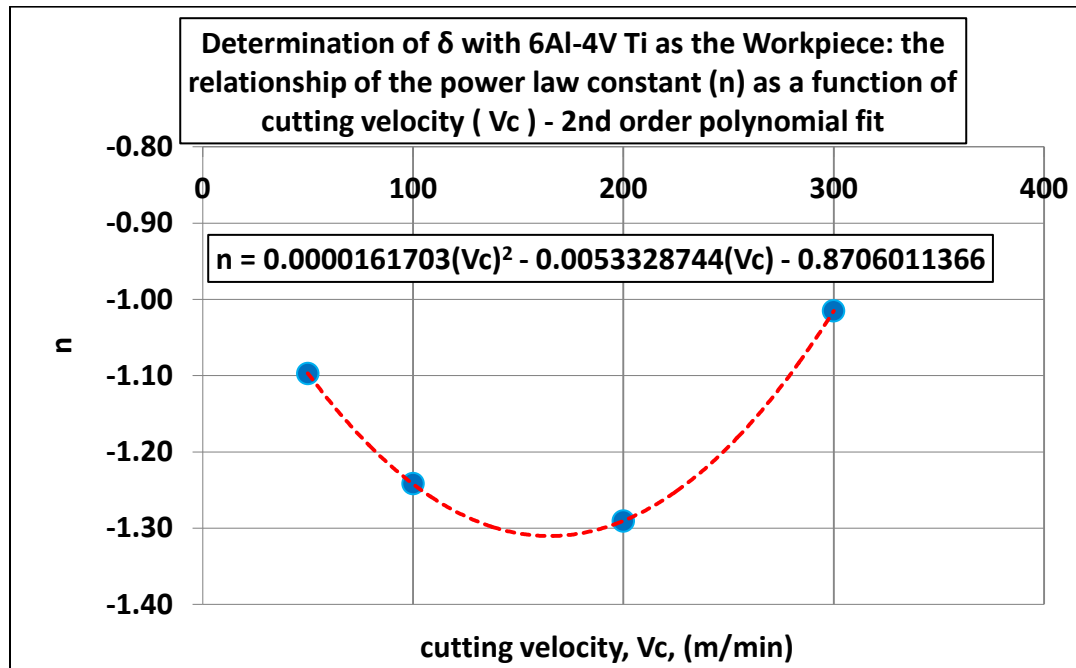


Figure 52:Determination of δ with 6Al-4V Ti as the workpiece: the relationship of the power law constant (n) as a function of cutting velocity (Vc) - 2nd order polynomial fit.

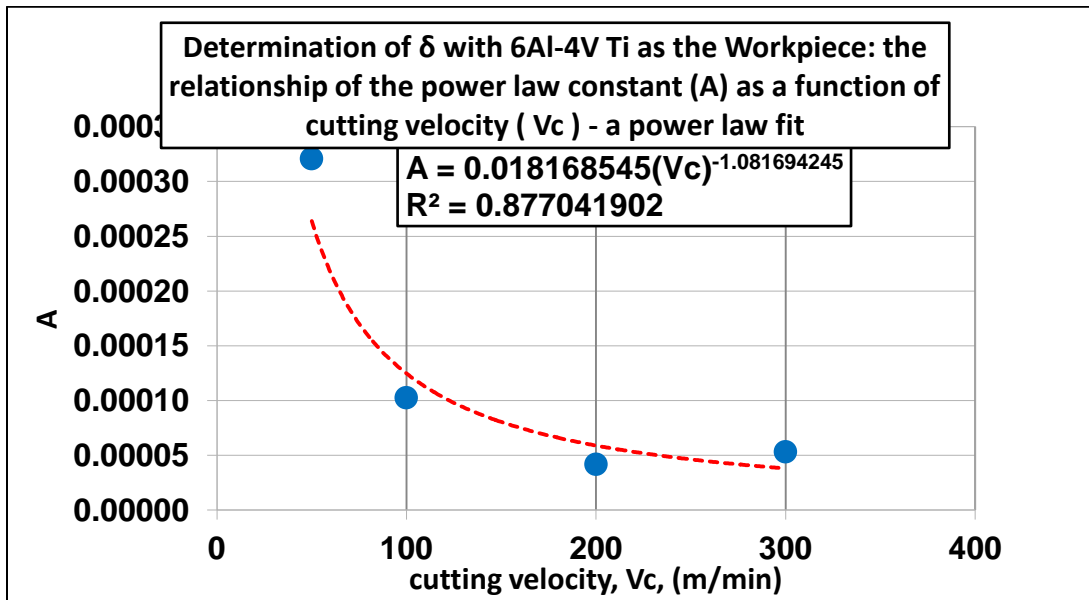


Figure 53:Determination of δ with 6Al-4V Ti as the workpiece: the relationship of the power law constant (A) as a function of cutting velocity (Vc) - a power law fit.

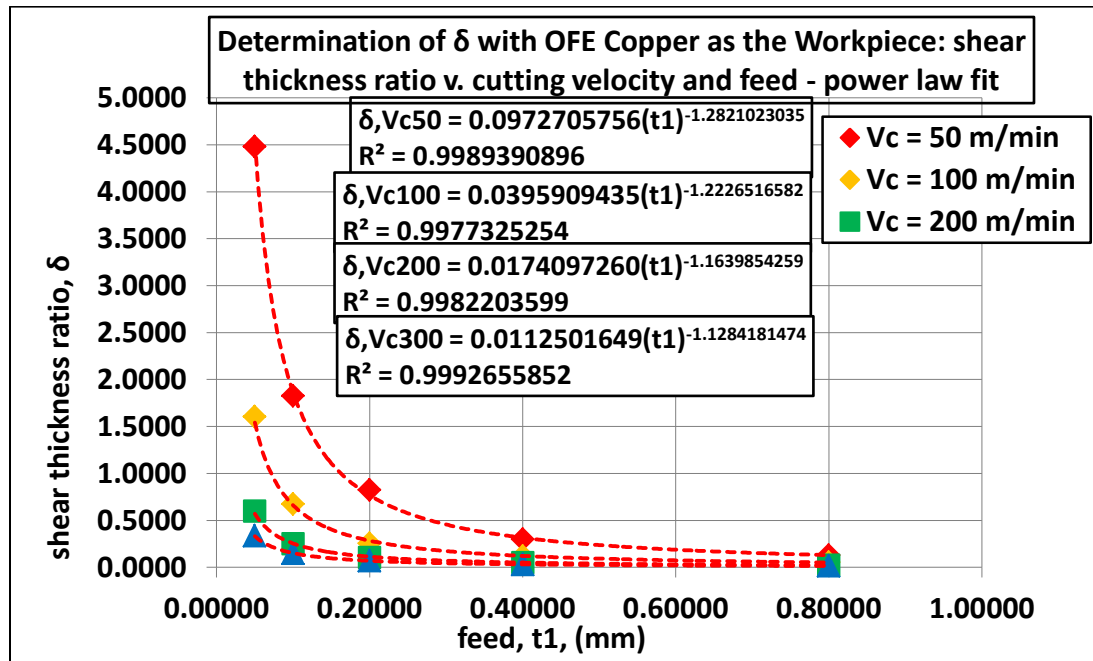


Figure 54:Determination of δ with OFE copper as the workpiece: shear thickness ratio v. cutting velocity and feed - power law fit.

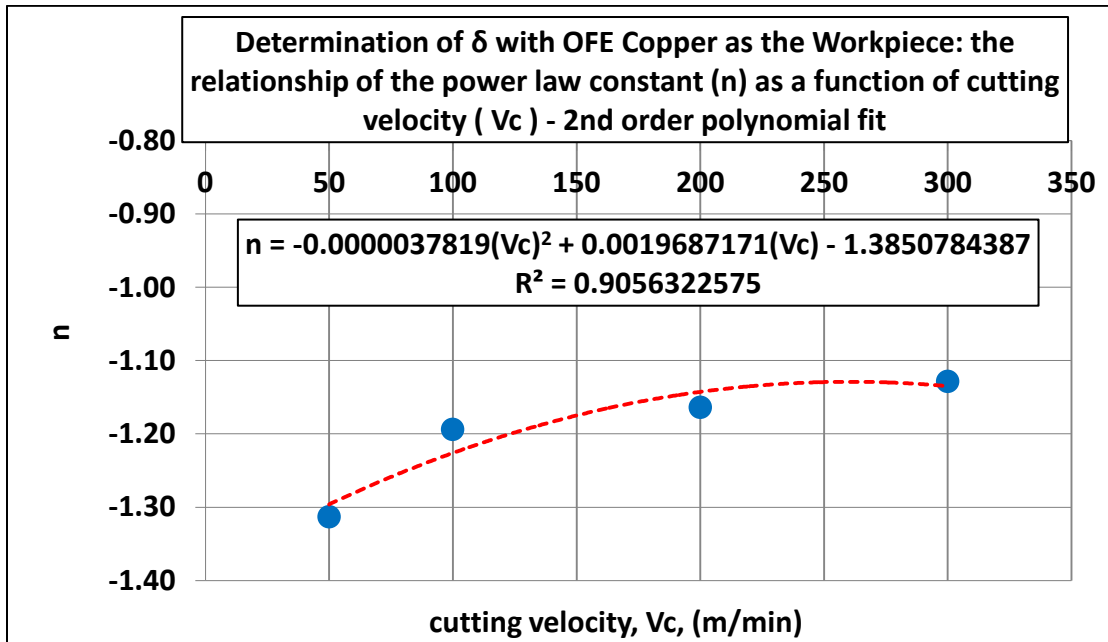


Figure 55:Determination of δ with OFE copper as the workpiece: the relationship of the power law constant (n) as a function of cutting velocity (V_c) - 2nd order polynomial fit.

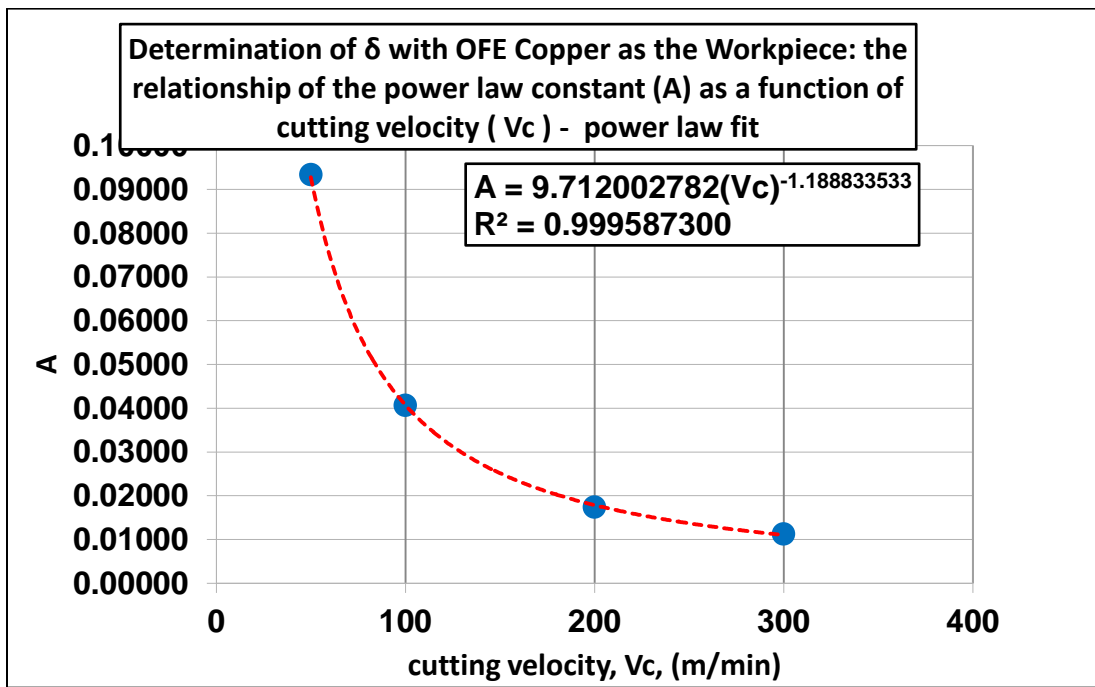


Figure 56:Determination of δ with OFE copper as the workpiece: the relationship of the power law constant (A) as a function of cutting velocity (Vc) - power law fit.

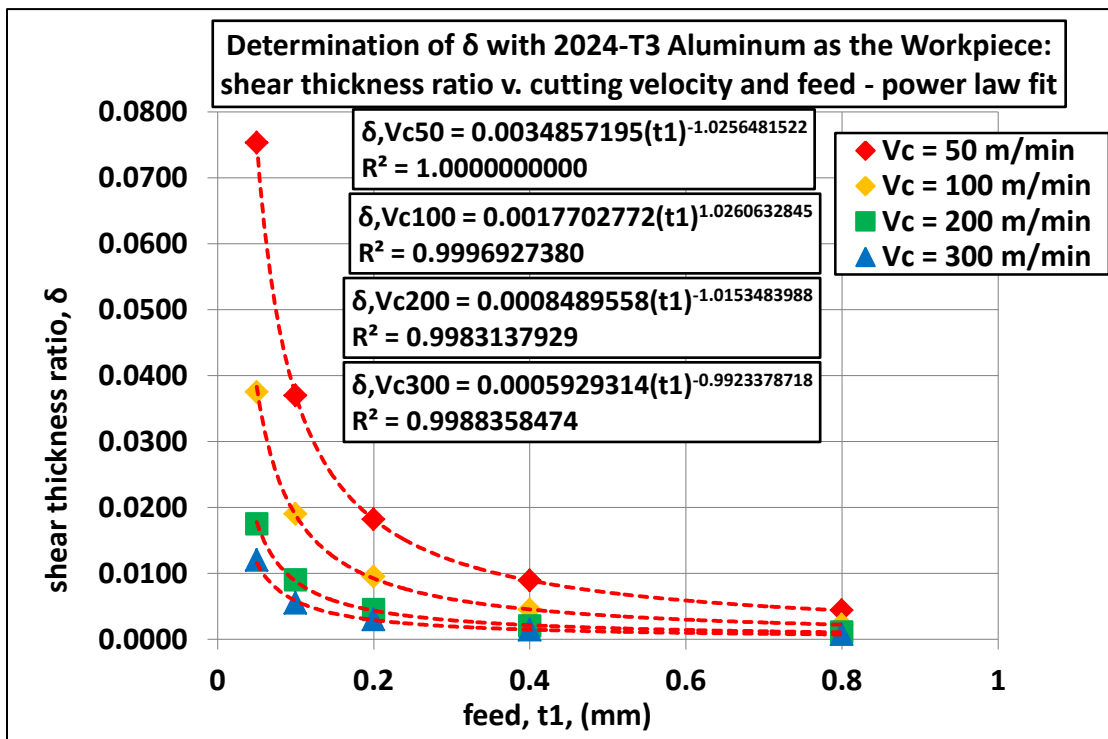


Figure 57: Determination of δ with 2024-T3 aluminum as the workpiece: shear thickness ratio v. cutting velocity and feed - power law fit.

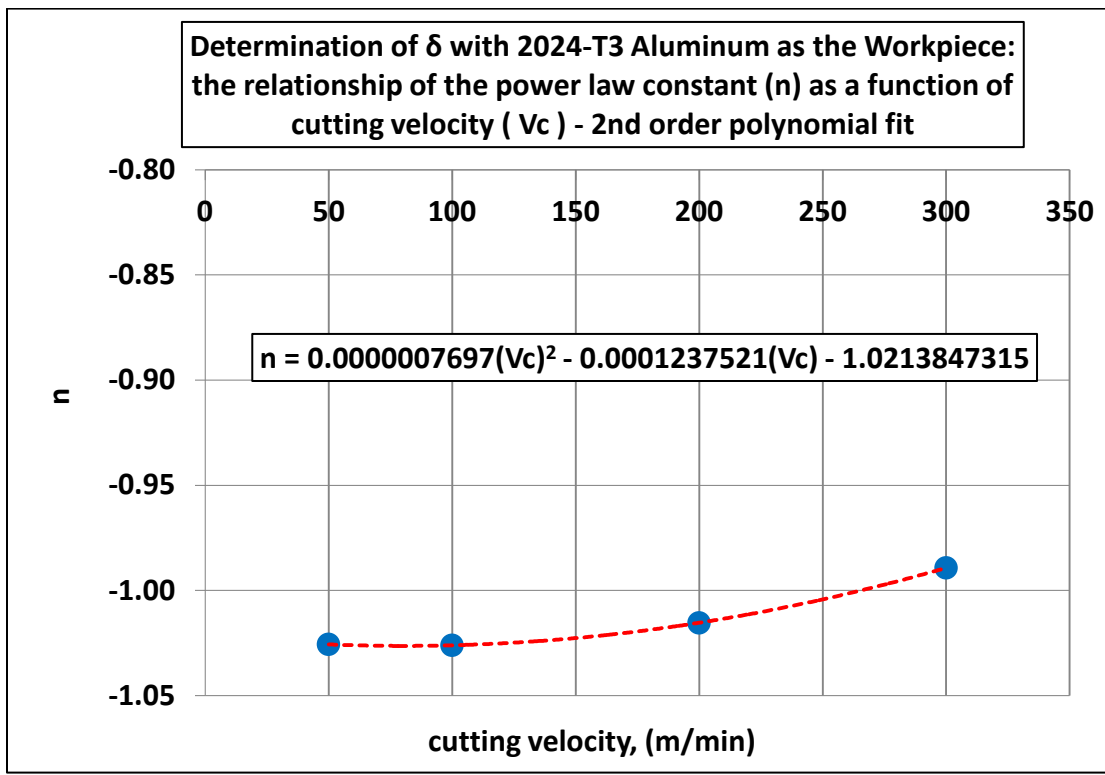


Figure 58: Determination of δ with 2024-T3 aluminum as the workpiece: the relationship of the power law constant (n) as a function of cutting velocity (Vc) - 2nd order polynomial fit.

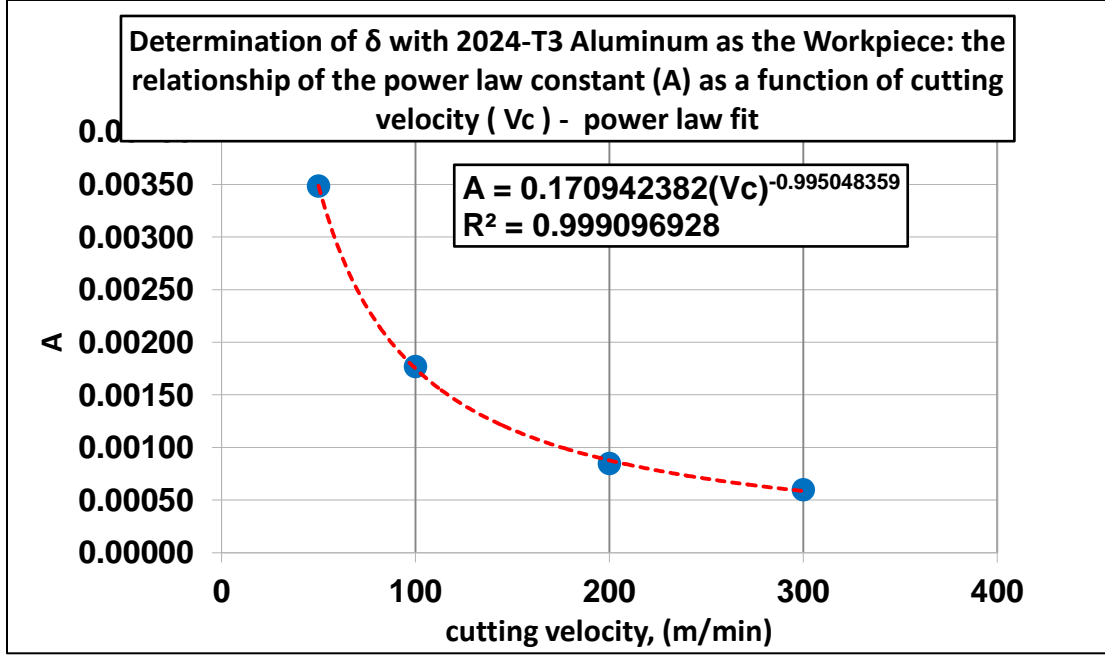


Figure 59: Determination of δ with 2024-T3 aluminum as the workpiece: the relationship of the power law constant (A) as a function of cutting velocity (Vc) - power law fit.

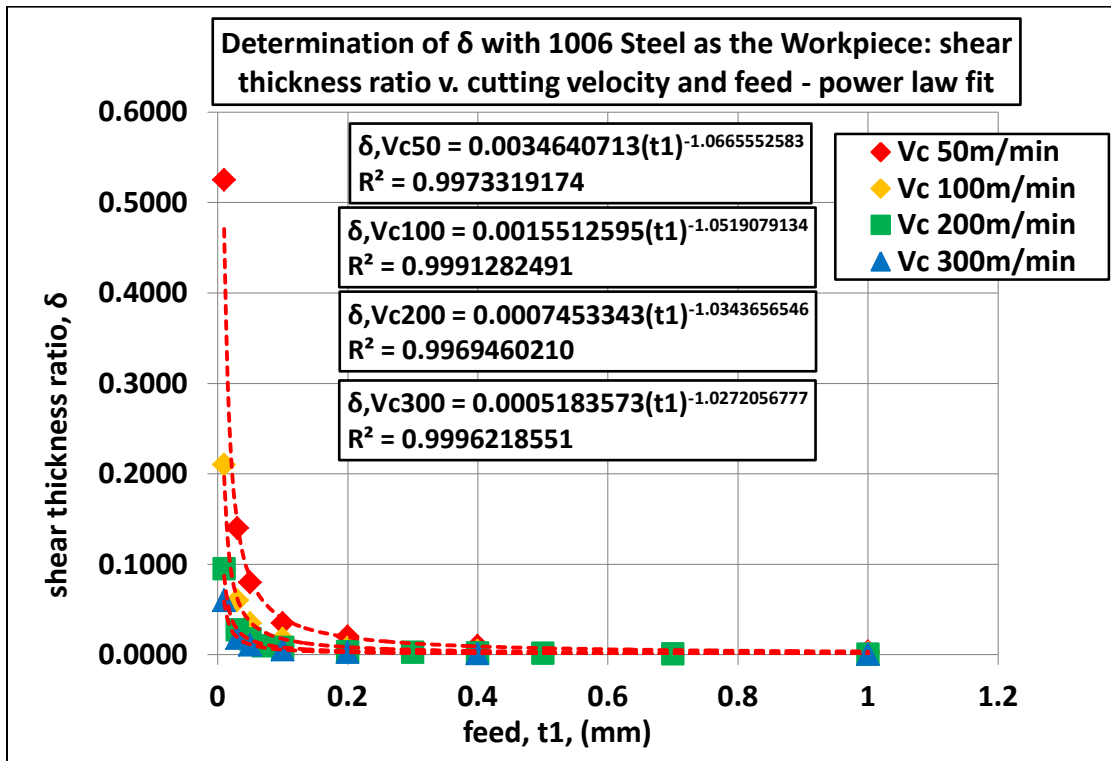


Figure 60: Determination of δ with 1006 steel as the workpiece: shear thickness ratio v. cutting velocity and feed - power law fit.

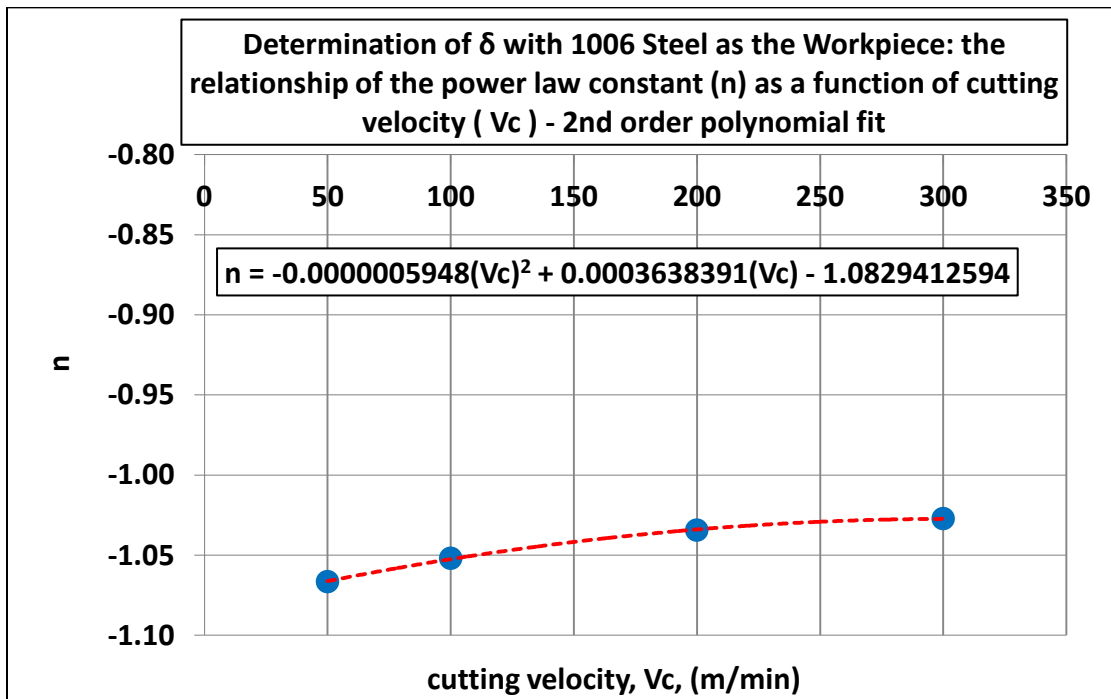


Figure 61: Determination of δ with 1006 steel as the workpiece: the relationship of the power law constant (n) as a function of cutting velocity (V_c) - 2nd order polynomial fit.

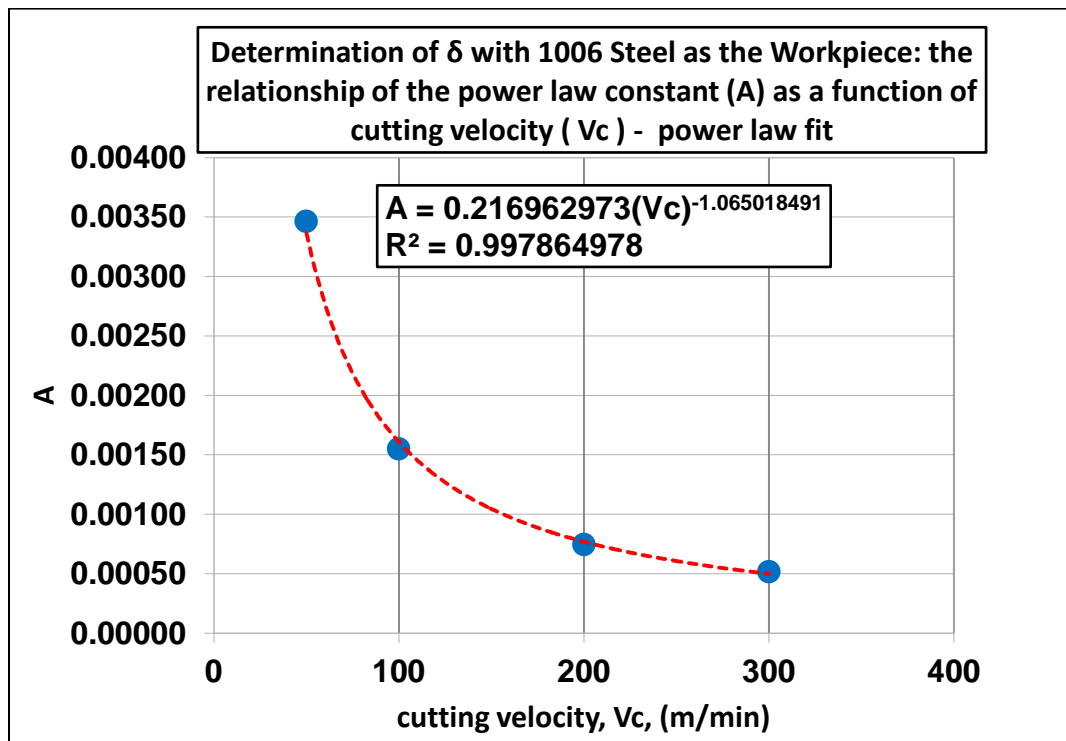


Figure 62: Determination of δ with 1006 steel as the workpiece: the relationship of the power law constant (A) as a function of cutting velocity (V_c) - power law fit.